Numerical solutions for steady flows with pressure dependent viscosities

Ms. Iffat Zehra

August 5, 2015

Preface

Fluid dynamics is a branch of mathematical sciences which deals with the study and analysis of fluid flow for different geometries as well as the rheological behavior of different fluids. The fluids are classified into different categories depending upon their rheological properties. The primary classifications of fluids are based upon the relation between shear stress and rate of deformation. This fluid parameter can be assumed as a constant for some fluids but in real scenario most fluids do not have constant viscosity. The viscosity of the fluids involved in real life problems is either pressure dependent or temperature dependent. Most of the literature both in experimental or in theoretical form the analysis on fluid flow with temperature dependent viscosities is available but the study of rheological properties of fluids with pressure dependent viscosities has not been given much attention. Viscosity is a function of pressure, which is a realistic model for technological applications, such as enhanced oil recovery and geological carbon sequestration. The fluid flow through porous media is of interest for various applications, i.e., penetration of glue in the surface, porosity of solid materials, injection of mud, slurries or cement grouts to reinforce soils, seepage of water in mud dams, propagation of blood through kidney, injection of fluids when drilling in rocks either for the reinforcement of the wells or for enhancing oil recovery, etc. Much work has been focused on the flow properties of purely

viscous fluids. In the present study flow problems of non- Newtonian fluids with pressure dependent viscosities is analyzed in porous media as the high pressure situations are witness there and the rheological properties of the fluids with pressure dependent viscosities in these cases are highly significant.

The present work is an attempt to investigate the pressure dependent viscosity problems which was less focused before. Different non-Newtonian fluid models are taken into account to study the two major categories of fluids, i.e., the (shear thinning) Pseudoplastic fluids and the (shear thickening) dilatant fluid as these fluid types covers a wide range of fluids actually used in real life problems, i.e., toxic fluids, blood, paper plumb, mud etc. The present work provides the mathematical analysis of Poiseuille flow, Couette flow and flow over a stretching sheet for various non-Newtonian fluids.

The thesis has been organized in the following manner:

Introduction section is the literature survey and opening on the subject. Chapter one confers the flow of Jeffrey fluid with pressure dependent viscosity and pressure dependent porosity. Chapter two is devoted to the numerical investigation for Williamson fluid with pressure dependent viscosity. Poiseuille and Couette flows of hyperbolic tangent fluid with pressure dependent viscosity through porous medium are examined in chapter three. In chapter four flows of Carreau fluid with pressure dependent viscosity in a variable porous medium is explored. Chapter five is dedicated to the numerical study of pressure dependent viscosity for Sutterby fluid through porous medium. Numerical simulations of Couple Stress fluid over an elastic stretching sheet with pressure dependent viscosity are carried out in chapter six. Chapter seven is committed to the flow of Jeffrey fluid with pressure dependent viscosity in the annulus of two infinitely long coaxial cylinders. Finally conclusions are carried out in chapter eight.

Contents

Nomenclature

ρ	density	A_1	first Rivlin-Ericksen tensor
$\mathbf{T}$	cauchy stress tensor	$\boldsymbol{\tau}$	extra stress tensor
Ω	angular velocity	Re	Reynolds number
h	height of inclined channel	α	porous medium parameter
θ	angle of inclination	$\mu(p)$	pressure dependent viscosity
μ_0	zero shear rate viscosity	μ_∞	infinite shear rate viscosity
λ_1	relaxation time	λ_2	retardation time
β	power law index	$\prod$	second invariant strain tensor
We	Weissenberg number	C	ratio of pressure due to gravity
η	couple stress parameter	χ	coefficient of the viscosity
α_0	stretching parameter	ε	pressure coefficient for the viscosity
U_c	characteristic velocity	g	acceleration due to gravity
p_0	pressure at the boundary	N	dimensionless couple stress parameter
Γ	time constant	E	dimensionless coefficient of pressure
R_{in}	radius of internal cylinder	ζ	dimensionless parameter
R_{out}	radius of outer cylinder	C_f	skin friction coefficient

Chapter 0

Introduction

Fluid dynamics is a branch of engineering science which deals with the study and analysis of fluid flow in different geometries as well as the rheological behavior of different fluids. The fluids are classified into different categories depending upon the variation exhibited by fluids with various rheological properties. Viscosity of the fluid which shows the rheological behavior, is the ratio of shear stress to the shear rate. Some fluids have constant viscosity but in general most fluids do not have constant viscosity. The viscosity of the fluids in many real life problems is either pressure dependent, temperature dependent or shear rate dependent.

Variable viscosity contributes as a drag force to the fluid flow. This can be explained in terms of the internal friction between adjacent layers. The fluid flows with the layer wise movement in a forward direction. The variable viscosity creates resistance between these adjacent layers. Andrade [1] contributed in this regard by establishing an empirical formula for the relationship between viscosity, pressure, density and temperature. However, much focus was given to the area of temperature dependent viscosity. Experimental and theoretical research is available in this regard.

In early study, Stokes [2] discussed that fluids viscosity can be a function of pressure.

Later on, various researchers explored experimental data which shows while dealing with the polymer melts, viscosity can be a function of pressure. Aho and Syrjala [3–4] determined through analysis that the viscosity of polystyrene is strongly dependent upon pressure. Some simple flows of viscous fluids with pressure dependent viscosities have been discussed numerically by Hron et. al. [5–6]. Barus [7] explored the variation in the viscosity of the liquids with pressure and provided the relationship between the viscosity and pressure. Thus, as the pressure is increased, the viscosity may change by several orders of magnitude. Some other experiments showed that the viscosity can be a factor of as much as 10 to the power 10%, the density changes are significant by comparison [8-14], such kind of pressure dependent viscosity is useful in elastohydrodynamics. Experimental results had revealed that the variation in the fluid viscosity is significantly notable with the change in the pressure i.e., fluid viscosity is a function of pressure. Bridgman [15–16] examined the dependence of fluid viscosity on the normal stress under high pressure experimentally. There has been considerable work on the flows of fluid with pressure dependent viscosity as they are relevant to several technologically significant problems. High pressure sufficient to cause major change in the viscosity appears in many polymer processing operations. The pressure dependence of the viscosity plays important role in fluid film lubrication (an application of elastohydrodynamics), microfluidics and geophysics. In elastohydrodynamic applications, the lubricant is forced to flow through a very narrow region which leads to very high pressures. In geophysical flows the fluid viscosity changes with the depth of the fluids. Bair and Winer [17] specifically examined the lubricants flow and their results verified the dependence of viscosity on the mean normal stress. There have been few rigorous mathematical studies concerning the existence and uniqueness of flows of fluids with pressure dependent viscosity. Mathematical issues arising in the case of incompressible Newtonian or non-Newtonian fluids with a pressure dependent viscosity have been addressed by Renardy [18], Gazzola [19] and Malek et.

al. [20–21]. The existence of flows of fluids with pressure dependent viscosity and the associated assumptions have been discussed by Bulicek et. al. [22]. Barus [7] proposed an exponential isothermal equation of state for viscosity, i.e. the viscosity was taken as an exponential function of pressure. The accumulation of other equations proposed for the pressure dependent viscosity has been considered by Kannan et. al. [23]. Viscosity is a function of pressure, which is a realistic model for technological applications, such as enhanced oil recovery and geological carbon sequestration.

The fluid flow through porous media is also important for various applications in civil, geotechnical, petroleum, biomedical engineering and material sciences. i.e., penetration of glue in the surface, porosity of solid materials, injection of mud, slurries or cement grouts to reinforce soils, seepage of water in mud dams, injection of drilling fluids in rocks either for the reinforcement of the wells or for enhancing oil recovery, etc. Mainly flow through porous media is commonly modeled by considering Darcy's equation. Darcy's equation establishes significant relationship between pressure drop and fluid velocity for fluids with constant viscosity [24–27]. In enhancing oil recovery and reinforcement of the wells fluid flow occurs under high pressure where the viscosity of the fluids cannot be considered a constant. For fluids having variable viscosities, experimental results doesn't obey the Darcy's equation. Thus for fluid flow with variable viscosities Darcy's equation is modified [28].

The study of non-Newtonian fluids through porous medium is an important aspect which occurs in a broad range of engineering applications such as transport processes in a chemical industry, storage of nuclear waste material, discoveries of the flow of oil in petroleum reservoirs, etc. Although there are number of researchers [29–33] who have addressed non-Newtonian fluids through porous medium with different geometries. There is limited work available for non-Newtonian fluids with the assumption of pressure dependent viscosity along with pressure dependent porosity. Some more relevant article related to the

topic are cited in the Refs.[34-36].

The purpose of the present research is to explore the effect of pressure dependent viscosity on the fluid flow problems for different fluids. In the present study flow problems of non-Newtonian fluids with pressure dependent viscosities are analyzed in porous media as the high pressure situations are witness there and the rheological properties of the fluids with pressure dependent viscosities in these cases are highly significant. The two major categories of fluids, i.e., the (shear thinning) pseudoplastic fluids and the (shear thickening) dilatant fluid are considered, as these fluid types covers a wide range of fluids actually used in real life problems i.e., toxic fluids, lubricants, paints, paper plumb, mud etc. Relevant recent articles discussing Couette flow, Poiseuille flow and a flow over a stretching sheet are cited in [37–42]. The present work provides the mathematical analysis of Poiseuille flow, Couette flow and flow over a stretching sheet for various non-Newtonian fluids. The geometry of the problem as well as the mathematical formulation of the problem is carried out in Cartesian and Cylindrical coordinates. For the purpose of simplification non dimensional form of the variables is used which will lead to a system of nonlinear differential equations subject to the appropriate boundary conditions. In order to study the fluid flow behavior of these nonlinear differential equations numerical schemes such as finite difference scheme and shooting method with Runge-Kutta Fehlberg technique [43–46] are incorporated. Finite difference technique is a useful numerical scheme based on central difference operator. The idea for finite difference method is to discretize the boundary interval and replace the derivatives with difference formulas. The solution at all discrete mesh points is simultaneously calculated. Shooting method is a numerical technique in which boundary value problem is converted into system of initial value problems and the solution points are achieved by iterative process from an initial point to the end point. Numerical investigation for the fluid velocity is carried out. Graphical results are presented to observe the physical behavior of various pertinent parameters on these flow

characteristics.

The present thesis consist of eight chapters which are briefly explained as

Chapter one discussed the flow of Jeffrey fluid with pressure dependent viscosity and pressure dependent porosity. Numerical investigation is made by finite difference scheme. Contents of this chapter are published in the International Journal for Numerical Methods in Fluids, 68 (2012) 196–209.

Pseudoplastic fluids with pressure dependent viscosity and porosity are examined numerically in chapter two. Shooting method with Runge-Kutta Fehlberg is implemented for the numerical study of Williamson fluid. Contents of this chapter are published in the Journal of Results in Physics, 5 (2015) 20–25.

Chapter three is devoted for the numerical investigation of hyperbolic tangent fluid in an inclined channel with pressure dependent viscosity and porosity. Numerical solutions for the problem are discussed with the help of graphs and tables. The chapter contents are submitted for publication in Zeitschrift fuer Naturforschung A.

Chapter four deals with the numerical study of Carreau fluid with pressure dependent viscosity. The coupled non–linear differential equations are numerically examined by shooting method along with Runge-Kutta Fehlberg technique. Content of this chapter are published in Alexandria Engineering Journal 53 (2014) 427435.

Sutterby fluid model covers the wide range of Newtonian, shear thinning and shear thickening fluids. Chapter 5 copes with the numerical treatment of dilatant (shear thickening) fluid with pressure dependent viscosity and porosity . Shooting method with Runge-Kutta Fehlberg is used for the numerical study of Sutterby fluid. The contents of this chapter are submitted for publication in the European Physical Journal - Plus.

Numerical investigation of couple stress fluid with pressure dependent viscosity between two parallel plates in which the lower plate is stretched while the upper plate is moving with constant velocity is carried out in chapter 6. The governing system of nonlinear

ordinary differential equations is solved numerically by using the trapezoid scheme with the enhancement of Richardson extrapolation. Results are shown through graphs and tables. Content of this research is submitted in the Journal of Applied Mathematics and Mechanics.

Chapter 7 is the numerical analysis of flow of Jeffrey fluid with pressure dependent viscosity in the annulus of two infinitely long coaxial cylinders. The mathematical analysis is carried out in cylindrical coordinates. Nonlinear ordinary differential equations are simplified by using appropriate non dimensional variables and quantities. Numerical results are carried out with the help of shooting method along with Runge-Kutta Fehlberg technique. The numerical results trends for different important parameters are discussed graphically. This chapter contents are submitted for publication in the Journal of Computational and Applied Mathematics.

Last chapter summarizes the conclusion extracted out from the numerical study for steady flows of non-Newtonian fluids with pressure dependent viscosities.

Chapter 1

Numerical treatment of Jeffrey fluid with pressure dependent viscosity

1.1 Introduction

In this chapter, mathematical analysis of Jeffrey fluid with pressure dependent viscosity in a porous medium is carried out. The equations of Jeffrey fluid model have been derived when the viscosity and porosity are considered to be pressure dependent. The solution of these equations is subjected to two types of boundary conditions named as (i) Poiseuille flow and (ii) Couette flow have been calculated numerically using finite difference scheme. Four different cases for pressure dependent viscosities and pressure dependent porosity are examined. The graphical description of certain parameters of interest are displayed and discussed.

1.2 Fluid model

Let us consider an incompressible unidirectional flow of a Jeffrey fluid with pressure dependent viscosity in an inclined channel of height h. Cartesian coordinates system is taken into account such that $(u(y), 0, 0)$ is velocity vector in which u is the x-component of velocity and y is perpendicular to the x-axis. The equations which govern the flow of an incompressible fluid through a porous medium are

$$div\mathbf{V} = 0, \tag{1.1}$$

$$\rho\frac{d\mathbf{V}}{dt} = div\mathbf{T} - \alpha(p)\mathbf{V} + \rho\mathbf{b}_e, \tag{1.2}$$

where $\mathbf{V}$ is the velocity vector, ρ is the density, t is the time, $\mathbf{b}_e$ is the body forces, $\alpha(p)$ is a pressure dependent porous medium parameter and $\mathbf{T}$ is the Cauchy stress tensor. For Jeffrey fluid model the Cauchy stress tensor is defined as [47]

$$\mathbf{T} = -p\mathbf{I} + \boldsymbol{\tau} \tag{1.3}$$

where

$$\boldsymbol{\tau} = \frac{\mu(p)}{1+\lambda_1}\left(\mathbf{A}_1 + \lambda_2\frac{d\mathbf{A}_1}{dt}\right) \tag{1.4}$$

in which p is the pressure, $\mathbf{I}$ is the unit tensor, λ_1 and λ_2 are the relaxation and retardation times, $\boldsymbol{\tau}$ is the extra stress tensor and $\mathbf{A}_1$ is the first Rivlin-Ericksen tensor which is as follows

$$\mathbf{A}_1 = \nabla\mathbf{V} + (\nabla\mathbf{V})^{\dagger}, \tag{1.5}$$

where $\dagger$ represents the transpose.

1.3 Mathematical formulation

The velocity and pressure fields are of the form

$$\mathbf{V} = (u(y), 0, 0), \qquad p = p(y), \tag{1.6}$$

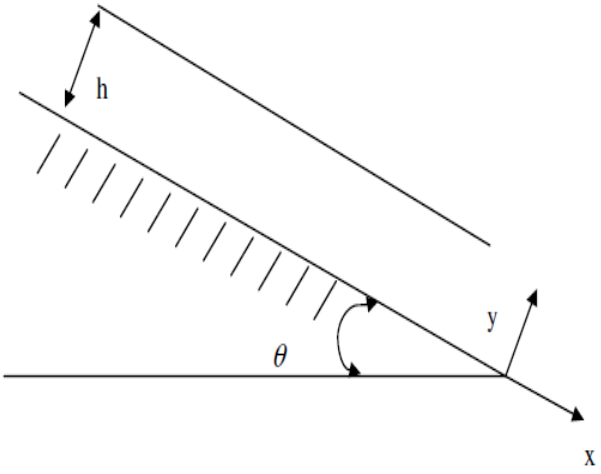

Figure 1.1: Fluid flows on an inclined plane

With the help of Eqs. (1.3) to (1.6) in the presence of gravity g and porous media effects, Eq. (1.2) takes the following component form

$$-\frac{\partial p}{\partial x}+\frac{\mu(p)}{1+\lambda_1}\frac{d^2u}{dy^2}+\frac{1}{1+\lambda_1}\frac{d\mu(p)}{dy}\frac{du}{dy}-\alpha(p)u(y)+\rho g\sin\theta=0, \tag{1.7}$$

and

$$-\frac{\partial p}{\partial y}-\rho g\cos\theta=0. \tag{1.8}$$

Introducing the following dimensionless variables

$$\bar{y}=\frac{y}{h}, \qquad \bar{u}=\frac{u}{U_c}, \tag{1.9}$$

where U_c is the characteristic velocity. With the help of Eq.(1.9), Eqs.(1.7) and (1.8) after dropping the bars can be written as

$$\frac{d^2u}{dy^2}+\frac{1}{\mu(p)}\frac{d\mu(p)}{dy}\frac{du}{dy}-h^2(1+\lambda_1)\frac{\alpha(p)}{\mu(p)}u(y)+(1+\lambda_1)\frac{\rho g h^2\sin\theta}{U_c\mu(p)}=0, \tag{1.10}$$

and

$$\frac{dp}{dy}+\rho g h\cos\theta=0. \tag{1.11}$$

The solution of Eq.(1.11) is

$$p = p_0 + \rho g h \cos\theta (1 - y). \tag{1.12}$$

where p_0 is the pressure at $y = h$.

With the help of Eq. (1.12), the solution of Eq. (1.10) has been computed in the next section for two types of boundary conditions known as

(i) Poiseuille flow

(ii) Couette flow

1.4 Poiseuille flow

In this case the rigid plates at $y = 0$ and $y = h$ are at rest. Therefore,

$$u(0) = 0, \qquad u(h) = 0. \tag{1.13}$$

To solve Eq. (1.10) subject to the boundary condition (1.13), we must choose the values of functions $\mu(p)$ and $\alpha(p)$. The following are few different functional forms chosen for illustration

Case I

$$\mu(p) = Aexp(ap), \quad \alpha(p) = Bexp(bp), A > 0, B, a, b \geq 0. \tag{1.14}$$

Case II

$$\mu(p) = Aexp(ap), \quad \alpha(p) = B(p/p_0)^m, A > 0, B, a, m \geq 0. \tag{1.15}$$

Case III

$$\mu(p) = A(p/p_0)^n, \quad \alpha(p) = Bexp(bp), A > 0, B, b, n \geq 0. \tag{1.16}$$

Case IV

$$\mu(p) = A(p/p_0)^n, \quad \alpha(p) = B(p/p_0)^m, A > 0, B, n, m \geq 0. \tag{1.17}$$

With the help of these expressions, for each case Eq. (1.10) takes the following form

$$\frac{d^2u}{dy^2} - \Gamma_1\frac{du}{dy} - \Gamma_2(1+\lambda_1)exp[\Gamma_4(1-y)]u(y) + \Gamma_3(1+\lambda_1)exp[-\Gamma_1(1-y)] = 0, \quad (1.18)$$

where

$$\Gamma_1 = \rho gh\cos\theta, \Gamma_2 = \frac{h^2Bexp[(b-a)p_0]}{A}, \Gamma_3 = \frac{\rho gh^2\sin\theta}{U_cAexp(ap_0)}, \Gamma_4 = (b-a)\rho gh\cos\theta. \quad (1.19)$$

$$\frac{d^2u}{dy^2} - \Gamma_1\frac{du}{dy} - \Gamma_2(1+\lambda_1)[1+\Gamma_4(1-y)]^m exp[-\Gamma_1(1-y)]u(y) + \Gamma_3(1+\lambda_1)exp[-\Gamma_1(1-y)] = 0, \quad (1.20)$$

in which

$$\Gamma_1 = a\rho gh\cos\theta, \Gamma_2 = \frac{Bh^2}{Aexp(ap_0)}, \Gamma_3 = \frac{\rho gh^2\sin\theta}{U_cAexp(ap_0)}, \Gamma_4 = \frac{\rho gh\cos\theta}{p_0}. \quad (1.21)$$

$$\frac{d^2u}{dy^2} - \frac{n\Gamma_1}{1+\Gamma_1(1-y)}\frac{du}{dy} - \Gamma_2(1+\lambda_1)[1+\Gamma_1(1-y)]^{-n}exp[\Gamma_4(1-y)]u(y) + \Gamma_3(1+\lambda_1)[1+\Gamma_1(1-y)]^{-n} = 0, \quad (1.22)$$

here

$$\Gamma_1 = \frac{\rho gh\cos\theta}{p_0}, \Gamma_2 = \frac{Bh^2exp(bp_0)}{A}, \Gamma_3 = \frac{\rho gh^2\sin\theta}{U_cA}, \Gamma_4 = b\rho gh\cos\theta. \quad (1.23)$$

$$\frac{d^2u}{dy^2} - \frac{n\Gamma_1}{1+\Gamma_1(1-y)}\frac{du}{dy} - \Gamma_2(1+\lambda_1)[1+\Gamma_1(1-y)]^{m-n}u(y) + \Gamma_3(1+\lambda_1)[1+\Gamma_1(1-y)]^{-n} = 0, \quad (1.24)$$

the non dimensional parameters are defined as

$$\Gamma_1 = \frac{\rho gh\cos\theta}{p_0}, \quad \Gamma_2 = \frac{Bh^2}{A}, \quad \Gamma_3 = \frac{\rho gh^2\sin\theta}{U_cA}. \quad (1.25)$$

The corresponding boundary conditions in non dimensional form are defined as

$$u(0) = 0, \qquad u(1) = 0. \quad (1.26)$$

1.5 Couette flow

In this case, the lower plate is at rest and the upper plate is moving with the velocity U_h. The boundary conditions for the problem in non dimensional form becomes

$$u(0) = 0, \qquad u(1) = U_0, \tag{1.27}$$

where $U_0 = U_h/U_c$. The governing equations are same as defined in previous section(Eqs.(1.18) – (1.25)).

1.6 Solution of the problem

1.6.1 Finite difference method

Finite difference method is a numerical tool to solve linear or non linear differential equations. In this technique the derivatives are approximated by using the central difference scheme and the resulting algebraic equations are solved numerically. In order to compute numerical solution of given problem in an interval $[y_0, y_J]$ where J is a positive integer, first divide the interval $[y_0, y_J]$ into J subintervals (if equally spaced) each of length Δy defined as

$$\Delta y = \frac{y_J - y_0}{J}, \tag{1.28}$$

with the mesh points $y_j = y_0 + j\Delta y$ for $j = 0, 1, ...J$. The value of dependent variable $u(y)$ at $y = y_j$ is denoted as

$$u(y_j) = u_j. \tag{1.29}$$

At the lower boundary or at initial node $y_0 = 0$

$$u(y_0) = u(0) = 0 \tag{1.30}$$

and the upper boundary condition i.e., at $y = y_J$

$$u(y_J) = u(1) = U_0 \tag{1.31}$$

In case of Poiseuille flow i.e., when $U_0 = 0$.

After using central difference scheme to approximate first and second order derivatives as

$$\frac{du}{dy} \approx \frac{u_{j+1} - u_{j-1}}{2(\Delta y)}, \qquad \frac{d^2u}{dy^2} \approx \frac{u_{j+1} - 2u_j + u_{j-1}}{(\Delta y)^2}, \tag{1.32}$$

Eqs. (1.18), (1.20), (1.22) and (1.24) gives the following system of equations.

Case I

$$a_j u_{j+1} + b_j u_j + c_j u_{j-1} = A exp[-\Gamma_1(1 - y_j)], \tag{1.33}$$

with

$$a_j = \frac{1}{(\Delta y)^2} - \frac{\Gamma_1}{2(\Delta y)}, \qquad c_j = \frac{1}{(\Delta y)^2} + \frac{\Gamma_1}{2(\Delta y)}, \qquad A = -\Gamma_3(1 + \lambda_1),$$

$$b_j = -\frac{2}{(\Delta y)^2} - \Gamma_2(1 + \lambda_1) exp[\Gamma_4(1 - y_j)].$$

Case II

$$a_j u_{j+1} + b_j u_j + c_j u_{j-1} = A exp[-\Gamma_1(1 - y_j)], \tag{1.34}$$

with

$$a_j = \frac{1}{(\Delta y)^2} - \frac{\Gamma_1}{2\Delta y}, \qquad c_j = \frac{1}{(\Delta y)^2} + \frac{\Gamma_1}{2(\Delta y)}, \qquad A = -\Gamma_3(1 + \lambda_1),$$

$$b_j = -\frac{2}{(\Delta y)^2} - \Gamma_2(1 + \lambda_1)[1 + \Gamma_4(1 - y_j)]^m exp[-\Gamma_1(1 - y_j)],$$

Case III

$$a_j u_{j+1} + b_j u_j + c_j u_{j-1} = \frac{A}{[1 + \Gamma_1(1 - y_j)]^n}, \tag{1.35}$$

with

$$a_j = \frac{1}{(\Delta y)^2} - \frac{n\Gamma_1}{2(\Delta y)[1 + \Gamma_1(1 - y_j)]}, \qquad c_j = \frac{1}{(\Delta y)^2} + \frac{n\Gamma_1}{2(\Delta y)[1 + \Gamma_1(1 - y_j)]},$$

$$b_j = -\frac{2}{(\Delta y)^2} - \Gamma_2 \frac{(1 + \lambda_1) exp[\Gamma_4(1 - y_j)]}{[1 + \Gamma_1(1 - y_j)]^n}, \qquad A = -\Gamma_3(1 + \lambda_1).$$

Case IV

$$a_j u_{j+1} + b_j u_j + c_j u_{j-1} = \frac{A}{[1 + \Gamma_1(1 - y_j)]^n}, \tag{1.36}$$

with

$$a_j = \frac{1}{(\Delta y)^2} - \frac{n\Gamma_1}{2(\Delta y)[1+\Gamma_1(1-y_j)]}, \qquad c_j = \frac{1}{(\Delta y)^2} + \frac{n\Gamma_1}{2(\Delta y)[1+\Gamma_1(1-y_j)]},$$

$$b_j = -\frac{2}{(\Delta y)^2} - \Gamma_2(1+\lambda_1)[1+\Gamma_1(1-y_j)]^{m-n}, \qquad A = -\Gamma_3(1+\lambda_1).$$

And the corresponding boundary conditions are modified as, For Poiseuille flow

$$u_0(0) = 0, \qquad u_J(1) = 0. \tag{1.37}$$

For Couette flow

$$u_0(0) = 0 \qquad u_J(1) = U_0. \tag{1.38}$$

This method has truncation error $O(\Delta y^2)$. Solution for both fluids are obtained numerically and the results are elaborated through tables and graphs.

1.6.2 Numerical results and discussion

The governing equations of Jeffrey fluid with pressure dependent viscosities have been solved numerically for Poiseuille flow and Couette flow. Table 1.1 is the numerical results of fluid velocity for four different cases of pressure dependent viscosity and porosity. This table illustrates the comparison of exponential and rational forms of viscosity as well as porosity. It reveals that when viscosity is considered to be a rational function of pressure fluid velocity is greater than the cases when viscosity depends on pressure exponentially. Moreover, by keeping the viscosity to be an exponential function of pressure and comparing the results for two different cases of porosity it is witness that the rational dependence of porosity on pressure contributes in raising the fluid velocity as compare to the case where porosity is an exponential function of pressure. Similarly when the same comparison is carried out by taking viscosity to be a rational function of pressure, exponential form of porosity increases the velocity as compare to the rational expression

for porosity. So, we can conclude that for Poiseuille flow a combination of exponential expression for pressure dependent viscosity and a rational form of porosity enhances velocity of Jeffrey fluid. It is found that for each case the velocity is maximum at the centre, this is because we are considering Poiseuille flow. The velocity field for different values of $\Gamma's$ are displayed in figures 1.2 to 1.5 for various values of pressure dependent viscosity. It is observed that with the increase in $\Gamma's$, the velocity field decreases for all the cases and the velocity is maximum in the absence of $\Gamma's$. Note that Γ_1 and Γ_4 equals to zero represents the case when the channel is considered to be vertical. The increasing values of Γ_1 and Γ_4 indicates the inclination of the channel. Thus, we can say that the variable pressure causes the decrease in velocity. The velocity field for various parameter λ_1 are shown in figures 1.6 to 1.9. It is depicted that the velocity field increases in each case of the viscosity with the increase in λ_1 and gives the maximum value in the centre due to the pressure gradient. The velocity for various values of power m and n are displayed in figures 1.10 to 1.13. It is observed that the velocity field decreases with the increase in m and n.

Table 1.2 displays the numerical results of Couette flow for four different cases of pressure dependent viscosity and porosity. The study of this table discloses that when comparison is done for all the four cases simultaneously, it is noted that exponentially pressure dependent viscosity and porosity being a rational function of pressure attain more fluid velocity than rest of the three cases. This leads to the conclusion that for both Poiseuille and Couette flow exponential form of viscosity and rational expression for porosity is the better choice. The graphically results for Couette flow are presented in figures 1.14 to 1.25. The velocity field for different values of $\Gamma's$ are shown in figures 1.14 to 1.17. It is observed that the velocity field decreases for each of the case and maximum value occurs in the middle. Thus in the presence of pressure dependent viscosity the velocity field decreases rapidly. The velocity field for different values of λ_1 when $\mu(p) = Aexp(ap)$,

$\alpha(p) = Bexp(bp)$ are shown in figure 1.18. It is observed that the velocity field decreases with the increase in λ_1. In case II, the velocity field increases with the increase in λ_1 (see figure 1.19). The velocity field for different values of λ_1 in case III and IV are shown in figures 1.20 and 1.21. It is seen that the velocity field decreases with the increase in λ_1. The velocity field for different values of m and n are shown in figures 1.22 to 1.25. It is observed that the velocity field increases with the increase in m for viscosity case I and IV and decrease with the increase in n for viscosity case II and III.

	u(y)			
y	**Case I**	**Case II**	**Case III**	**Case IV**
0	0	0	0	0
0.090909091	0.074851658	0.097232957	0.090105257	0.058345789
0.181818182	0.134275824	0.169301186	0.167039530	0.105553749
0.272727273	0.185134630	0.228047422	0.232448176	0.146186738
0.363636364	0.230436913	0.276341593	0.286915152	0.182679749
0.454545455	0.270310280	0.314937157	0.329835263	0.215640251
0.545454545	0.302221425	0.342287300	0.359109886	0.243719640
0.636363636	0.320693855	0.354052690	0.370575904	0.263043912
0.727272727	0.316633671	0.342264590	0.356999486	0.266100060
0.818181818	0.276302256	0.294109527	0.306319034	0.239863348
0.909090909	0.179936811	0.190327956	0.198530137	0.162786752
1.000000000	0	0	0	0

Table 1.1: Velocity for $\Gamma_1 = 1, \Gamma_2 = 10, \Gamma_3 = 10, \Gamma_4 = 1, m = 2, n = 2, \lambda_1 = 0.2$ for Poiseuille flow

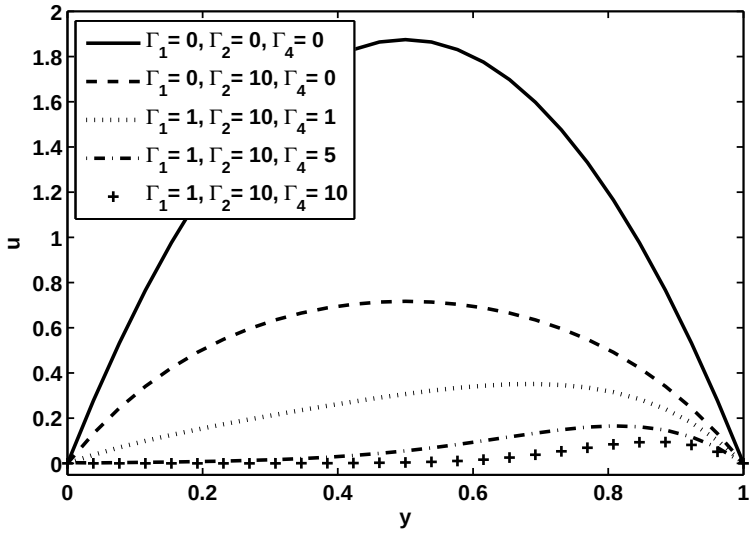

Figure 1.2: Velocity profile for $\mu(p) = Aexp(ap)$ and $\alpha(p) = Bexp(bp)$ with $\Gamma_3 = 10$ and $\lambda_1 = 0.5$ in Poiseuille flow.

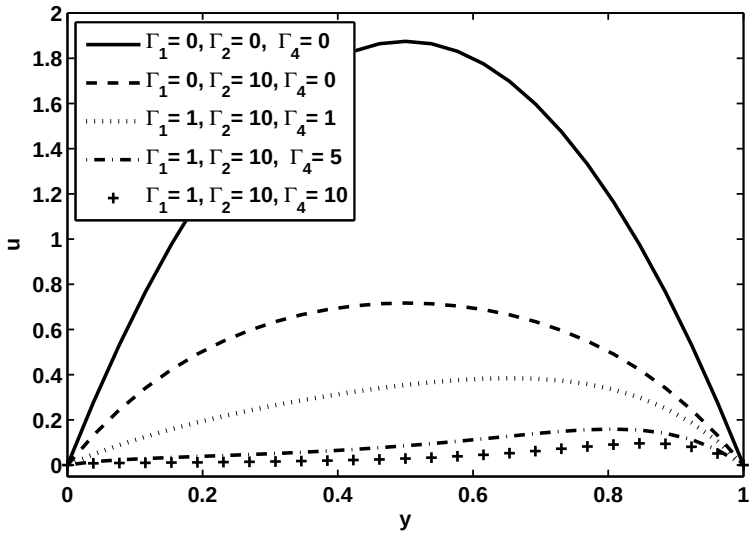

Figure 1.3: Velocity profile for $\mu(p) = Aexp(ap)$ and $\alpha(p) = B(\frac{p}{p_0})^m$ with $\Gamma_3 = 10, \lambda_1 = 0.5$ and $m = 2$ in Poiseuille flow.

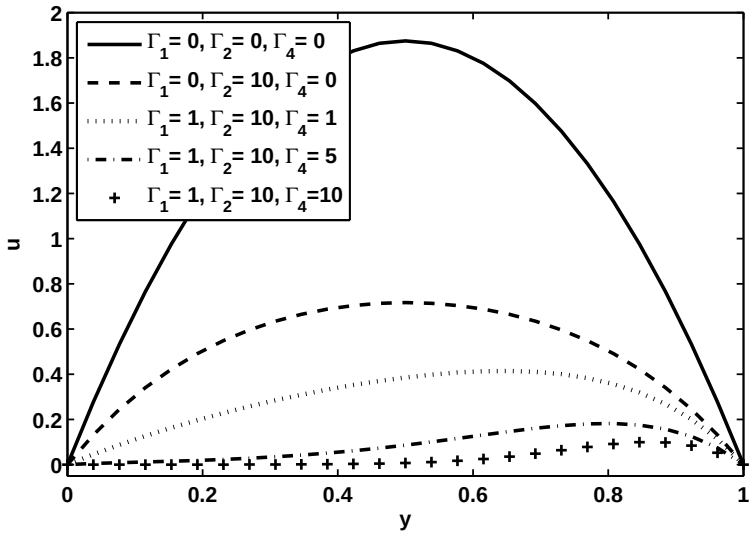

Figure 1.4: Velocity profile for $\mu(p) = A(\frac{p}{p_0})^n$ and $\alpha(p) = Bexp(bp)$ with $\Gamma_3 = 10, \lambda_1 = 0.5$ and $n = 2$ in Poiseuille flow.

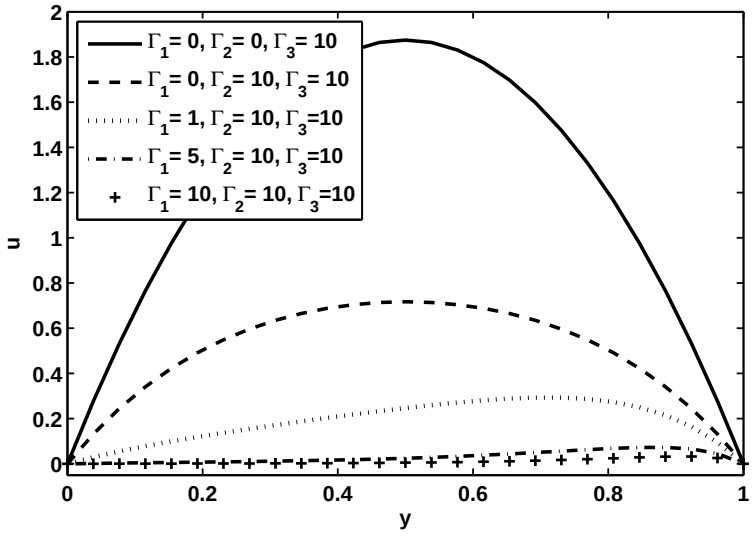

Figure 1.5: Velocity profile for $\mu(p) = A(\frac{p}{p_0})^n$ and $\alpha(p) = B(\frac{p}{p_0})^m$ with $\Gamma_3 = 10, \lambda_1 = 0.5$ and $m = 2$ in Poiseuille flow.

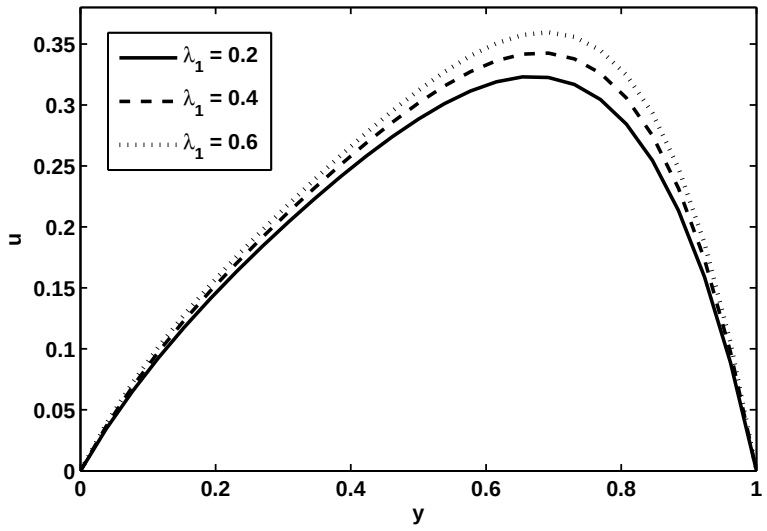

Figure 1.6: Velocity profile for $\mu(p) = Aexp(ap)$ and $\alpha(p) = Bexp(bp)$ with $\Gamma_1 = 1, \Gamma_2 = 10, \Gamma_3 = 10$ and $\Gamma_4 = 1$ in Poiseuille flow.

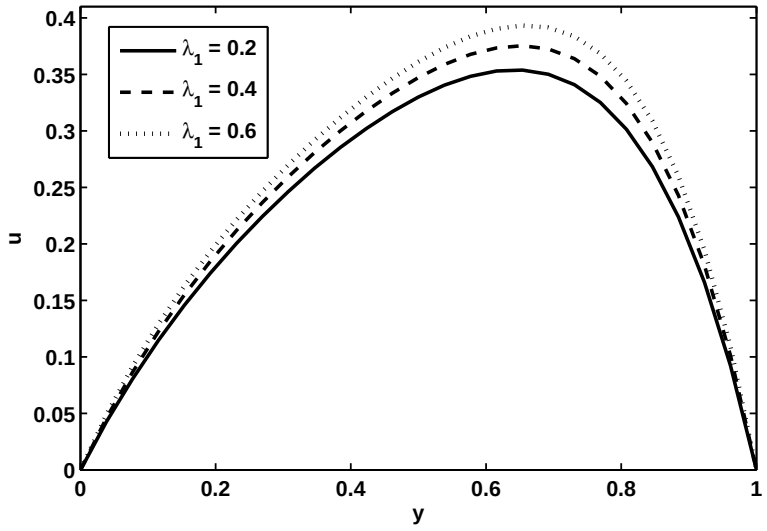

Figure 1.7: Velocity profile for $\mu(p) = Aexp(ap)$ and $\alpha(p) = B(\frac{p}{p_0})^m$ with $\Gamma_1 = 1, \Gamma_2 = 10, \Gamma_3 = 10, \Gamma_4 = 1$ and $m = 2$ in Poiseuille flow.

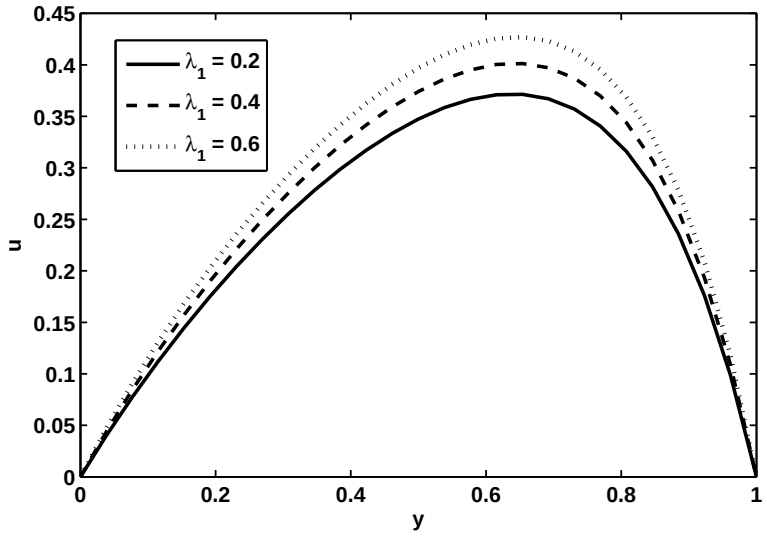

Figure 1.8: Velocity profile for $\mu(p) = A(\frac{p}{p_0})^n$ and $\alpha(p) = Bexp(bp)$ with $\Gamma_1 = 1, \Gamma_2 = 10, \Gamma_3 = 10, \Gamma_4 = 1$ and $n = 2$ in Poiseuille flow.

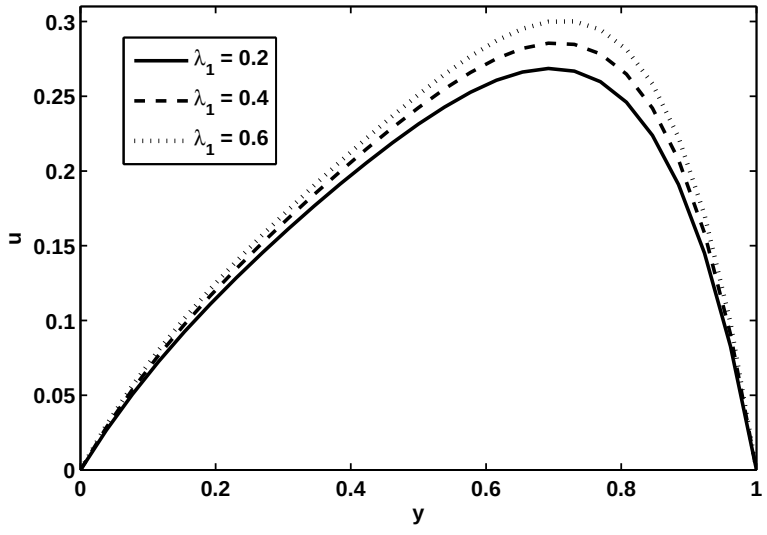

Figure 1.9: Velocity profile for $\mu(p) = A(\frac{p}{p_0})^n$ and $\alpha(p) = B(\frac{p}{p_0})^m$ with $\Gamma_1 = 1, \Gamma_2 = 10, \Gamma_3 = 10, m = 1$ and $n = 2$ in Poiseuille flow.

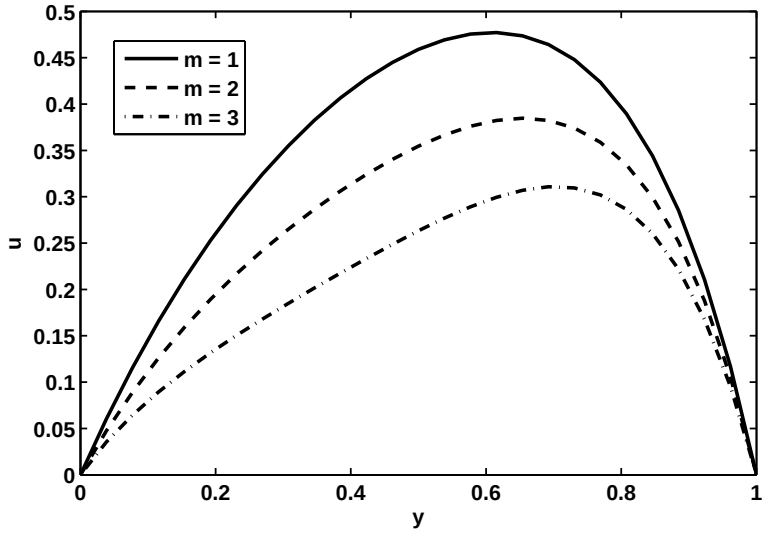

Figure 1.10: Velocity profile for $\mu(p) = Aexp(ap)$ and $\alpha(p) = B(\frac{p}{p_0})^m$ with $\Gamma_1 = 1, \Gamma_2 = 10, \Gamma_3 = 10, \Gamma_4 = 1$ and $\lambda_1 = 0.5$ in Poiseuille flow.

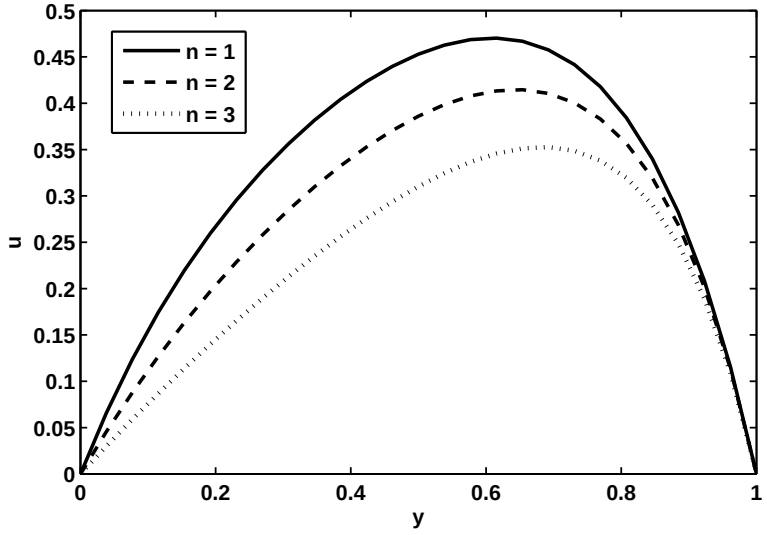

Figure 1.11: Velocity profile for $\mu(p) = A(\frac{p}{p_0})^n$ and $\alpha(p) = Bexp(bp)$ with $\Gamma_1 = 1, \Gamma_2 = 10, \Gamma_3 = 10, \Gamma_4 = 1$ and $\lambda_1 = 0.5$ in Poiseuille flow.

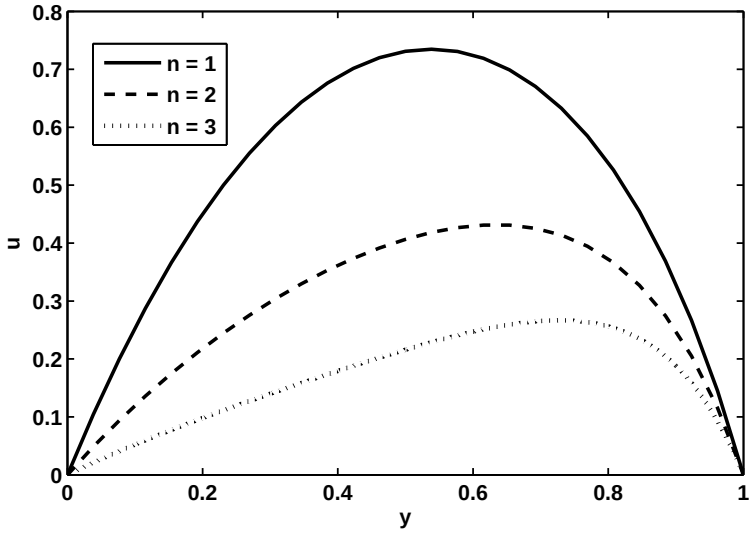

Figure 1.12: Velocity profile for $\mu(p) = A(\frac{p}{p_0})^n$ and $\alpha(p) = B(\frac{p}{p_0})^m$ with $\Gamma_1 = 1, \Gamma_2 = 10, \Gamma_3 = 10, m = 3$ and $\lambda_1 = 0.5$ in Poiseuille flow.

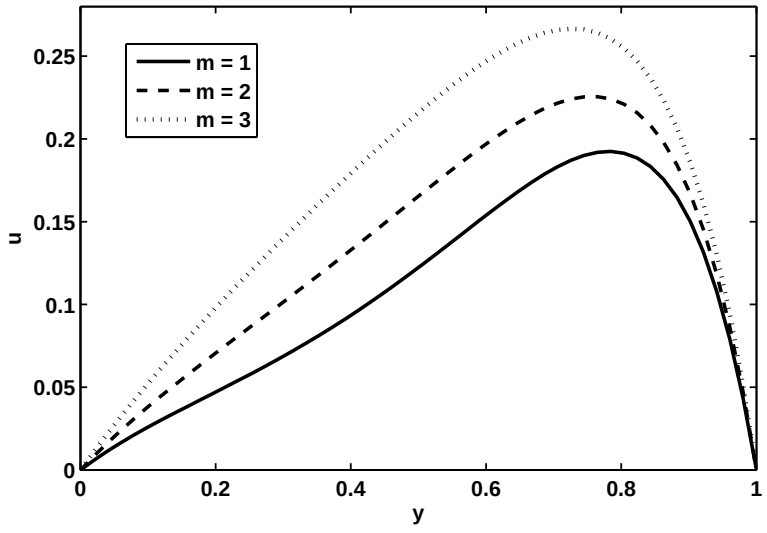

Figure 1.13: Velocity profile for $\mu(p) = A(\frac{p}{p_0})^n$ and $\alpha(p) = B(\frac{p}{p_0})^m$ with $\Gamma_1 = 1, \Gamma_2 = 10, \Gamma_3 = 10, n = 3$ and $\lambda_1 = 0.5$ in Poiseuille flow.

y	u(y)			
	Case I	**Case II**	**Case III**	**Case IV**
0	0	0	0	0
0.090909091	0.023352527	0.068821553	0.039275318	0.055417077
0.181818182	0.043445438	0.131777763	0.075720014	0.109650577
0.272727273	0.065693775	0.192166840	0.112785885	0.163701973
0.363636364	0.093844187	0.252691770	0.153423713	0.218855735
0.454545455	0.131387137	0.315673610	0.200561167	0.276796662
0.545454545	0.182157761	0.383263553	0.257516282	0.339786894
0.636363636	0.250597894	0.457701385	0.328444137	0.410939234
0.727272727	0.341844000	0.541687169	0.418916972	0.494650273
0.818181818	0.461700676	0.638966222	0.536774409	0.597307142
0.909090909	0.616524988	0.755286620	0.693466745	0.728479729
1.000000000	0.900000000	0.900000000	0.900000000	0.900000000

Table 1.2: Velocity for $\Gamma_1 = 1, \Gamma_2 = 10, \Gamma_3 = 5, \Gamma_4 = 2, m = 2, n = 2, \lambda_1 = 0.1, U_0 = 0.9$ for Couette flow

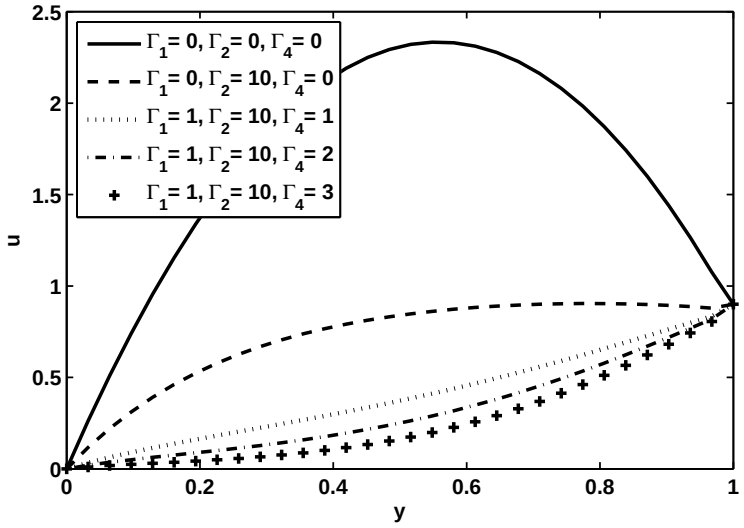

Figure 1.14: Velocity profile for $\mu(p) = Aexp(ap)$ and $\alpha(p) = Bexp(bp)$ with $\Gamma_3 = 10, U_0 = 0.9$ and $\lambda_1 = 0.5$ in Couette flow.

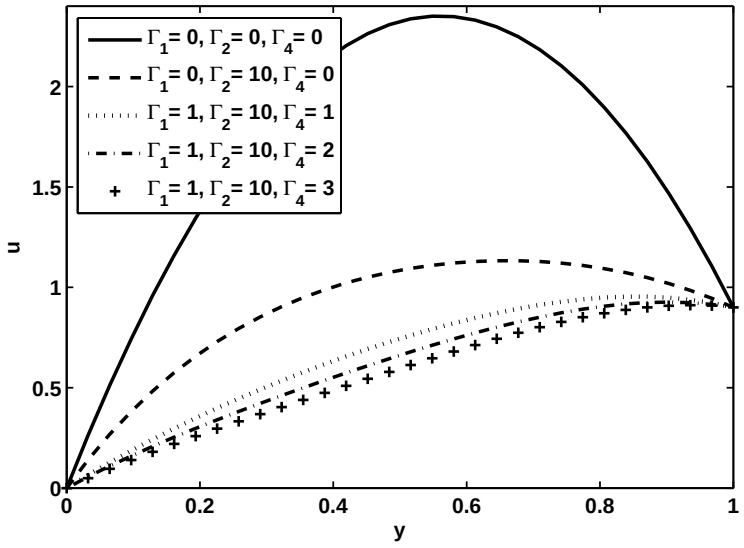

Figure 1.15: Velocity profile for $\mu(p) = Aexp(ap)$ and $\alpha(p) = B(\frac{p}{p_0})^m$ with $\Gamma_3 = 10, U_0 = 0.9, \lambda_1 = 0.5$ and $m = 2$ in Couette flow.

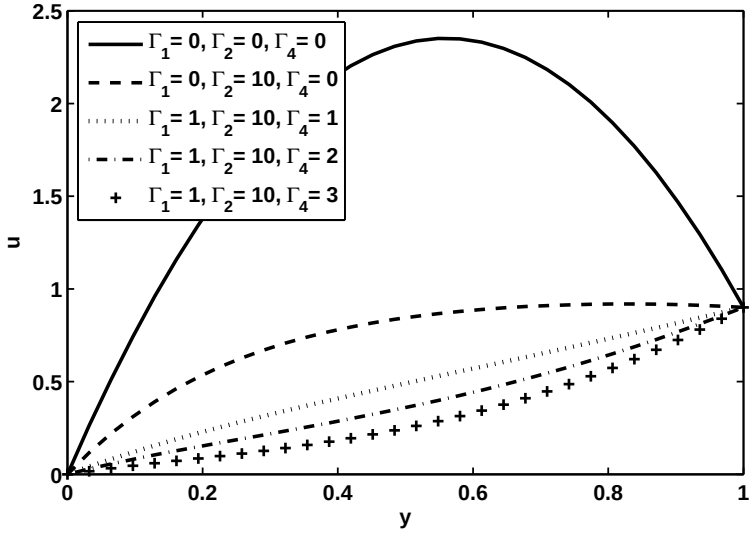

Figure 1.16: Velocity profile for $\mu(p) = A(\frac{p}{p_0})^n$ and $\alpha(p) = Bexp(bp)$ with $\Gamma_3 = 10, U_0 = 0.9, \lambda_1 = 0.5$ and $n = 2$ in Couette flow.

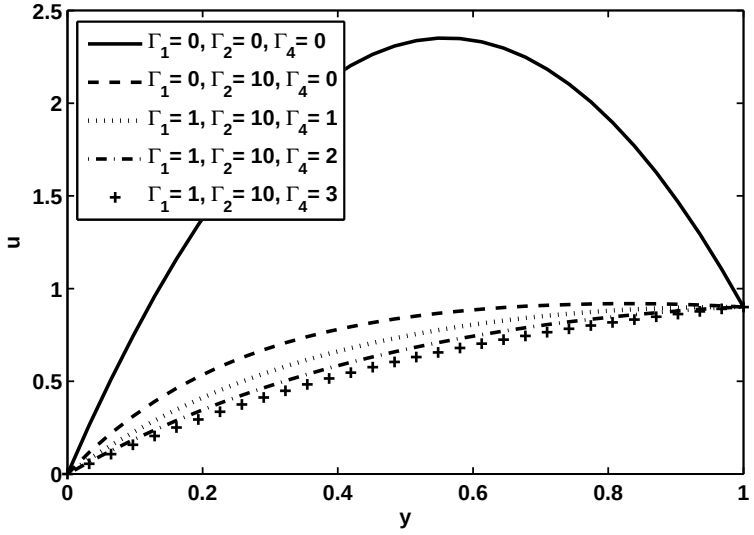

Figure 1.17: Velocity profile for $\mu(p) = A(\frac{p}{p_0})^n$ and $\alpha(p) = B(\frac{p}{p_0})^m$ with $\Gamma_3 = 10, U_0 = 0.9, \lambda_1 = 0.5, n = 1$ and $m = 2$ in Couette flow.

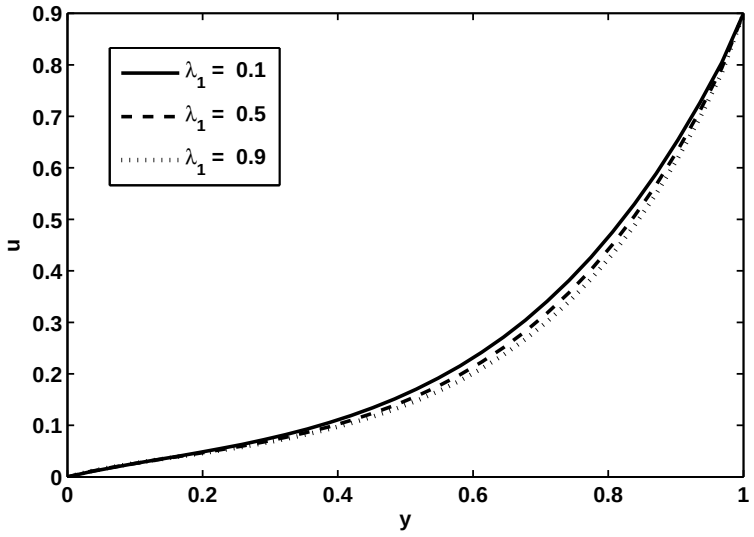

Figure 1.18: Velocity profile for $\mu(p) = Aexp(ap)$ and $\alpha(p) = Bexp(bp)$ with $\Gamma_1 = 1, \Gamma_2 = 10, \Gamma_3 = 5, \Gamma_4 = 1$ and $U_0 = 0.9$ in Couette flow.

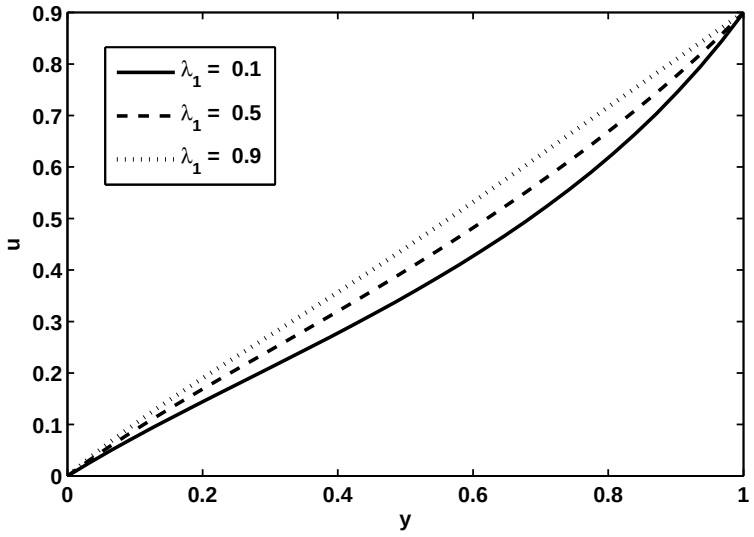

Figure 1.19: Velocity profile for $\mu(p) = Aexp(ap)$ and $\alpha(p) = B(\frac{p}{p_0})^m$ with $\Gamma_1 = 1, \Gamma_2 = 10, \Gamma_3 = 5, \Gamma_4 = 2, U_0 = 0.9$ and $m = 2$ in Couette flow.

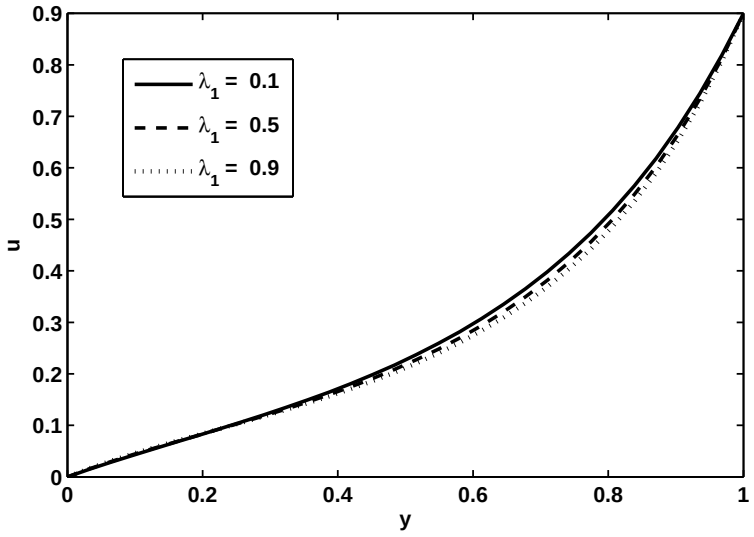

Figure 1.20: Velocity profile for $\mu(p) = A(\frac{p}{p_0})^n$ and $\alpha(p) = Bexp(bp)$ with $\Gamma_1 = 1, \Gamma_2 = 10, \Gamma_3 = 5, \Gamma_4 = 2, U_0 = 0.9$ and $n = 2$ in Couette flow.

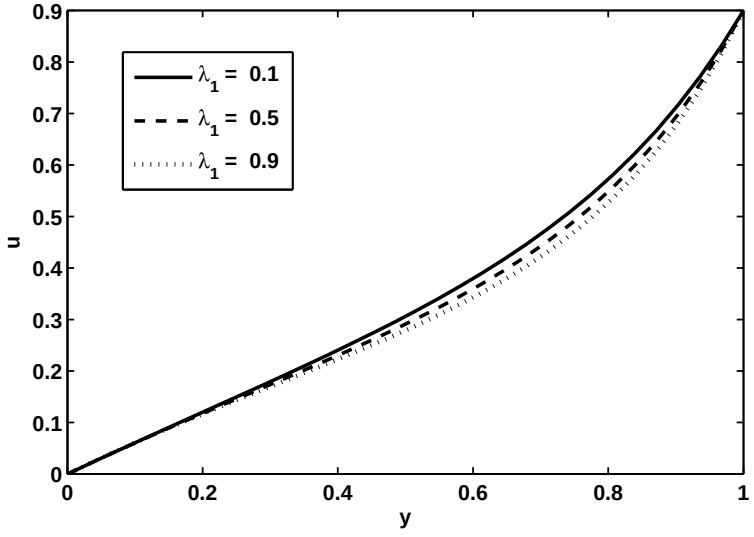

Figure 1.21: Velocity profile for $\mu(p) = A(\frac{p}{p_0})^n$ and $\alpha(p) = B(\frac{p}{p_0})^m$ with $\Gamma_1 = 1, \Gamma_2 = 7, \Gamma_3 = 1, U_0 = 0.9, m = 3$ and $n = 1$ in Couette flow.

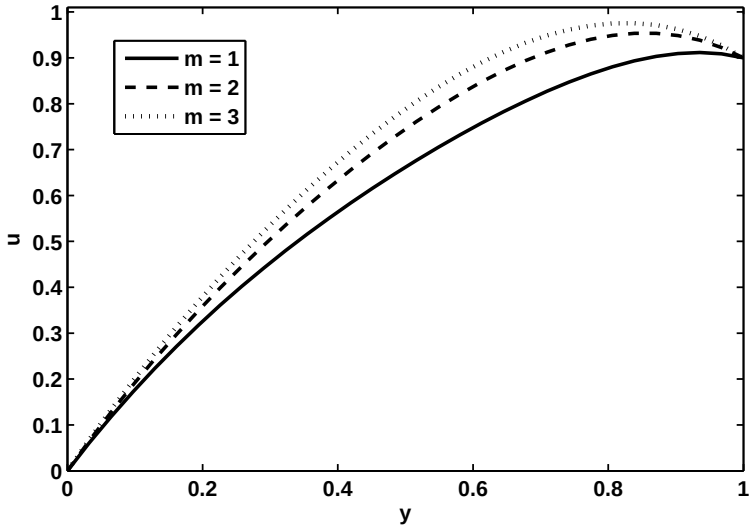

Figure 1.22: Velocity profile for $\mu(p) = Aexp(ap)$ and $\alpha(p) = B(\frac{p}{p_0})^m$ with $\Gamma_1 = 1, \Gamma_2 = 10, \Gamma_3 = 10, \Gamma_4 = 1, U_0 = 0.9$ and $\lambda_1 = 0.5$ in Couette flow.

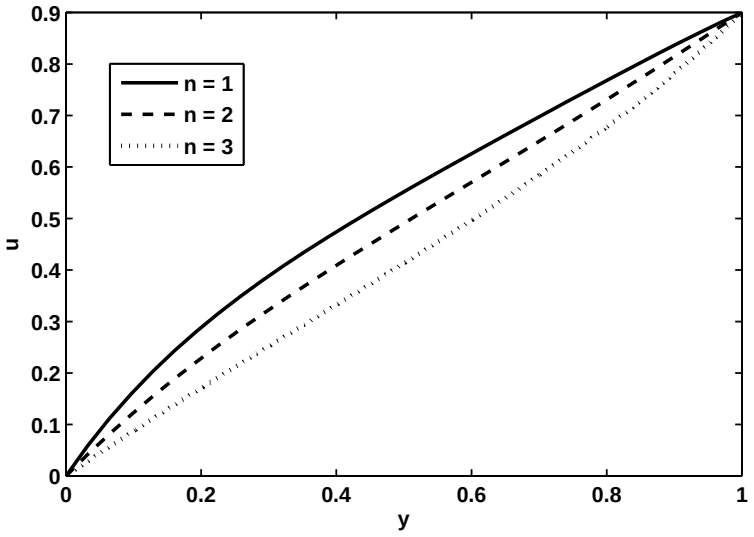

Figure 1.23: Velocity profile for $\mu(p) = A(\frac{p}{p_0})^n$ and $\alpha(p) = Bexp(bp)$ with $\Gamma_1 = 1, \Gamma_2 = 10, \Gamma_3 = 10, \Gamma_4 = 1, U_0 = 0.9$ and $\lambda_1 = 0.5$ in Couette flow.

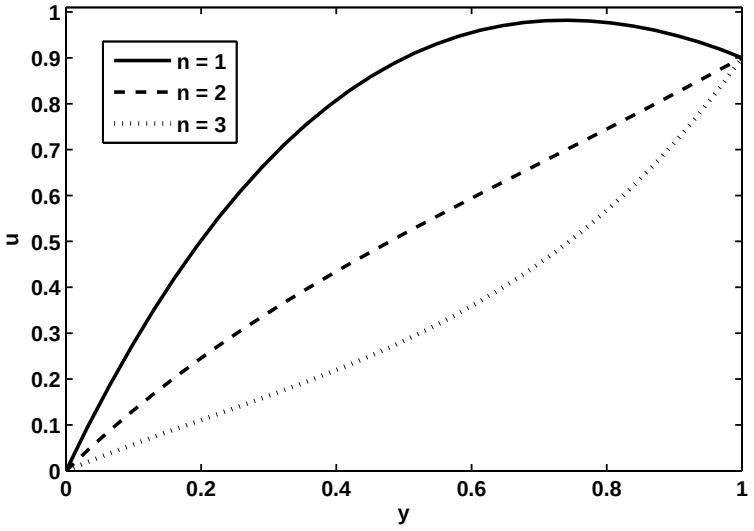

Figure 1.24: Velocity profile for $\mu(p) = A(\frac{p}{p_0})^n$ and $\alpha(p) = B(\frac{p}{p_0})^m$ with $\Gamma_1 = 1, \Gamma_2 = 10, \Gamma_3 = 10, U_0 = 0.9, m = 3$ and $\lambda_1 = 0.5$ in Couette flow.

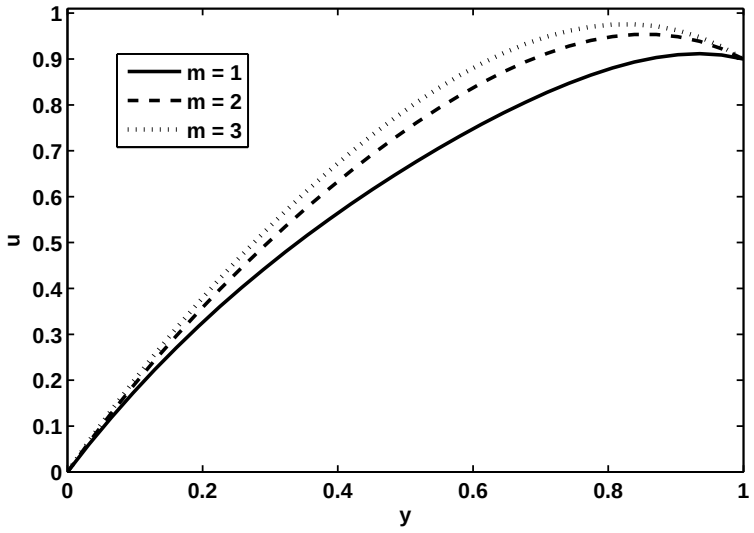

Figure 1.25: Velocity profile for $\mu(p) = A(\frac{p}{p_0})^n$ and $\alpha(p) = B(\frac{p}{p_0})^m$ with $\Gamma_1 = 1, \Gamma_2 = 10, \Gamma_3 = 10, U_0 = 0.9, n = 3$ and $\lambda_1 = 0.5$ in Couette flow.

Chapter 2

Numerical Solutions of Williamson fluid with pressure dependent viscosity

2.1 Introduction

In the present chapter, we have examined the flow of Williamson fluid in an inclined channel with pressure dependent viscosity. The governing equation of motion for Williamson fluid model under the effects of pressure dependent viscosity and pressure dependent porosity are modelled and solved for two types of geometries i.e., (i) Poiseuille flow and (ii) Couette flow. Four different cases for pressure dependent viscosity and pressure dependent porosity are examined. The numerical analysis of governing problems are carried out by using Shooting method with Runge Kutta Fehlberg technique. The physical features of pertinent parameters are discussed through tables and graphs.

2.2 Fluid model

An incompressible unidirectional flow of a Williamson fluid with pressure dependent viscosity through porous medium in an inclined channel is considered. The equation of momentum under these assumptions is

$$\rho\frac{d\mathbf{V}}{dt} = div\mathbf{T} + \rho b_e - \alpha(p)\boldsymbol{\tau}\mathbf{V}. \tag{2.1}$$

The extra stress tensor $\boldsymbol{\tau}$ for Williamson fluid [48–49] is given by

$$\boldsymbol{\tau} = [\mu_\infty + (\mu_0 - \mu_\infty)(1 - \Gamma|\dot{\gamma}|)^{-1}]\dot{\gamma}, \tag{2.2}$$

in which μ_∞ is the infinite shear rate viscosity, μ_0 is the zero shear rate viscosity, Γ is the time constant and $\dot{\gamma}$ is defined as

$$\dot{\gamma} = \sqrt{\frac{1}{2}\sum_i\sum_j \dot{\gamma}_{ij}\dot{\gamma}_{ji}} = \sqrt{\frac{1}{2}\prod} \tag{2.3}$$

where

$$\prod = \frac{1}{2}tr(\nabla\mathbf{V} + (\nabla\mathbf{V})^\dagger)^2. \tag{2.4}$$

Here $\prod$ is the second invariant strain tensor. We consider the constitutive Eq. (2.2), the case for which $\mu_\infty = 0, \mu_0 = \mu$ and $\Gamma\dot{\gamma} < 1$. The component of extra stress tensor therefore, can be written as

$$\boldsymbol{\tau} = \mu(p)[(1 - \Gamma\dot{\gamma})^{-1}]\dot{\gamma}_{ij} = \mu(p)[1 + \Gamma\dot{\gamma})\dot{\gamma}_{ij}. \tag{2.5}$$

2.3 Mathematical formulation

With the help of Eqs. (1.6) and (2.5), the component form of Eq. (2.1) in the presence of gravity and porous medium take the following form

$$-\frac{\partial p}{\partial x} + \mu(p)(1 + 2\Gamma\frac{du}{dy})\frac{d^2u}{dy^2} + \frac{d\mu(p)}{dy}(1 + \Gamma\frac{du}{dy})\frac{du}{dy} - \alpha(p)(1 + \Gamma\frac{du}{dy})u(y) + \rho g\sin\theta = 0, \tag{2.6}$$

and

$$-\frac{\partial p}{\partial y} - \rho g \cos\theta = 0. \tag{2.7}$$

Using the following dimensionless quantity

$$We = \frac{\Gamma U_c}{h}, \tag{2.8}$$

where We is the Weissenberg number. With the help of Eq.(2.8), Eqs.(2.6) and (2.7) can be written as

$$(1 + 2We\frac{du}{dy})\frac{d^2u}{dy^2} + \frac{1}{\mu(p)}\frac{d\mu(p)}{dy}(1 + We\frac{du}{dy})\frac{du}{dy} - h^2\frac{\alpha(p)}{\mu(p)}(1 + We\frac{du}{dy})u(y) + \frac{\rho g h^2 \sin\theta}{U_c\mu(p)} = 0, \tag{2.9}$$

and

$$\frac{dp}{dy} + \rho g h \cos\theta = 0. \tag{2.10}$$

The solution of Eq.(2.10) is

$$p = p_0 + \rho g h \cos\theta(1 - y). \tag{2.11}$$

where p_0 is the pressure at $y = h$.

With the help of Eq. (2.11), the solution of Eq. (2.9) has been computed in the next section for two types of boundary conditions known as

(i) Poiseuille flow

(ii) Couette flow

2.4 Poiseuille flow

In the Poiseuille flow the rigid plates at $y = 0$ and $y = h$ are stationary which yields boundary conditions Eq. (1.13)

$$u(0) = 0, \qquad u(h) = 0. \tag{2.12}$$

By using Eqs.(1.14) to (1.17), Eq. (2.9) take the following forms respectively

$$(1+2We\frac{du}{dy})\frac{d^2u}{dy^2}-\Gamma_1(1+We\frac{du}{dy})\frac{du}{dy}-\Gamma_2(1+We\frac{du}{dy})exp[\Gamma_4(1-y)]u(y) + \Gamma_3 exp[-\Gamma_1(1-y)]=0, \quad (2.13)$$

$$(1+2We\frac{du}{dy})\frac{d^2u}{dy^2}-\Gamma_1(1+We\frac{du}{dy})\frac{du}{dy}-\Gamma_2(1+We\frac{du}{dy})[1+\Gamma_4(1-y)]^m exp[-\Gamma_1(1-y)]u(y)+\Gamma_3 exp[-\Gamma_1(1-y)]=0, \quad (2.14)$$

$$(1+2We\frac{du}{dy})\frac{d^2u}{dy^2}-\frac{n\Gamma_1}{1+\Gamma_1(1-y)}(1+We\frac{du}{dy})\frac{du}{dy}-\Gamma_2(1+We\frac{du}{dy})[1+\Gamma_1(1-y)]^{-n} exp[\Gamma_4(1-y)]u(y)+\Gamma_3[1+\Gamma_1(1-y)]^{-n}=0, \quad (2.15)$$

$$(1+2We\frac{du}{dy})\frac{d^2u}{dy^2}-\frac{n\Gamma_1}{1+\Gamma_1(1-y)}(1+We\frac{du}{dy})\frac{du}{dy}-\Gamma_2(1+We\frac{du}{dy})[1+\Gamma_1(1-y)]^{m-n}u(y) + \Gamma_3[1+\Gamma_1(1-y)]^{-n}=0, \quad (2.16)$$

and the corresponding non dimensional boundary conditions are defined in Eq.(1.26).

2.5 Couette flow

In this case, the lower plate is at rest and the upper plate is moving with the velocity U_h. The boundary conditions for the problem in non dimensional form is defined in Eq.(1.27) The governing equations are same as defined in previous section (Eqs.(2.13) to (2.16)).

2.6 Solution of the problem

2.6.1 Shooting method

Shooting method is a numerical technique to get approximate solution of linear or non linear boundary value problems. Main theme of the Shooting method is to reduce boundary value problem into a system of initial value problems and choosing one boundary condition as an initial condition and second boundary condition to be the final destiny needs to be computed. There are various numerical methods available to solve initial value problems. The sub method Runge Kutta Felhberg has been used for the present case because it acquires less iterative steps and achieves better accuracy as compared to available methods in literature. Thus, the system of initial value problems by introducing a fictitious slope s can be written as

$$\frac{du}{dy} = U_2 \qquad U_1(0) = 0, \tag{2.17}$$

$$\frac{dU_2}{dy} = f(y, U_1, U_2) \qquad U_2(0) = s, \tag{2.18}$$

where $U_1 = u(y)$ and $U_2 = \frac{dU}{dy}$. We approximate the solution to boundary value problem by considering sequence of initial value problems involving a parameter s_k such that

$$\lim_{k\to\infty} u(1, s_k) = u(1) = U_0. \tag{2.19}$$

The sequence $\{s_k\}$ is generated by using Newton's Raphson method

$$s_k = s_{k-1} - \frac{U_1(s_{k-1})}{U_2(s_{k-1})}. \tag{2.20}$$

Finally, solution for both the cases can be calculated by Shooting method in conjunction with Runge Kutta Fehlberg method. Following the above procedure, Eqs. (2.13) to (2.16) can be reduced as

Case I

$$f(y,U_1,U_2)=\frac{\Gamma_1(1+WeU_2)U_2+\Gamma_2(1+WeU_2)exp[\Gamma_4(1-y)]U_1-\Gamma_3exp[-\Gamma_1(1-y)]}{1+2WeU_2}, \tag{2.21}$$

$$\frac{\partial f}{\partial U_1}=\frac{\Gamma_2(1+WeU_2)}{1+2WeU_2}exp[\Gamma_4(1-y)], \tag{2.22}$$

$$\frac{\partial f}{\partial U_2}=\frac{1}{(1+2WeU_2)^2}\big[(1+2WeU_2)(\Gamma_1(1+2WeU_2)+\Gamma_2exp[\Gamma_4(1-y)]WeU_1)$$
$$-2We((1+WeU_2)(\Gamma_1U_2+\Gamma_2exp[\Gamma_4(1-y)]U_1)-\Gamma_3exp[-\Gamma_1(1-y)])\big]. \tag{2.23}$$

Case II

$$f(y,U_1,U_2)=\frac{(1+WeU_2)\big(\Gamma_1U_2+\Gamma_2[1+\Gamma_4(1-y)]^mexp[-\Gamma_1(1-y)]U_1\big)-\Gamma_3exp[-\Gamma_1(1-y)]}{(1+2WeU_2)}, \tag{2.24}$$

$$\frac{\partial f}{\partial U_1}=\frac{\Gamma_2(1+WeU_2)}{1+2WeU_2}exp[-\Gamma_1(1-y)][1+\Gamma_4(1-y)]^m, \tag{2.25}$$

$$\frac{\partial f}{\partial U_2}=\frac{1}{(1+2WeU_2)^2}\big[(1+2WeU_2)(\Gamma_1(1+2WeU_2)+\Gamma_2exp[-\Gamma_1(1-y)][1+\Gamma_4(1-y)]^mWeU_1)$$
$$-2We((1+WeU_2)(\Gamma_1U_2+\Gamma_2exp[-\Gamma_1(1-y)][1+\Gamma_4(1-y)]^mU_1)-\Gamma_3exp[-\Gamma_1(1-y)])\big]. \tag{2.26}$$

Case III

$$f(y,U_1,U_2)=\frac{(1+WeU_2)\left(\frac{n\Gamma_1U_2}{1+\Gamma_1(1-y)}+\frac{\Gamma_2U_1exp[\Gamma_4(1-y)]}{(1+\Gamma_1(1-y))^n}\right)-\frac{\Gamma_3}{(1+\Gamma_1(1-y))^n}}{1+2WeU_2}, \tag{2.27}$$

$$\frac{\partial f}{\partial U_1}=\frac{\Gamma_2(1+WeU_2)}{(1+2WeU_2)(1+\Gamma_1(1-y))^n}exp[\Gamma_4(1-y)], \tag{2.28}$$

$$\frac{\partial f}{\partial U_2}=\frac{1}{(1+2WeU_2)^2}\left[(1+2WeU_2)\big(\frac{n\Gamma_1(1+2WeU_2)}{1+\Gamma_1(1-y)}+\frac{\Gamma_2exp[\Gamma_4(1-y)]WeU_1}{(1+\Gamma_1(1-y))^n}\big)\right.$$
$$\left.-2We\left((1+WeU_2)\big(\frac{n\Gamma_1}{(1+\Gamma_1(1-y))^n}U_2+\frac{\Gamma_2exp[\Gamma_4(1-y)]}{(1+\Gamma_1(1-y))^n}U_1\big)-\frac{\Gamma_3}{(1+\Gamma_1(1-y))^n}\right)\right]. \tag{2.29}$$

Case IV

$$f(y,U_1,U_2)=\frac{(1+WeU_2)\big(\frac{n\Gamma_1U_2}{1+\Gamma_1(1-y)}+\Gamma_2U_1(1+\Gamma_1(1-y))^{m-n}\big)-\frac{\Gamma_3}{(1+\Gamma_1(1-y))^n}}{1+2WeU_2}, \quad (2.30)$$

$$\frac{\partial f}{\partial U_1}=\frac{\Gamma_2(1+WeU_2)}{(1+2WeU_2)}(1+\Gamma_1(1-y))^{m-n}, \quad (2.31)$$

$$\frac{\partial f}{\partial U_2}=\frac{1}{(1+2WeU_2)^2}\Bigg[(1+2WeU_2)\big(\frac{n\Gamma_1(1+2WeU_2)}{1+\Gamma_1(1-y)}+\Gamma_2WeU_1(1+\Gamma_1(1-y))^{m-n}\big)$$
$$-2We\bigg((1+WeU_2)\big(\frac{n\Gamma_1U_2}{(1+\Gamma_1(1-y))^n}+\Gamma_2(1+\Gamma_1(1-y))^{m-n}U_1\big)-\frac{\Gamma_3}{(1+\Gamma_1(1-y))^n}\bigg)\Bigg]. \quad (2.32)$$

The results have been analyzed through tables and graphs in the proceeding section.

2.6.2 Numerical results and discussion

Numerical solutions for the governing equation of motion for Williamson fluid for four different cases of pressure dependent viscosity and porosity are evaluated by shooting method with Runge-Kutta Fehlberg technique. The numerical analysis is carried out for Poiseuille flow and Couette flow. Table 2.1 features the results for Poiseuille flow. Numerical results are listed for all the four cases. The comparison of four cases demonstrates that the combination of exponential form of viscosity and polynomial form of porosity improves fluid velocity and this combination is the most suitable one. It is found that for each case the velocity is maximum at the centre due to pressure gradient. This phenomena occurs because we are considering the Poiseuille flow in which the channel walls are at rest like a canal flow and flow occur due to the constant motion of pressure gradient. The velocity field for different values of $\Gamma's$ and for various values of power m and n are displayed in figures 2.1 to 2.4. It predicts that with the increase in $\Gamma's$ and the power m and n, the velocity field decreases for each case of viscosity and porosity. It is observed that velocity gives maximum values in the absence of $\Gamma's$. Thus we can say that

the variable viscosity and porosity cause a decay in the fluid velocity. This result is also indisputable with the fact that by the increase of pressure, viscosity $\mu(p)$ and porosity $\alpha(p)$ increases which causes the velocity point wise decreases. Figures 2.5 to 2.8 show the velocity field for different values of Weissenberg number We. Weissenberg number equals zero corresponds to a purely Newtonian fluid. It depicts that with an increase in We, velocity field increases for all the cases of viscosities $\mu(p)$ and porosity $\alpha(p)$.

Table 2.2 exhibits the numerical results of Couette flow for four different cases of pressure dependent viscosity and porosity. The comparison of these numerical results yields the similar conclusion as for the cases of Poiseuille flow. The overall examination of all the four cases divulges that case II is the appropriate choice to attain more fluid velocity. Figures 2.9 to 2.16 are the graphical results for Couette flow. The maximum velocity occurs in the centre of channel. The velocity profile for different values of $\Gamma's$ and the power m and n for Couette flow are shown through the figures 2.9 to 2.12. It is analyzed that velocity field decreases with an increase in the values of $\Gamma's$ and the power m and n for all the four cases of viscosity and porosity. Similar role is examined for the Poiseuille flow. Variation of Weissenberg number We for velocity profile of Couette flow is shown through Figures 2.13 to 2.16. Fluid velocity raises with a raise in the values of Weissenberg number and this behavior is quite similar to that for the Poiseuille flow.

	u(y)			
y	**Case I**	**Case II**	**Case III**	**Case IV**
0	0	0	0	0
0.10	0.054541180	0.062006688	0.033678834	0.031600971
0.20	0.100990725	0.114706620	0.066014430	0.061738948
0.30	0.140989749	0.158778166	0.096415696	0.090022209
0.40	0.174476943	0.193948547	0.123896565	0.115687707
0.50	0.199779943	0.218778319	0.146845206	0.137364549
0.60	0.213500068	0.230336409	0.162626372	0.152663985
0.70	0.210209260	0.223731321	0.166866894	0.157443291
0.80	0.181925602	0.191435995	0.152099736	0.144420481
0.90	0.117259625	0.122298335	0.104990975	0.100387898
1.00	0	0	0	0

Table 2.1: Velocity for $\Gamma_1 = 1, \Gamma_2 = 5, \Gamma_3 = 5, \Gamma_4 = 1, m = 2, n = 3, We = 0.05$ for Poiseuille flow

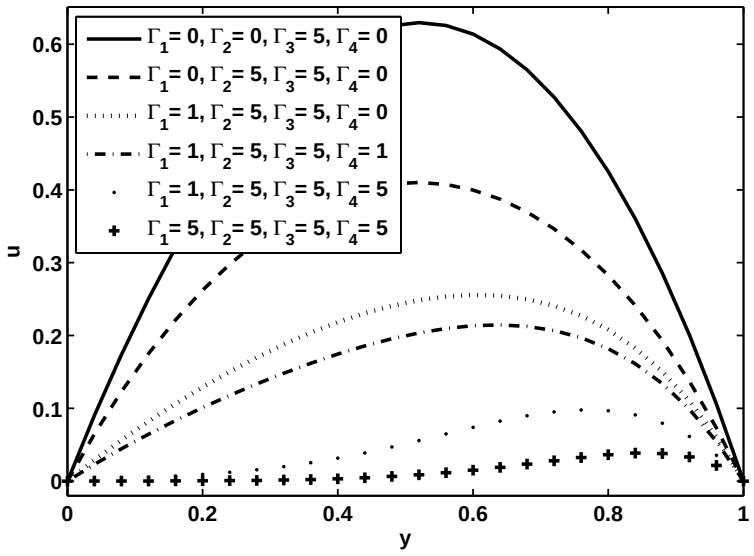

Figure 2.1: Velocity profile for $\mu(p) = Aexp(ap)$ and $\alpha(p) = Bexp(bp)$ with $We = 0.05$ in Poiseuille flow.

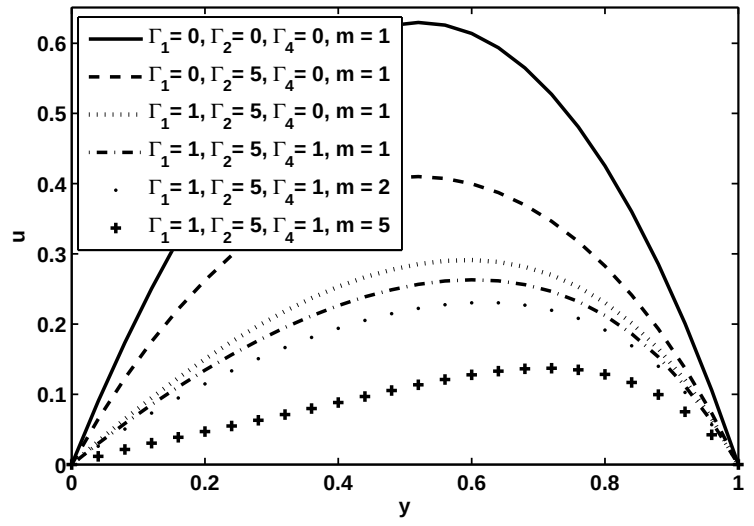

Figure 2.2: Velocity profile for $\mu(p) = Aexp(ap)$ and $\alpha(p) = B(\frac{p}{p_0})^m$ with $\Gamma_3 = 5$ and $We = 0.05$ in Poiseuille flow.

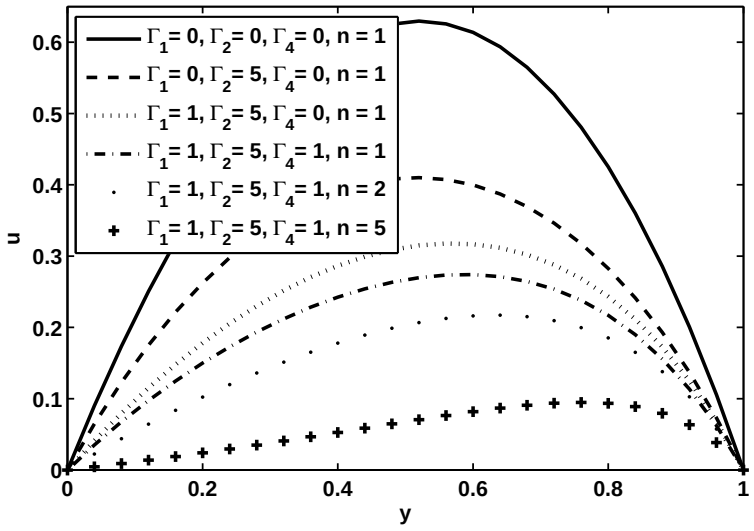

Figure 2.3: Velocity profile for $\mu(p) = A(\frac{p}{p_0})^n$ and $\alpha(p) = Bexp(bp)$ with $\Gamma_3 = 5$ and $We = 0.05$ in Poiseuille flow.

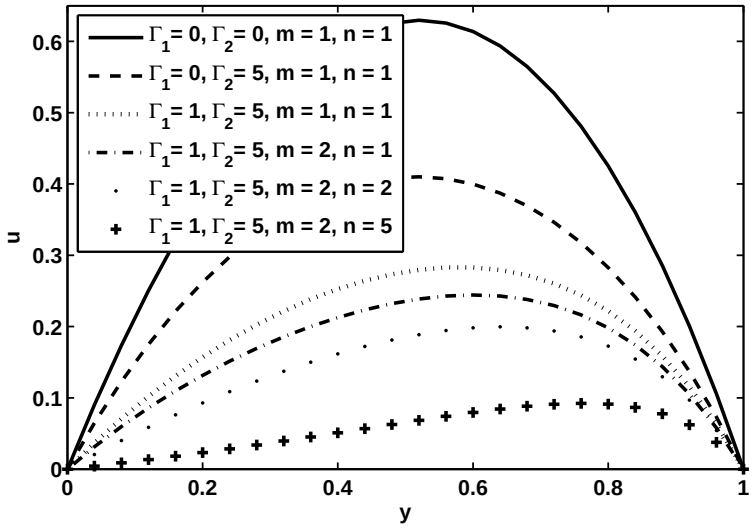

Figure 2.4: Velocity profile for $\mu(p) = A(\frac{p}{p_0})^n$ and $\alpha(p) = B(\frac{p}{p_0})^m$ with $\Gamma_3 = 5$ and $We = 0.05$ in Poiseuille flow.

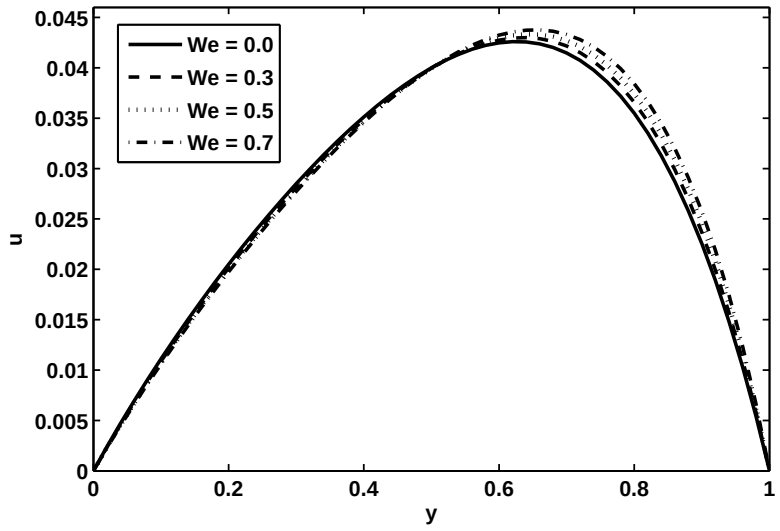

Figure 2.5: Velocity profile for $\mu(p) = Aexp(ap)$ and $\alpha(p) = Bexp(bp)$ with $\Gamma_1 = 1, \Gamma_2 = 5, \Gamma_3 = 1$ and $\Gamma_4 = 1$ in Poiseuille flow.

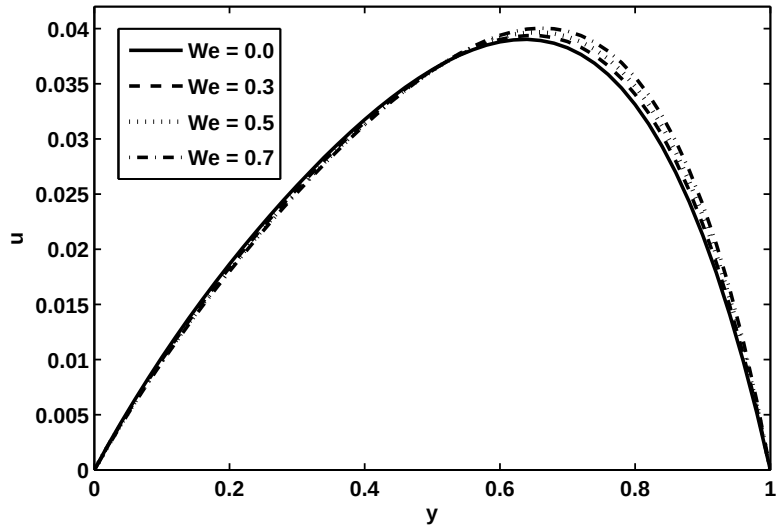

Figure 2.6: Velocity profile for $\mu(p) = Aexp(ap)$ and $\alpha(p) = B(\frac{p}{p_0})^m$ with $\Gamma_1 = 1, \Gamma_2 = 1, \Gamma_3 = 1, \Gamma_4 = 1$ and $m = 3$ in Poiseuille flow.

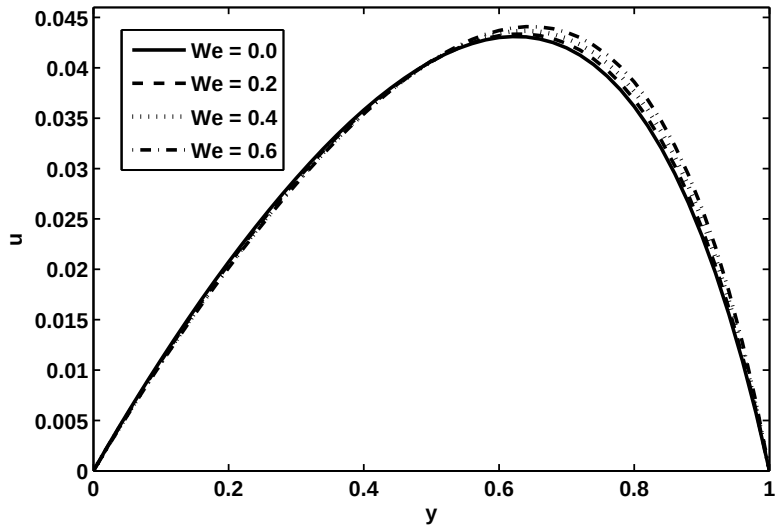

Figure 2.7: Velocity profile for $\mu(p) = A(\frac{p}{p_0})^n$ and $\alpha(p) = Bexp(bp)$ with $\Gamma_1 = 1, \Gamma_2 = 1, \Gamma_3 = 1, \Gamma_4 = 1$ and $n = 2$ in Poiseuille flow.

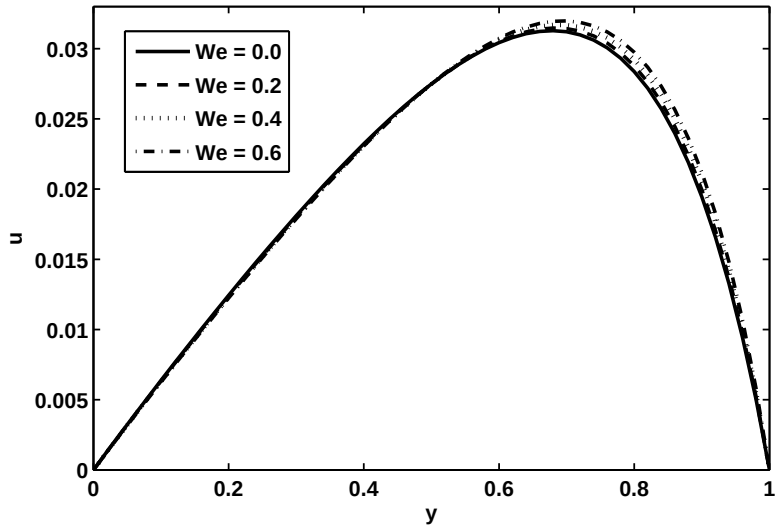

Figure 2.8: Velocity profile for $\mu(p) = A(\frac{p}{p_0})^n$ and $\alpha(p) = B(\frac{p}{p_0})^m$ with $\Gamma_1 = 1, \Gamma_2 = 10, \Gamma_3 = 10, m = 2$ and $n = 3$ in Poiseuille flow.

	u(y)			
y	**Case I**	**Case II**	**Case III**	**Case IV**
0	0	0	0	0
0.10	0.071849704	0.082903740	0.055371996	0.051104847
0.20	0.139777528	0.160491132	0.113526143	0.104640455
0.30	0.208173483	0.235775069	0.175408706	0.161859564
0.40	0.280328873	0.311519199	0.242218835	0.224354648
0.50	0.358794105	0.390277106	0.315529025	0.294199928
0.60	0.445574843	0.474397252	0.397477274	0.374166211
0.70	0.542221669	0.565980417	0.491082861	0.468050633
0.80	0.649845865	0.666773958	0.600787224	0.581196473
0.90	0.769080825	0.777985615	0.733419290	0.721336059
1.00	0.9	0.9	0.9	0.9

Table 2.2: Velocity for $\Gamma_1 = 1, \Gamma_2 = 5, \Gamma_3 = 5, \Gamma_4 = 1, m = 2, n = 3, We = 0.05$ and $U_0 = 0.9$ for Couette flow

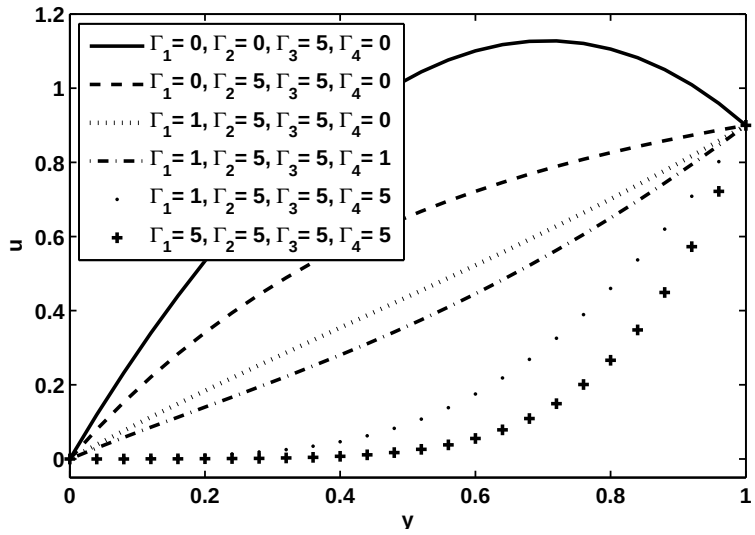

Figure 2.9: Velocity profile for $\mu(p) = Aexp(ap)$ and $\alpha(p) = Bexp(bp)$ with $W_e = 0.05$, and $U_0 = 0.9$ in Couette flow.

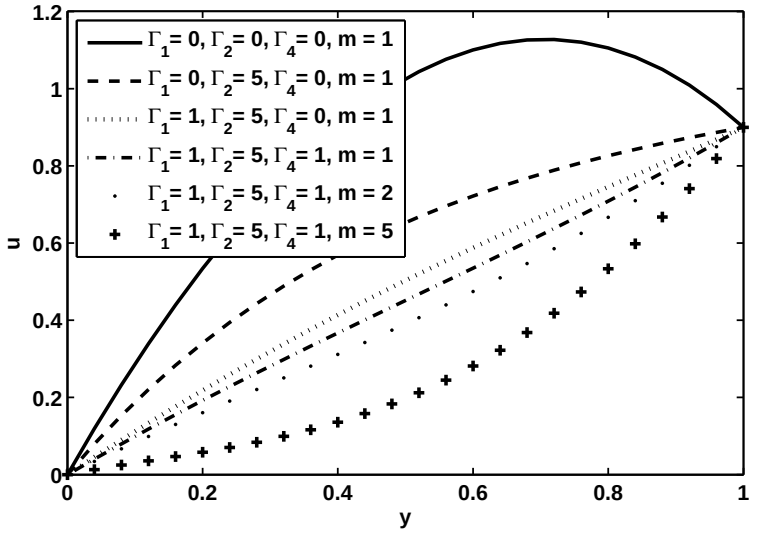

Figure 2.10: Velocity profile for $\mu(p) = Aexp(ap)$ and $\alpha(p) = B(\frac{p}{p_0})^m$ with $\Gamma_3 = 5, W_e = 0.05$ and $U_0 = 0.9$ in Couette flow.

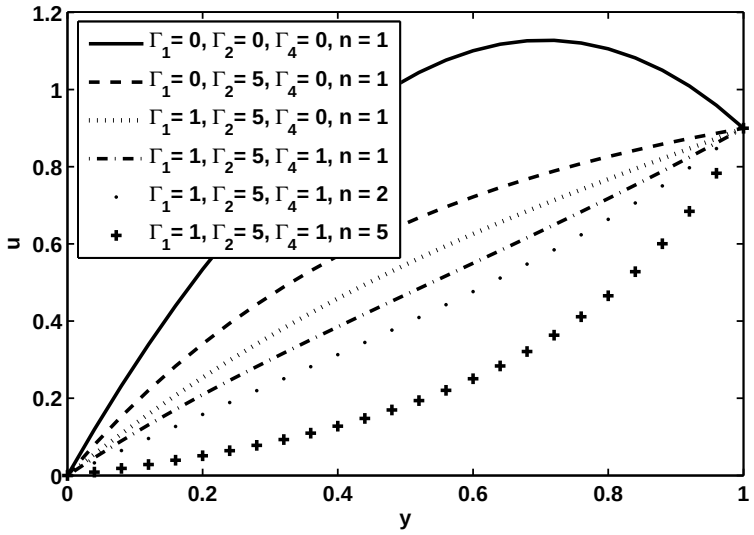

Figure 2.11: Velocity profile for $\mu(p) = A(\frac{p}{p_0})^n$ and $\alpha(p) = Bexp(bp)$ with $\Gamma_3 = 5, W_e = 0.05$ and $U_0 = 0.9$ in Couette flow.

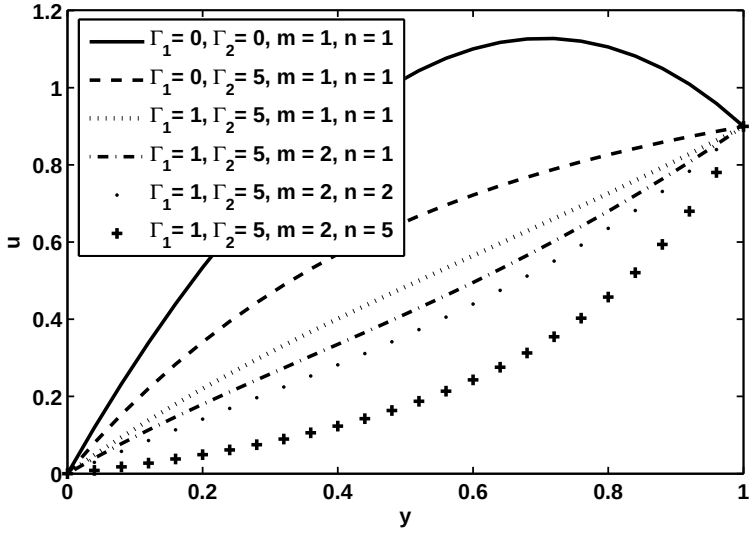

Figure 2.12: Velocity profile for $\mu(p) = A(\frac{p}{p_0})^n$ and $\alpha(p) = B(\frac{p}{p_0})^m$ with $\Gamma_3 = 5, W_e = 0.05$ and $U_0 = 0.9$ in Couette flow.

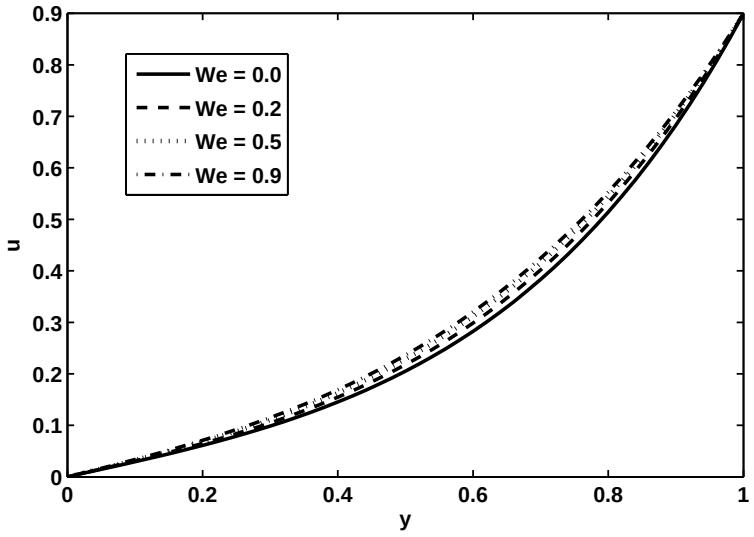

Figure 2.13: Velocity profile for $\mu(p) = Aexp(ap)$ and $\alpha(p) = Bexp(bp)$ with $\Gamma_1 = 1, \Gamma_2 = 5, \Gamma_3 = 1, \Gamma_4 = 1$ and $U_0 = 0.9$ in Couette flow.

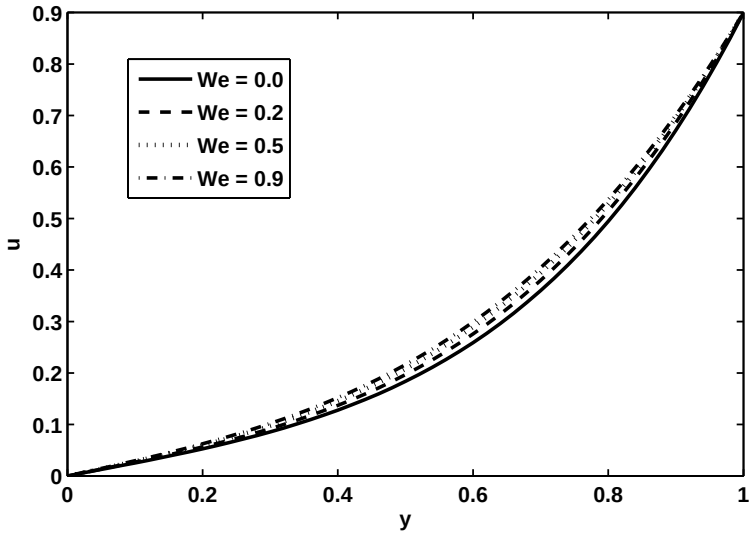

Figure 2.14: Velocity profile for $\mu(p) = Aexp(ap)$ and $\alpha(p) = B(\frac{p}{p_0})^m$ with $\Gamma_1 = 1, \Gamma_2 = 5, \Gamma_3 = 1, \Gamma_4 = 1, U_0 = 0.9$ and $m = 3$ in Couette flow.

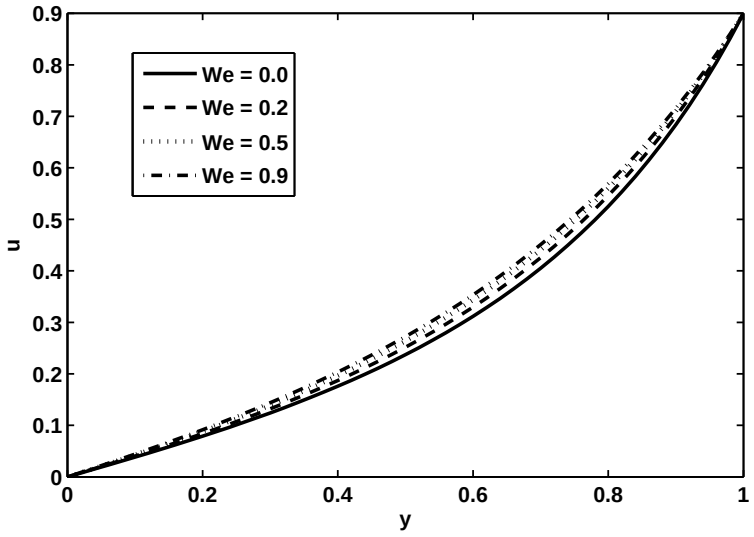

Figure 2.15: Velocity profile for $\mu(p) = A(\frac{p}{p_0})^n$ and $\alpha(p) = Bexp(bp)$ with $\Gamma_1 = 1, \Gamma_2 = 5, \Gamma_3 = 1, \Gamma_4 = 1, U_0 = 0.9$ and $n = 2$ in Couette flow.

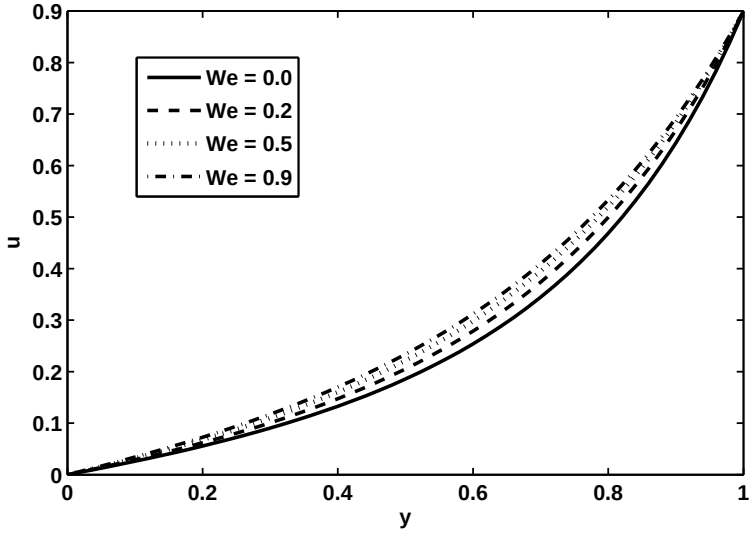

Figure 2.16: Velocity profile for $\mu(p) = A(\frac{p}{p_0})^n$ and $\alpha(p) = B(\frac{p}{p_0})^m$ with $\Gamma_1 = 1, \Gamma_2 = 5, \Gamma_3 = 1, U_0 = 0.9, m = 2$ and $n = 3$ in Couette flow.

Chapter 3

Poiseuille and Couette flows of hyperbolic tangent fluid model with pressure dependent viscosity through variable porous medium

3.1 Introduction

This chapter is devoted to the study of Poiseuille and Couette flows of hyperbolic tangent fluid with variable pressure dependent viscosities and porous medium. Both Poiseuille and Couette flows have been examined for four types of pressure dependent viscosities and porosity parameters. Numerical investigations have been done by shooting method along with Runge Kutta Fehlberg method. It is noted that this kind of Poiseuille and Couette flow for hyperbolic tangent fluid have been not discussed so for the case of constant viscosity. Graphs and tables are made to illustrate the physical features of pertinent parameters of hyperbolic tangent fluid.

3.2 Fluid model

Consider a steady unidirectional flow of a hyperbolic tangent fluid with pressure dependent viscosity in an inclined channel. The constitutive equation for incompressible hyperbolic tangent fluid is given by [50]

$$\boldsymbol{\tau} = [\mu_\infty + (\mu_0 + \mu_\infty)\tanh(\Gamma|\dot{\gamma}|)^\beta]\dot{\gamma} \tag{3.1}$$

in which β is the power law index and $\dot{\gamma}$ is defined in Eq.(2.3). We have considered the case for which $\mu_\infty = 0$ and $\Gamma\dot{\gamma} < 1$. The component of extra stress tensor therefore, can be written as

$$\boldsymbol{\tau} = -\mu_0[(\Gamma\dot{\gamma})^\beta]\dot{\gamma} = \mu_0[(1 + \Gamma\dot{\gamma} - 1)^\beta]\dot{\gamma}$$

$$\boldsymbol{\tau} = \mu_0[1 + \beta(\Gamma\dot{\gamma} - 1)]\dot{\gamma} \tag{3.2}$$

here μ_0 is the viscosity which depends upon pressure. For our convenience we use $\mu(p)$ instead of $\mu_0(p)$.

3.3 Mathematical formulation

With the help of Eq. (3.2), the component form of equation of motion for hyperbolic tangent fluid model with pressure dependent viscosity take the following form

$$\mu(p)(1 - \beta + 2\beta\Gamma\frac{du}{dy})\frac{d^2u}{dy^2} + \frac{d\mu(p)}{dy}(1 - \beta + \beta\Gamma\frac{du}{dy})\frac{du}{dy} - \alpha(p)(1 - \beta + \beta\Gamma\frac{du}{dy})u(y) + \rho g\sin\theta = 0, \tag{3.3}$$

and

$$-\frac{\partial p}{\partial y} - \rho g\cos\theta = 0. \tag{3.4}$$

Making use of Eqs.(1.9) and (2.8), Eqs.(3.3) and (3.4) after dropping the bars can be written as

$$(1-\beta+2\beta We\frac{du}{dy})\frac{d^2u}{dy^2}+\frac{1}{\mu(p)}\frac{d\mu(p)}{dy}(1-\beta+\beta We\frac{du}{dy})\frac{du}{dy}-h^2\frac{\alpha(p)}{\mu(p)}$$
$$(1-\beta+\beta We\frac{du}{dy})u(y)+\frac{\rho gh^2\sin\theta}{U_c\mu(p)}=0, \quad (3.5)$$

and

$$\frac{dp}{dy}+\rho gh\cos\theta=0. \quad (3.6)$$

The solution of Eq.(3.6) is

$$p=p_0+\rho gh\cos\theta(1-y). \quad (3.7)$$

where p_0 is the pressure at $y=h$.

With the help of Eq. (1.12), the solution of Eq. (3.5) has been computed in the next section for two types of boundary conditions known as

(i) Poiseuille flow

(ii) Couette flow

3.4 Poiseuille flow

In this case we assumed that the rigid plates at $y=0$ and $y=h$ are at rest. Therefore,

$$u(0)=0, \qquad u(h)=0. \quad (3.8)$$

By using Eq.(1.14) to Eq. (1.17), Eq. (3.5) take the following forms

$$(1-\beta+2\beta We\frac{du}{dy})\frac{d^2u}{dy^2}-\Gamma_1(1-\beta+\beta We\frac{du}{dy})\frac{du}{dy}-\Gamma_2(1-\beta+\beta We\frac{du}{dy})$$
$$exp[\Gamma_4(1-y)]u(y)+\Gamma_3 exp[-\Gamma_1(1-y)]=0, \quad (3.9)$$

$$(1-\beta+2\beta We\frac{du}{dy})\frac{d^2u}{dy^2}-\Gamma_1(1-\beta+\beta We\frac{du}{dy})\frac{du}{dy}-\Gamma_2(1-\beta+\beta We\frac{du}{dy})[1+\Gamma_4(1-y)]^m$$
$$exp[-\Gamma_1(1-y)]u(y)+\Gamma_3 exp[-\Gamma_1(1-y)]=0, \quad (3.10)$$

$$(1-\beta+2\beta We\frac{du}{dy})\frac{d^2u}{dy^2}-\frac{n\Gamma_1}{1+\Gamma_1(1-y)}(1-\beta+\beta We\frac{du}{dy})\frac{du}{dy}-\Gamma_2(1-\beta+\beta We\frac{du}{dy})$$
$$[1+\Gamma_1(1-y)]^{-n}exp[\Gamma_4(1-y)]u(y)+\Gamma_3[1+\Gamma_1(1-y)]^{-n}=0, \quad (3.11)$$

$$(1-\beta+2\beta We\frac{du}{dy})\frac{d^2u}{dy^2}-\frac{n\Gamma_1}{1+\Gamma_1(1-y)}(1-\beta+\beta We\frac{du}{dy})\frac{du}{dy}-\Gamma_2(1-\beta+\beta We\frac{du}{dy})$$
$$[1+\Gamma_1(1-y)]^{m-n}u(y)+\frac{\Gamma_3}{[1+\Gamma_1(1-y)]^n}=0. \quad (3.12)$$

For the Poiseuille flow, the corresponding boundary conditions in non dimensional form are defined in Eq.(1.26)

$$u(0)=0, \qquad u(1)=0. \quad (3.13)$$

3.5 Couette flow

For the Couette flow, the upper plate is moving with the velocity U_h and the lower plate is at rest. The boundary conditions for the problem in non dimensional form are defined as Eq.(1.27). The governing equations are same as defined in previous section (Eqs.(3.8) to (3.11)).

3.6 Numerical solution and discussion

The solution for both the cases have been calculated by Shooting method in conjunction with Runge-Kutta Fehlberg method. Analysis is carried out using the same scheme defined in previous chapter i.e., Eqs. (2.17) to (2.31). The results have been discussed through

tables and graphs as follows.

Numerical solutions are computed from the governing equations of hyperbolic tangent fluid for Poiseuille and Couette flow. Numerical results of Poiseuille flow for the four different cases of viscosity and porosity depending upon pressure are listed in Table 3.1. It is observed from relating case I and case III that the viscosity having exponential relation of pressure upsurges fluid flow as compare to the viscosity having rational relation of pressure. Further the comparison of case I and case II yields that fluid velocity elevates when porosity is taken to be a rational function of pressure. The comparison of case III and case IV exposes that exponential form of porosity enhances fluid flow. Moreover, the overall analysis of the four cases conclude that the best possible combination for attaining maximum fluid velocity is to consider case III. The velocity field for various values of $\Gamma's$ and for different values of power m and n are displayed in figures 3.1 to 3.4. It indicates that with the increase in $\Gamma's$ and the power m and n, fluid velocity reduces for each case of viscosity and porosity. Due to the pressure gradient the velocity is maximum at the centre of the channel. Also it is observed that velocity gives maximum values in the absence of $\Gamma's$. The velocity profile for different values of power law index β is depicted through figures 3.5 to 3.8. Shear thinning effects are observed with an increase in the power law index β for four different cases of viscosity and porosity parameter. Figures 3.9 to 3.12 show the velocity field for different values of Weissenberg number We. It illustrates that with a raise in We, velocity field increases for all the cases of viscosities and porosity.

Table 3.2 is the exhibition of numerical results for Couette flow when four different cases are considered. The analysis of Table 3.2 shows the similar results as for the cases of Poiseuille flow. So for both Poiseuille flow and Couette flow the inspection of all the four cases discloses that case II is the appropriate choice to attain more fluid velocity. Figures 3.13 to 3.24 illustrates the graphical results for Couette flow problem. The velocity profile for different values of $\Gamma's$ and the power m and n for Couette flow are shown in figures

3.13 to 3.16. It is analyzed that fluid velocity falls with a rise in the values of $\Gamma's$ and the power m and n for all the four cases of viscosity and porosity. Thus we can say that the pressure dependent viscosity causes a drag in fluid flow. It is also seen that the velocity field for Couette flow in the absence of $\Gamma's$ becomes high in magnitude. The velocity profile for different values of power law index β are displayed in figures 3.17 to 3.20. Pseudoplastic fluid effects are analysed with the different values of power law index β. Variation of Weissenberg number We for velocity profile of Couette flow are shown through figures 3.21 to 3.24. Velocity profile descend with an increase in the values of Weissenberg number.

	u(y)			
y	**Case I**	**Case II**	**Case III**	**Case IV**
0	0	0	0	0
0.10	0.090729910	0.103129455	0.056081235	0.052621502
0.20	0.168062432	0.190858888	0.109941319	0.102821166
0.30	0.234719902	0.264308404	0.160601546	0.149951185
0.40	0.290603495	0.323022409	0.206427618	0.192747513
0.50	0.332936073	0.364604330	0.244745245	0.228936155
0.60	0.356060768	0.384167393	0.271176332	0.254549264
0.70	0.350913158	0.373531589	0.278441284	0.262692513
0.80	0.304099441	0.320051827	0.254072578	0.241212177
0.90	0.196374225	0.204857061	0.175691128	0.167955317
1.00	0	0	0	0

Table 3.1: Velocity for $\Gamma_1 = 1, \Gamma_2 = 5, \Gamma_3 = 5, \Gamma_4 = 1, \beta = 0.4, m = 2, n = 3$ and $We = 0.05$ for Poiseuille flow

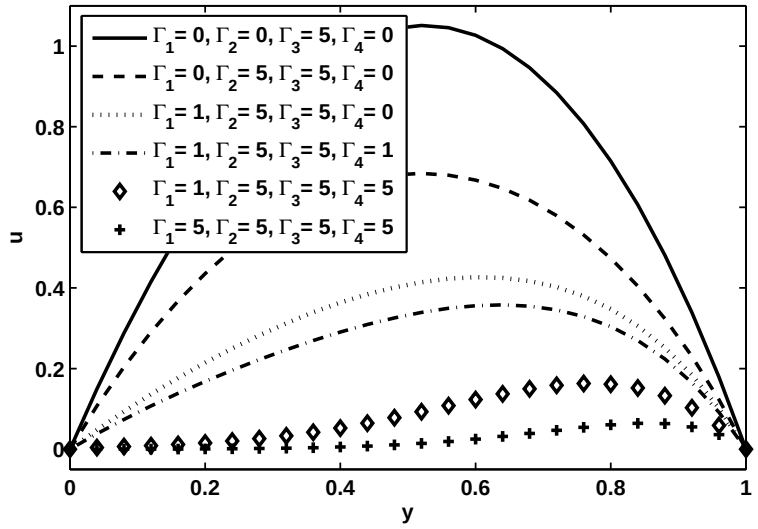

Figure 3.1: Velocity profile for $\mu(p) = Aexp(ap)$ and $\alpha(p) = Bexp(bp)$ with $\beta = 0.4$ and $We = 0.05$ in Poiseuille flow.

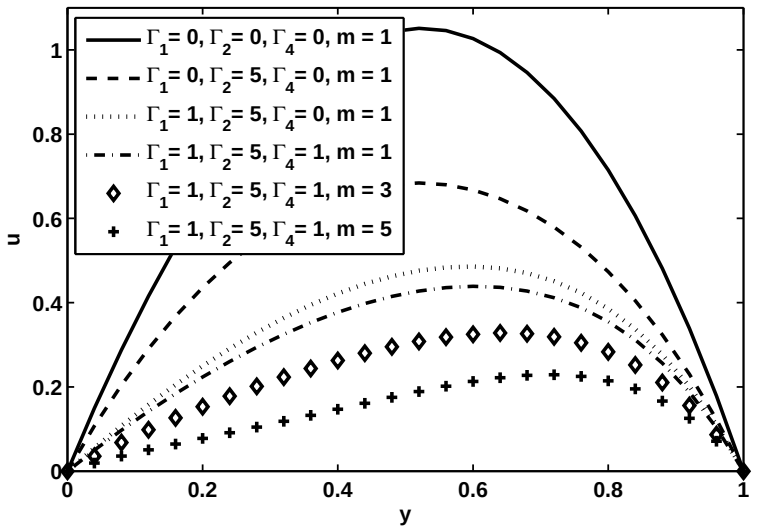

Figure 3.2: Velocity profile for $\mu(p) = Aexp(ap)$ and $\alpha(p) = B(\frac{p}{p_0})^m$ with $\Gamma_3 = 5, \beta = 0.4$ and $We = 0.05$ in Poiseuille flow.

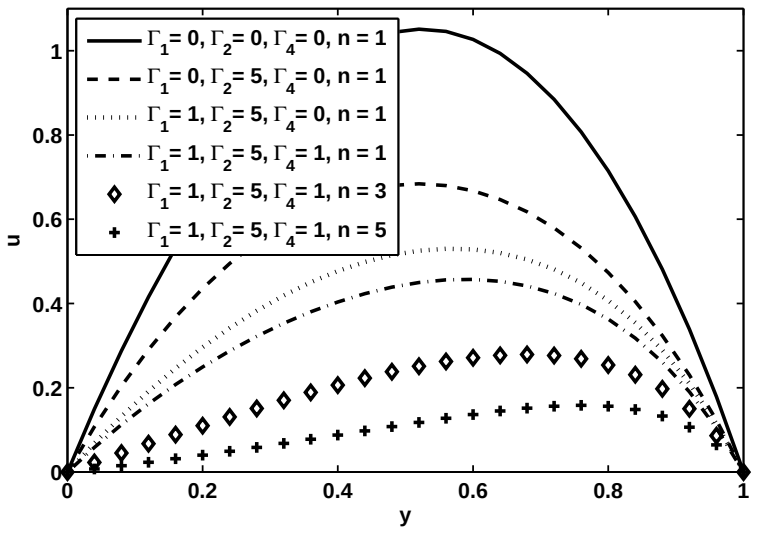

Figure 3.3: Velocity profile for $\mu(p) = A(\frac{p}{p_0})^n$ and $\alpha(p) = Bexp(bp)$ with $\Gamma_3 = 5, \beta = 0.4$ and $We = 0.05$ in Poiseuille flow.

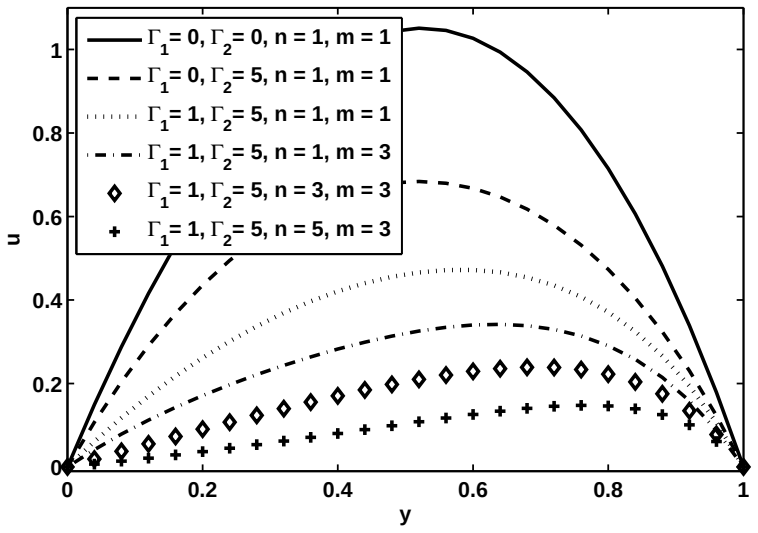

Figure 3.4: Velocity profile for $\mu(p) = A(\frac{p}{p_0})^n$ and $\alpha(p) = B(\frac{p}{p_0})^m$ with $\Gamma_3 = 5, \beta = 0.4$ and $We = 0.05$ in Poiseuille flow.

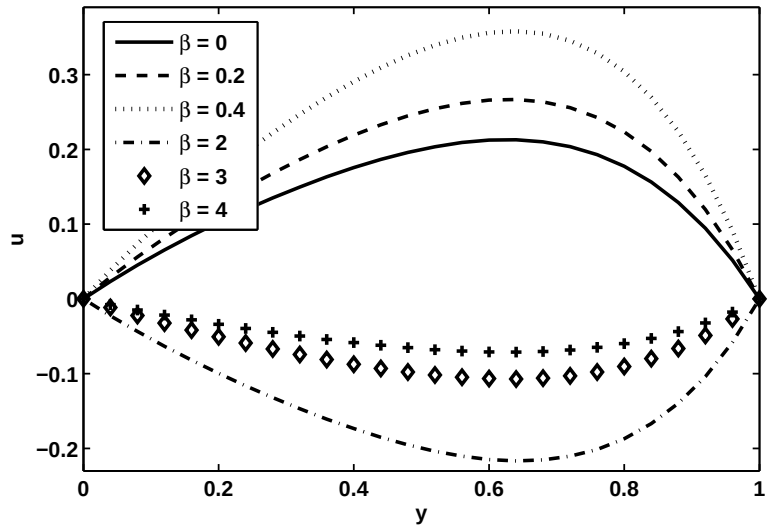

Figure 3.5: Velocity profile for $\mu(p) = Aexp(ap)$ and $\alpha(p) = Bexp(bp)$ with $\Gamma_1 = 1, \Gamma_2 = 10, \Gamma_3 = 10$ and $\Gamma_4 = 1$ in Poiseuille flow.

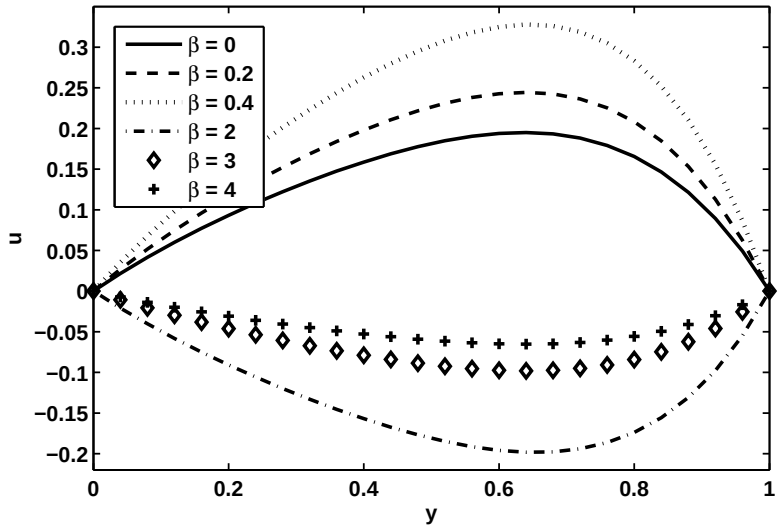

Figure 3.6: Velocity profile for $\mu(p) = Aexp(ap)$ and $\alpha(p) = B(\frac{p}{p_0})^m$ with $\Gamma_1 = 1, \Gamma_2 = 10, \Gamma_3 = 10, \Gamma_4 = 1$ and $m = 2$ in Poiseuille flow.

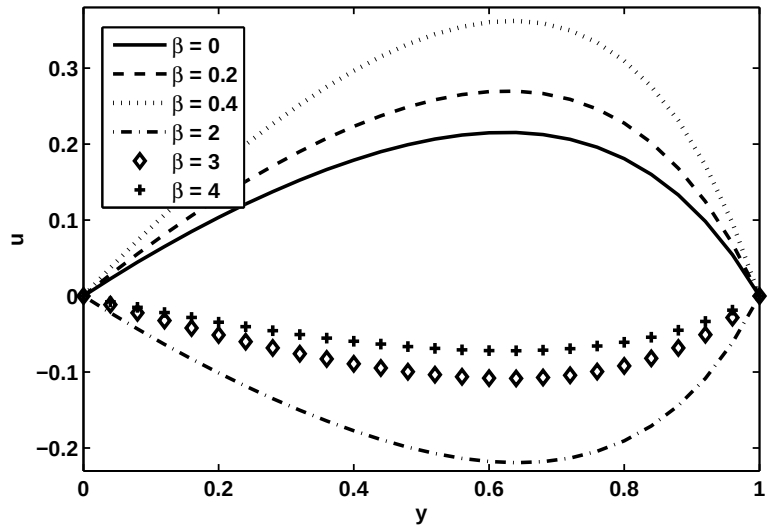

Figure 3.7: Velocity profile for $\mu(p) = A(\frac{p}{p_0})^n$ and $\alpha(p) = Bexp(bp)$ with $\Gamma_1 = 1, \Gamma_2 = 10, \Gamma_3 = 10, \Gamma_4 = 1$ and $n = 2$ in Poiseuille flow.

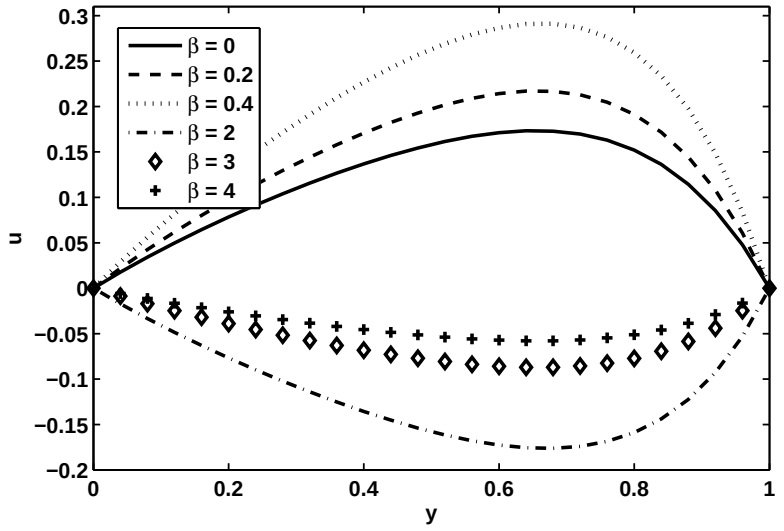

Figure 3.8: Velocity profile for $\mu(p) = A(\frac{p}{p_0})^n$ and $\alpha(p) = B(\frac{p}{p_0})^m$ with $\Gamma_1 = 1, \Gamma_2 = 10, \Gamma_3 = 10, m = 1$ and $n = 2$ in Poiseuille flow.

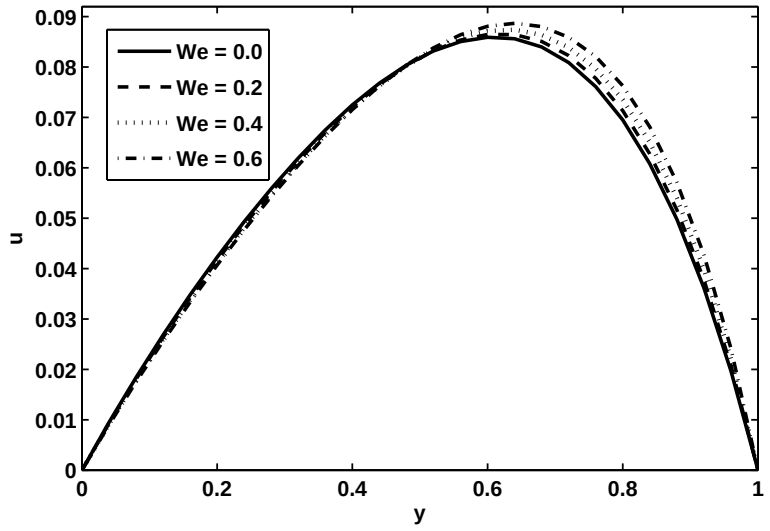

Figure 3.9: Velocity profile for $\mu(p) = Aexp(ap)$ and $\alpha(p) = B(\frac{p}{p_0})^m$ with $\Gamma_1 = 1, \Gamma_2 = 10, \Gamma_3 = 10, \Gamma_4 = 1$ and $\lambda_1 = 0.5$ in Poiseuille flow.

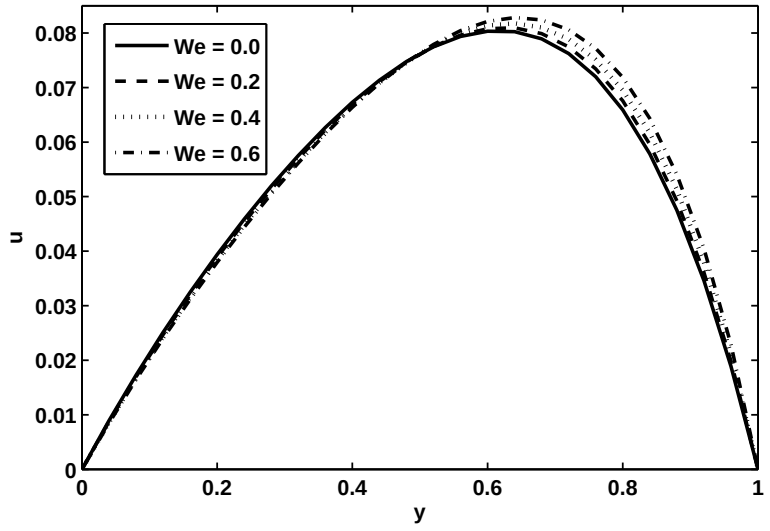

Figure 3.10: Velocity profile for $\mu(p) = A(\frac{p}{p_0})^n$ and $\alpha(p) = Bexp(bp)$ with $\Gamma_1 = 1, \Gamma_2 = 10, \Gamma_3 = 10, \Gamma_4 = 1$ and $\lambda_1 = 0.5$ in Poiseuille flow.

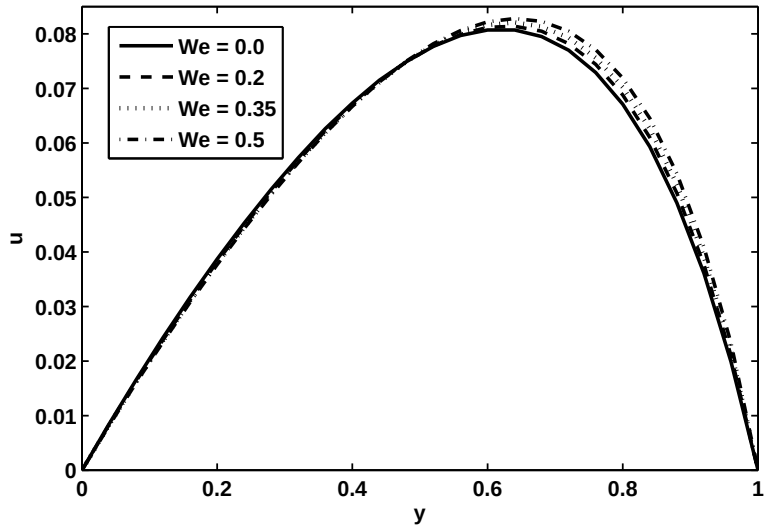

Figure 3.11: Velocity profile for $\mu(p) = A(\frac{p}{p_0})^n$ and $\alpha(p) = B(\frac{p}{p_0})^m$ with $\Gamma_1 = 1, \Gamma_2 = 10, \Gamma_3 = 10, m = 3$ and $\lambda_1 = 0.5$ in Poiseuille flow.

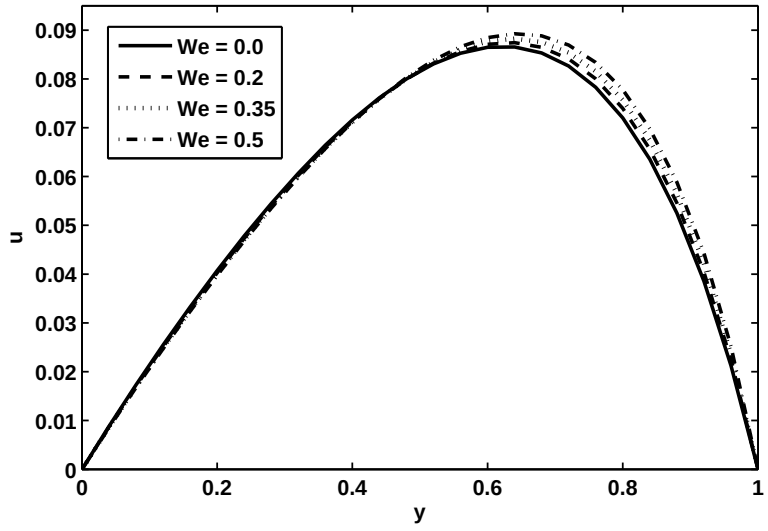

Figure 3.12: Velocity profile for $\mu(p) = A(\frac{p}{p_0})^n$ and $\alpha(p) = B(\frac{p}{p_0})^m$ with $\Gamma_1 = 1, \Gamma_2 = 10, \Gamma_3 = 10, n = 3$ and $\lambda_1 = 0.5$ in Poiseuille flow.

	u(y)			
y	**Case I**	**Case II**	**Case III**	**Case IV**
0	0	0	0	0
0.10	0.107536364	0.123422435	0.077182135	0.071582864
0.20	0.205754557	0.235356710	0.156176475	0.144547405
0.30	0.300072948	0.339218052	0.237518153	0.219861853
0.40	0.393705906	0.437556133	0.321733954	0.298586220
0.50	0.488091976	0.531963156	0.409318210	0.381866539
0.60	0.583042666	0.622891895	0.500682867	0.470900859
0.70	0.676687633	0.709358264	0.596057983	0.566844277
0.80	0.765251920	0.788499380	0.695294010	0.670583947
0.90	0.842668959	0.854951276	0.797460670	0.782233238
1.00	0.9	0.9	0.9	0.9

Table 3.2: Velocity for $\Gamma_1 = 1, \Gamma_2 = 5, \Gamma_3 = 5, \Gamma_4 = 1, \beta = 0.4, m = 2, n = 3, We = 0.05$ and $U_0 = 0.9$ for Couette flow

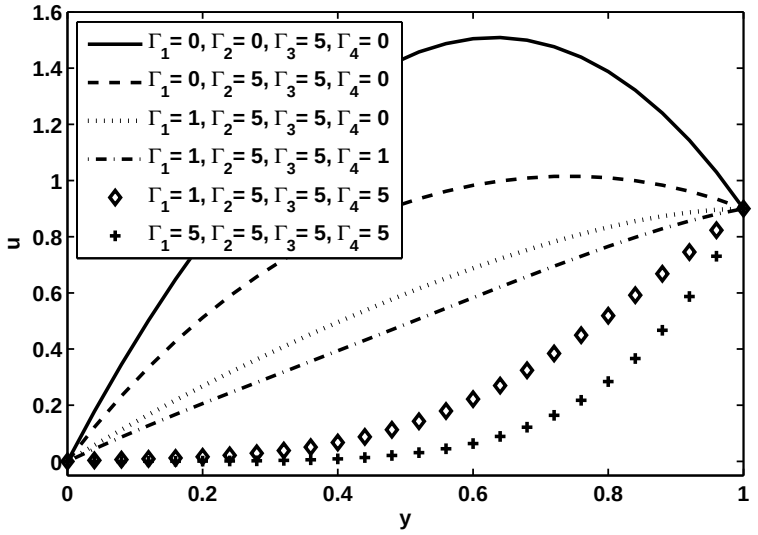

Figure 3.13: Velocity profile for $\mu(p) = Aexp(ap)$ and $\alpha(p) = Bexp(bp)$ with $W_e = 0.05$, and $U_0 = 0.9$ in Couette flow.

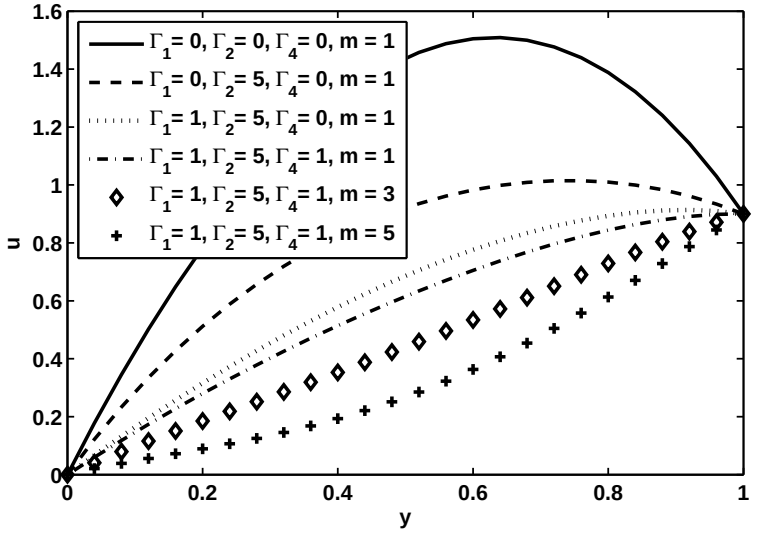

Figure 3.14: Velocity profile for $\mu(p) = Aexp(ap)$ and $\alpha(p) = B(\frac{p}{p_0})^m$ with $\Gamma_3 = 5, W_e = 0.05$ and $U_0 = 0.9$ in Couette flow.

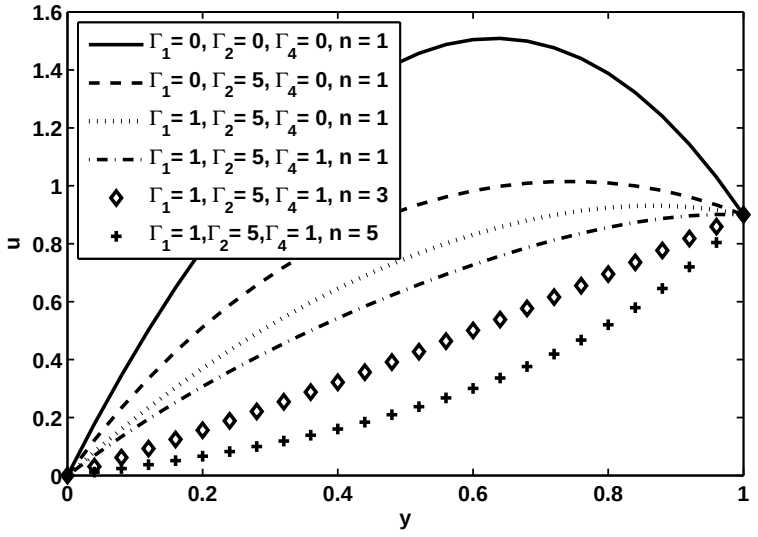

Figure 3.15: Velocity profile for $\mu(p) = A(\frac{p}{p_0})^n$ and $\alpha(p) = Bexp(bp)$ with $\Gamma_3 = 5, W_e = 0.05$ and $U_0 = 0.9$ in Couette flow.

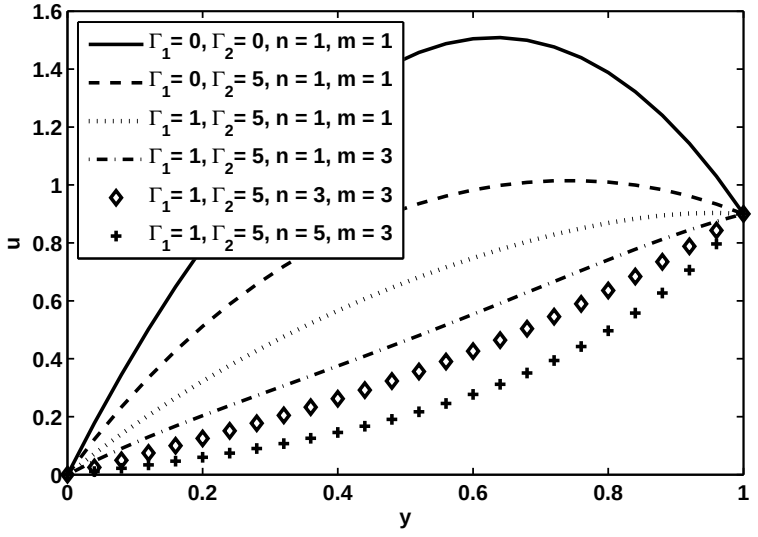

Figure 3.16: Velocity profile for $\mu(p) = A(\frac{p}{p_0})^n$ and $\alpha(p) = B(\frac{p}{p_0})^m$ with $\Gamma_3 = 5, W_e = 0.05$ and $U_0 = 0.9$ in Couette flow.

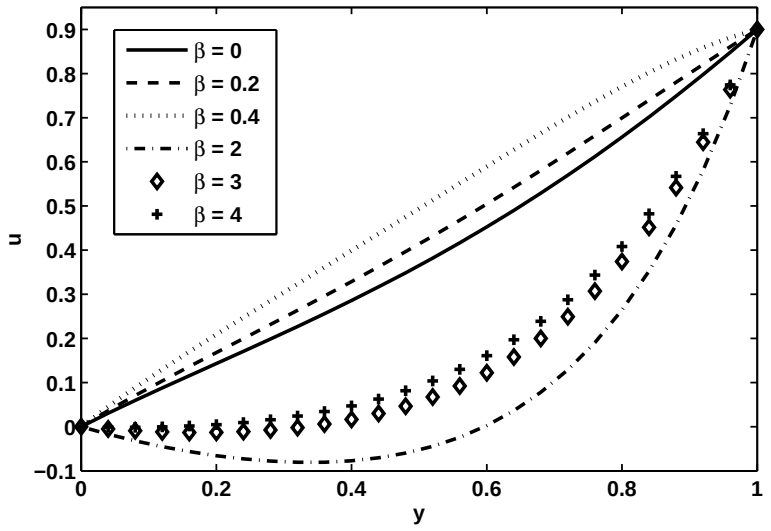

Figure 3.17: Velocity profile for $\mu(p) = Aexp(ap)$ and $\alpha(p) = Bexp(bp)$ with $\Gamma_1 = 1, \Gamma_2 = 5, \Gamma_3 = 1, \Gamma_4 = 1$ and $U_0 = 0.9$ in Couette flow.

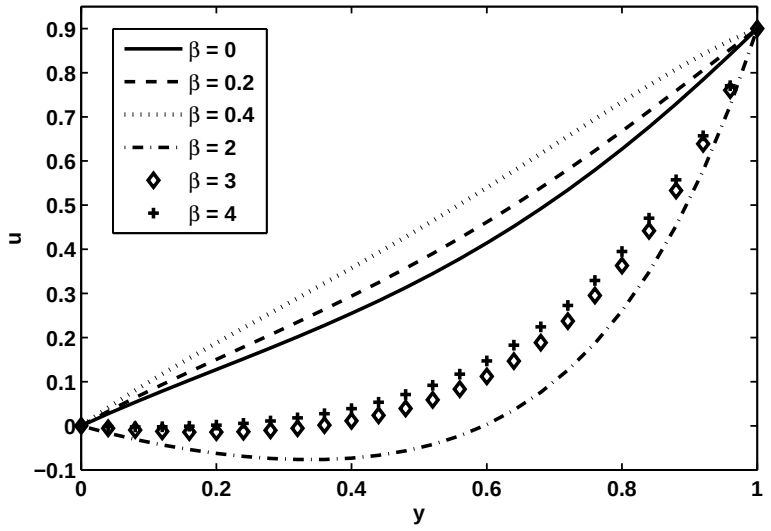

Figure 3.18: Velocity profile for $\mu(p) = Aexp(ap)$ and $\alpha(p) = B(\frac{p}{p_0})^m$ with $\Gamma_1 = 1, \Gamma_2 = 5, \Gamma_3 = 1, \Gamma_4 = 1, U_0 = 0.9$ and $m = 3$ in Couette flow.

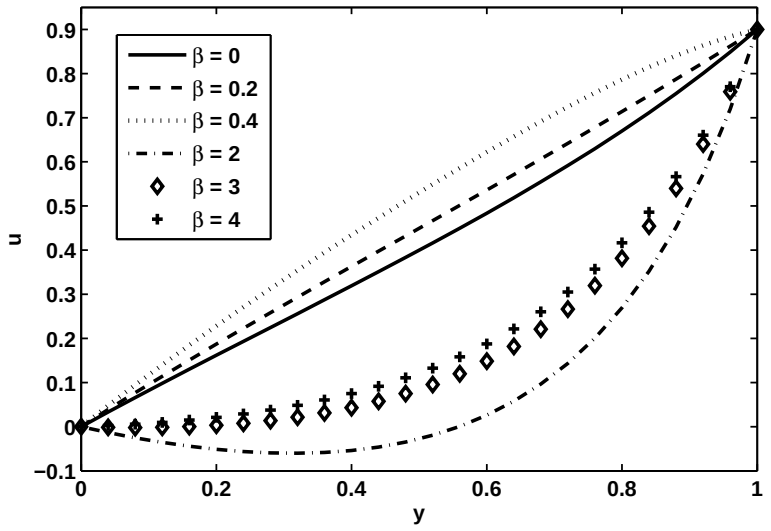

Figure 3.19: Velocity profile for $\mu(p) = A(\frac{p}{p_0})^n$ and $\alpha(p) = Bexp(bp)$ with $\Gamma_1 = 1, \Gamma_2 = 5, \Gamma_3 = 1, \Gamma_4 = 1, U_0 = 0.9$ and $n = 2$ in Couette flow.

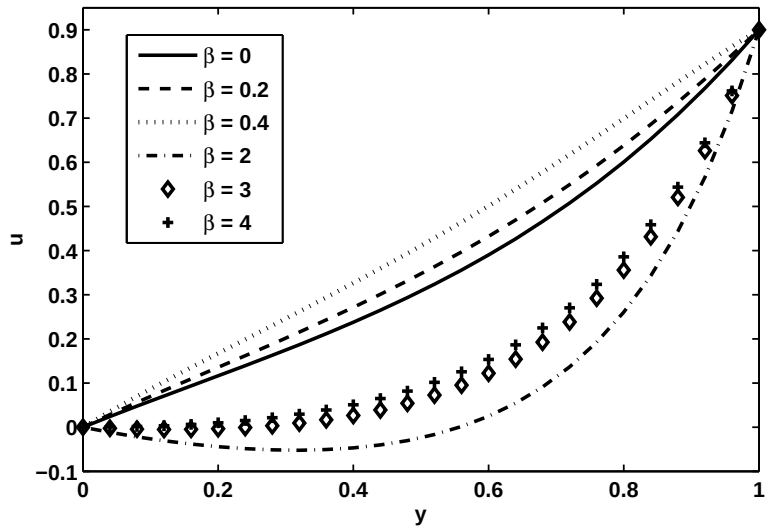

Figure 3.20: Velocity profile for $\mu(p) = A(\frac{p}{p_0})^n$ and $\alpha(p) = B(\frac{p}{p_0})^m$ with $\Gamma_1 = 1, \Gamma_2 = 5, \Gamma_3 = 1, U_0 = 0.9, m = 2$ and $n = 3$ in Couette flow.

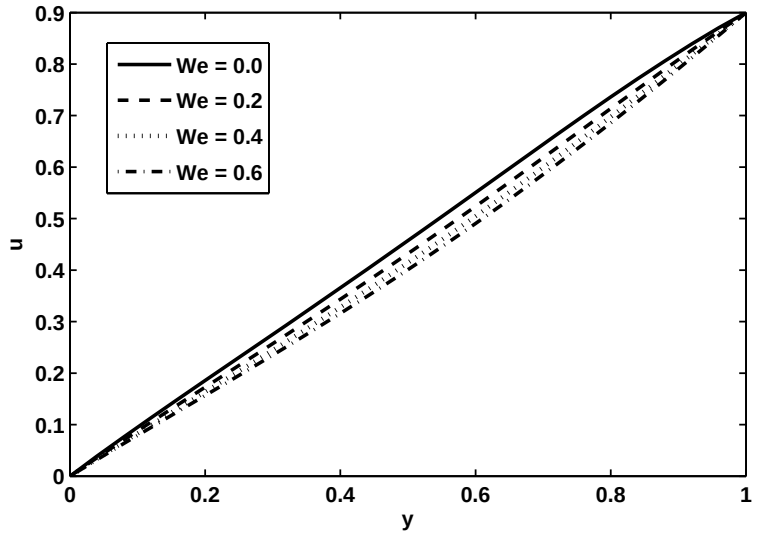

Figure 3.21: Velocity profile for $\mu(p) = Aexp(ap)$ and $\alpha(p) = Bexp(bp)$ with $\Gamma_1 = 1, \Gamma_2 = 5, \Gamma_3 = 1, \Gamma_4 = 1$ and $U_0 = 0.9$ in Couette flow.

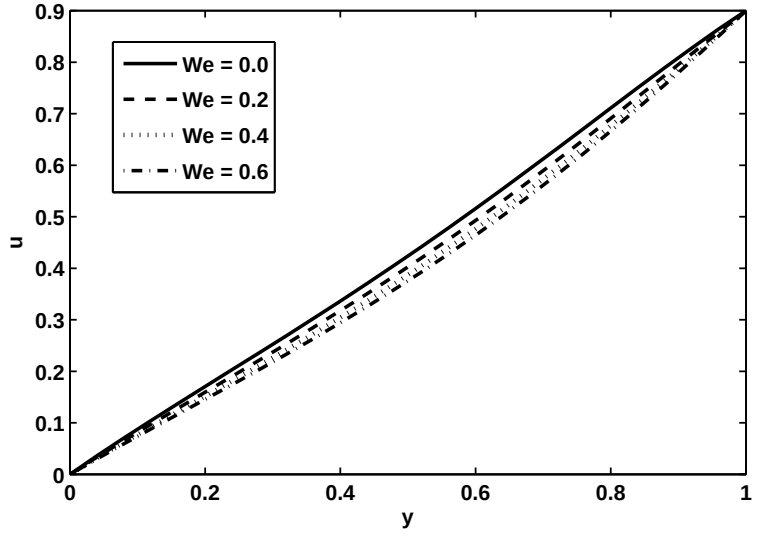

Figure 3.22: Velocity profile for $\mu(p) = Aexp(ap)$ and $\alpha(p) = B(\frac{p}{p_0})^m$ with $\Gamma_1 = 1, \Gamma_2 = 5, \Gamma_3 = 1, \Gamma_4 = 1, U_0 = 0.9$ and $m = 3$ in Couette flow.

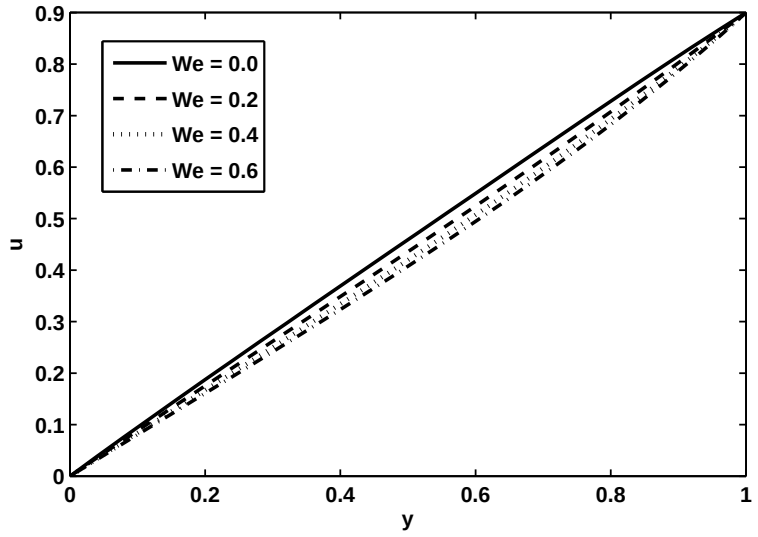

Figure 3.23: Velocity profile for $\mu(p) = A(\frac{p}{p_0})^n$ and $\alpha(p) = Bexp(bp)$ with $\Gamma_1 = 1, \Gamma_2 = 5, \Gamma_3 = 1, \Gamma_4 = 1, U_0 = 0.9$ and $n = 2$ in Couette flow.

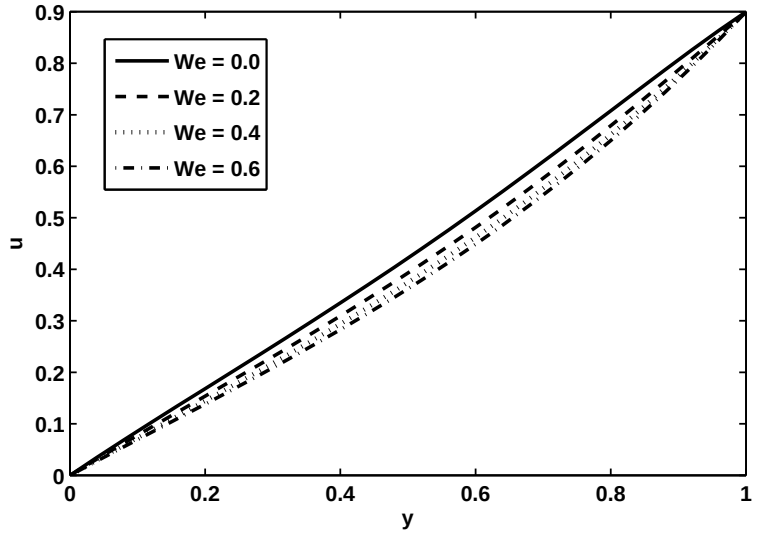

Figure 3.24: Velocity profile for $\mu(p) = A(\frac{p}{p_0})^n$ and $\alpha(p) = B(\frac{p}{p_0})^m$ with $\Gamma_1 = 1, \Gamma_2 = 5, \Gamma_3 = 1, U_0 = 0.9, m = 2$ and $n = 3$ in Couette flow.

Chapter 4

Flows of Carreau fluid with pressure dependent viscosity in a variable porous medium: Application of polymer melt

4.1 Introduction

The present work concerns the pressure dependent viscosity in Carreau fluid through porous medium. Four different combinations of pressure dependent viscosity and pressure dependent porous medium parameters are considered for two types of flow situations namely (i) Poiseuille flow (ii) Couette flow. The solutions of non linear equations have been evaluated numerically by Shooting method along with Runge-Kutta Fehlberg method. The physical features of pertinent parameters have been discussed through graphs.

4.2 Fluid model

The constitutive equation of Carreau fluid for incompressible and unidirectional flow for an inclined channel is given by [51]

$$\frac{\mu-\mu_\infty}{\mu_0-\mu_\infty}=[1+(\Gamma|\dot{\gamma}|)^2]^{\frac{\beta-1}{2}} \tag{4.1}$$

Consider the case when $\mu_\infty = 0$ and $\Gamma|\dot{\gamma}| << 1$. Therefore component of extra stress tensor becomes

$$\boldsymbol{\tau}=\mu_0[1+\frac{\beta-1}{2}(\Gamma|\dot{\gamma}|)^2]\dot{\gamma}. \tag{4.2}$$

4.3 Mathematical formulation

The component form of momentum equation in the presence of gravity and porosity take the following form

$$-\frac{\partial p}{\partial x}+\mu(p)[1+\frac{3}{2}(\beta-1)(\Gamma\frac{du}{dy})^2]\frac{d^2u}{dy^2}+\frac{d\mu(p)}{dy}[1+\frac{1}{2}(\beta-1)(\Gamma\frac{du}{dy})^2]\frac{du}{dy} \\ -\alpha(p)[1+\frac{1}{2}(\beta-1)(\Gamma\frac{du}{dy})^2]u(y)+\rho g\sin\theta=0, \tag{4.3}$$

and

$$-\frac{\partial p}{\partial y}-\rho g\cos\theta=0. \tag{4.4}$$

With the help of Eqs.(1.9) and (2.8), Eqs.(4.3) and (4.4) after dropping the bars can be written as

$$[1+\frac{3}{2}(\beta-1)(We\frac{du}{dy})^2]\frac{d^2u}{dy^2}+\frac{1}{\mu(p)}\frac{d\mu(p)}{dy}[1+\frac{1}{2}(\beta-1)(We\frac{du}{dy})^2]\frac{du}{dy} \\ -h^2\frac{\alpha(p)}{\mu(p)}[1+\frac{1}{2}(\beta-1)(We\frac{du}{dy})^2]u(y)+\frac{\rho g h^2\sin\theta}{U_c\mu(p)}=0, \tag{4.5}$$

and

$$\frac{dp}{dy}+\rho g h\cos\theta=0. \tag{4.6}$$

The solution of Eq.(4.6) is

$$p = p_0 + \rho g h \cos\theta (1 - y). \tag{4.7}$$

With the help of Eq. (4.6), the solution of Eq. (4.5) has been computed in the next section for two types of boundary conditions known as

(i) Poiseuille flow

(ii) Couette flow

4.4 Poiseuille flow

In this case the boundaries are at rigid surfaces Eq.(1.26), therefore, by using Eqs.(1.14) to (1.17), Eq. (4.5) take the following forms

$$(1+\frac{3}{2}(\beta-1)(We\frac{du}{dy})^2)\frac{d^2u}{dy^2}-\Gamma_1[1+\frac{1}{2}(\beta-1)(We\frac{du}{dy})^2]\frac{du}{dy}-\Gamma_2[1+\frac{1}{2}(\beta-1)(We\frac{du}{dy})^2]$$
$$exp[\Gamma_4(1-y)]u(y)+\Gamma_3 exp[-\Gamma_1(1-y)]=0, \tag{4.8}$$

$$[1+\frac{3}{2}(\beta-1)(We\frac{du}{dy})^2]\frac{d^2u}{dy^2}-\Gamma_1[1+\frac{1}{2}(\beta-1)(We\frac{du}{dy})^2]\frac{du}{dy}-\Gamma_2[1+\frac{1}{2}(\beta-1)(We\frac{du}{dy})^2][1+\Gamma_4(1-y)]^m$$
$$exp[-\Gamma_1(1-y)]u(y)+\Gamma_3 exp[-\Gamma_1(1-y)]=0, \tag{4.9}$$

$$[1+\frac{3}{2}(\beta-1)(We\frac{du}{dy})^2]\frac{d^2u}{dy^2}-\frac{n\Gamma_1}{1+\Gamma_1(1-y)}[1+\frac{1}{2}(\beta-1)(We\frac{du}{dy})^2]\frac{du}{dy}-\Gamma_2[1+\frac{1}{2}(\beta-1)(We\frac{du}{dy})^2]$$
$$[1+\Gamma_1(1-y)]^{-n}exp[\Gamma_4(1-y)]u(y)+\frac{\Gamma_3}{[1+\Gamma_1(1-y)]^n}=0, \tag{4.10}$$

$$[1+\frac{3}{2}(\beta-1)(We\frac{du}{dy})^2]\frac{d^2u}{dy^2}-\frac{n\Gamma_1}{1+\Gamma_1(1-y)}[1+\frac{1}{2}(\beta-1)(We\frac{du}{dy})^2]\frac{du}{dy}-\Gamma_2[1+\frac{1}{2}(\beta-1)(We\frac{du}{dy})^2]$$
$$[1+\Gamma_1(1-y)]^{m-n}u(y)+\frac{\Gamma_3}{[1+\Gamma_1(1-y)]^n}=0. \tag{4.11}$$

4.5 Couette flow

In this case, the lower plate is at rest and the upper plate is moving with the velocity U_h. The boundary conditions for the problem in non dimensional form are Eq. (1.27) The governing equations are same as defined in previous section (Eqs.(4.8) to (4.11)).

4.6 Numerical solution and discussion

The solution for both the cases has been calculated by Shooting method using Runge-Kutta Fehlberg and the results have been discussed through tables and graphs as follow. The brief method is already defined in Chapter two. Therefore to avoid the repetition we have only discussed the solutions through graphs and tables. The governing equations of Carreau fluid with pressure dependent viscosities have been solved numerically for Poiseuille and Couette flow.

Table 4.1 explains the results for Poiseuille flow. Numerical results are recorded for all the four cases. The comparison of case I and case III leads to the fact that viscosity depending upon pressure by a polynomial function elevates fluid flow as compare to the viscosity depending upon pressure exponentially. Case I and Case II shows the values of fluid velocity when viscosity is an exponential function of pressure but porosity expression varies. It is notable that more fluid velocity is attained for case I. Also the comparison of four cases demonstrates that the case III improves fluid velocity and this combination is the most appropriate one. It is found that for each case the velocity is maximum at the centre of the channel. The velocity field for different values of $\Gamma's$ are displayed in figures 4.1 to 4.4 for various values of pressure dependent viscosity. It predicts that with the increase in $\Gamma's$, the velocity field decreases for each case of viscosity and porosity. Also, the maximum velocity is observed in the absence of $\Gamma's$. As the pressure increases with depth, the viscosity $\mu(p)$ and porosity $\alpha(p)$ increases, i.e., the resistance to flow

rises and subsequently the velocity falls. The Carreau model attempts to describe a wide range of fluids by the establishment of a curve-fit with functions for Newtonian and shear-thinning ($\beta < 1$) non-Newtonian laws. The velocity profile for different values of power law index β is shown through figures 4.5 to 4.8. It is observed that with an increase in the power law index β, the velocity profile decreases for four different cases of viscosity and porosity parameter. The Weissenberg number designates the orientation generated by the deformation (see figures 4.9 to 4.12), for different values of Weissenberg number We. Furthermore, with an increase in We, velocity field decreases for all the cases of viscosity and porosity.

Table 4.2 shows the numerical results of Couette flow for four different cases of pressure dependent viscosity and porosity. The comparison of numerical results for case I and case III shows that viscosity depending upon pressure rationally increases fluid velocity. Also comparison of case I and case II reveals that case I contributes in improving fluid flow. The examination of all the four cases exhibit that case III is the appropriate choice to attain more fluid velocity. The graphical results for Couette flow are displayed in figures 4.13 to 4.24. The velocity profile of $\Gamma's$ for Couette flow are shown through the figures 4.13 to 4.16. It is analyzed that velocity field decreases with an increase in the values of $\Gamma's$ for all the four cases of viscosity and porous medium parameter. Thus, we can say that the pressure dependent viscosity causes decrease in velocity. It has been realized that the velocity field for Couette flow gives larger values in the absence of $\Gamma's$ as Poiseuille flow does. The velocity profile for different values of power law index β is given in figures 4.17 to 4.20. It is seen that the velocity field increases with an increase in power law index β for the case I and case IV. Variation of Weissenberg number We for velocity profile in Couette flow is shown through figures 4.21 to 4.24. Velocity profile increases with an increase in the values of Weissenberg number We for each case of viscosity and porosity.

	u(y)			
y	**Case I**	**Case II**	**Case III**	**Case IV**
0	0	0	0	0
0.10	0.055579371	0.051044719	0.055151524	0.042118556
0.20	0.102536473	0.093309623	0.103730943	0.078386160
0.30	0.142608319	0.129056253	0.145398995	0.109939917
0.40	0.175733294	0.158846514	0.179218386	0.136886144
0.50	0.200198540	0.181544924	0.203458657	0.158178047
0.60	0.212593918	0.194145427	0.215275424	0.171315410
0.70	0.207626102	0.191476439	0.210182167	0.171810341
0.80	0.177813392	0.165838613	0.181162621	0.152310543
0.90	0.113052792	0.106631915	0.117120498	0.101167906
1.00	0	0	0	0

Table 4.1: Velocity for $\Gamma_1 = 1, \Gamma_2 = 5, \Gamma_3 = 5, \Gamma_4 = 1, \beta = 0.4, m = 3, n = 2$ and $We = 0.1$ for Poiseuille flow

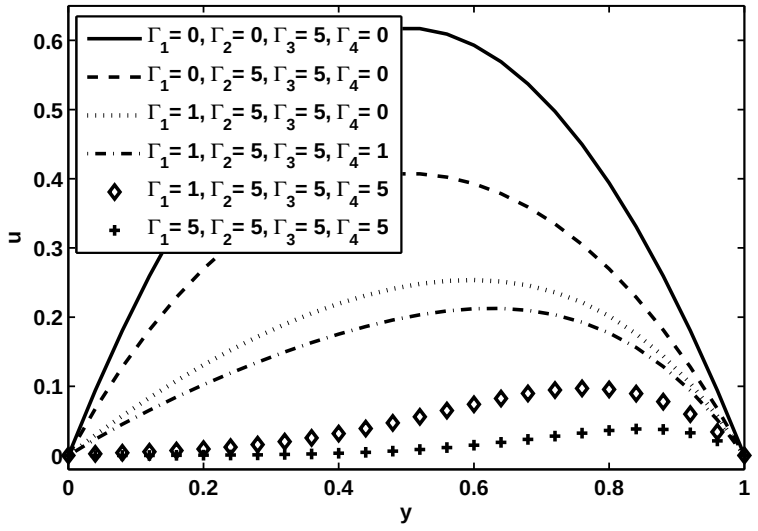

Figure 4.1: Velocity profile for $\mu(p) = Aexp(ap)$ and $\alpha(p) = Bexp(bp)$ with $\beta = 0.4$ and $We = 0.05$ in Poiseuille flow.

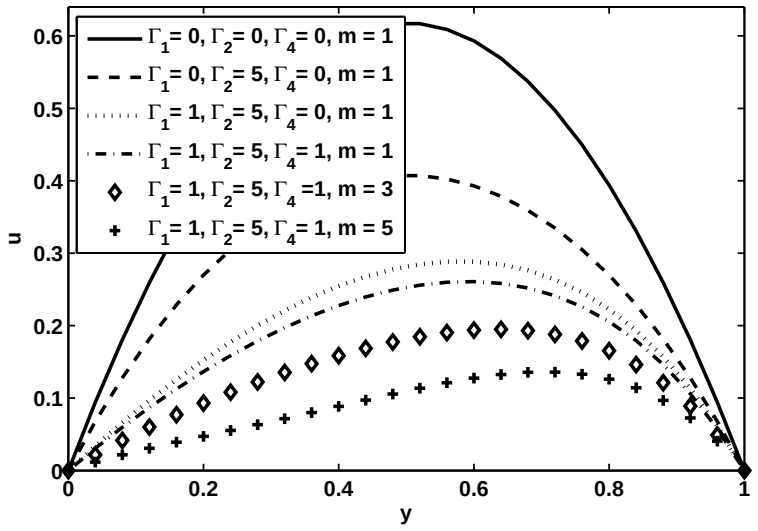

Figure 4.2: Velocity profile for $\mu(p) = Aexp(ap)$ and $\alpha(p) = B(\frac{p}{p_0})^m$ with $\Gamma_3 = 5, \beta = 0.4$ and $We = 0.05$ in Poiseuille flow.

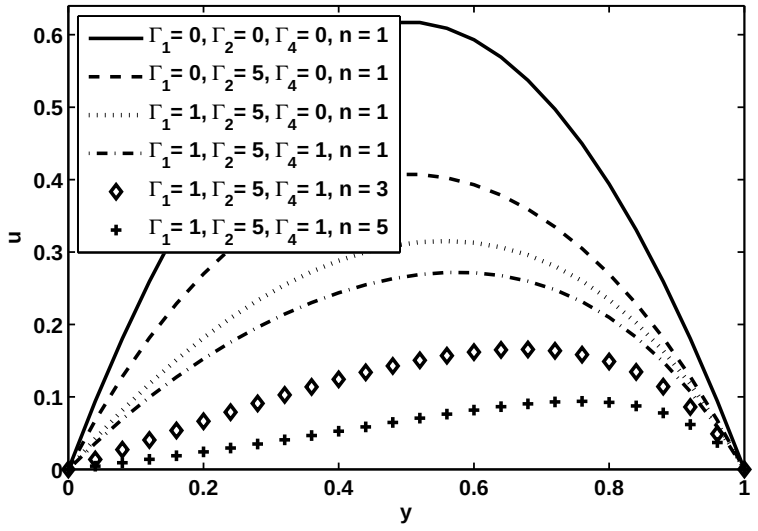

Figure 4.3: Velocity profile for $\mu(p) = A(\frac{p}{p_0})^n$ and $\alpha(p) = Bexp(bp)$ with $\Gamma_3 = 5, \beta = 0.4$ and $We = 0.05$ in Poiseuille flow.

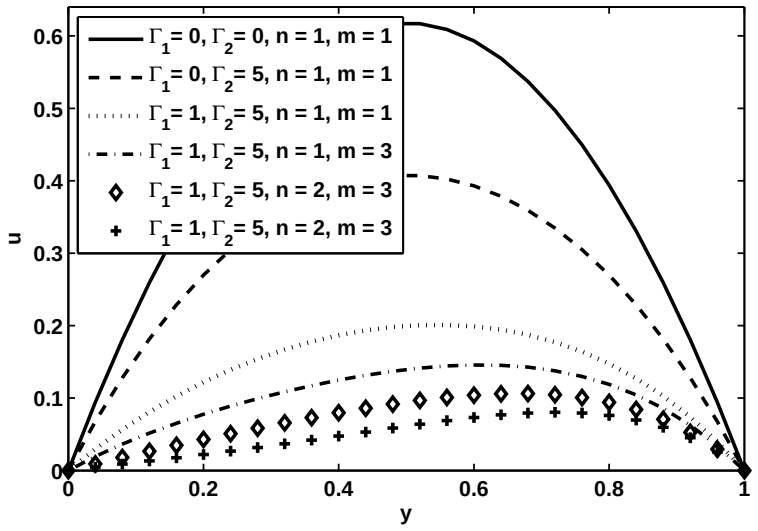

Figure 4.4: Velocity profile for $\mu(p) = A(\frac{p}{p_0})^n$ and $\alpha(p) = B(\frac{p}{p_0})^m$ with $\Gamma_3 = 5, \beta = 0.4$ and $We = 0.05$ in Poiseuille flow.

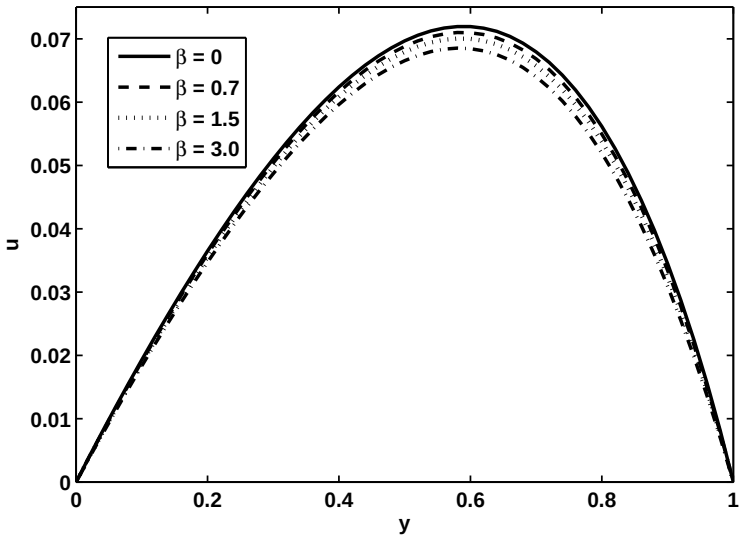

Figure 4.5: Velocity profile for $\mu(p) = Aexp(ap)$ and $\alpha(p) = Bexp(bp)$ with $\Gamma_1 = 1, \Gamma_2 = 10, \Gamma_3 = 10$ and $\Gamma_4 = 1$ in Poiseuille flow.

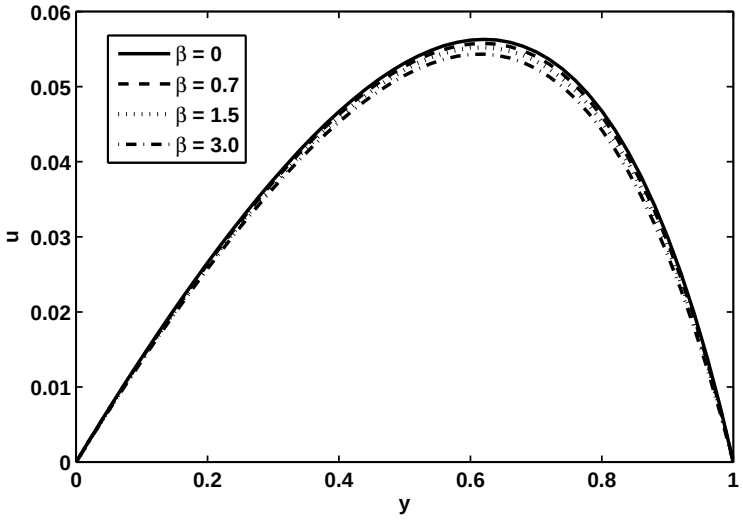

Figure 4.6: Velocity profile for $\mu(p) = Aexp(ap)$ and $\alpha(p) = B(\frac{p}{p_0})^m$ with $\Gamma_1 = 1, \Gamma_2 = 10, \Gamma_3 = 10, \Gamma_4 = 1$ and $m = 2$ in Poiseuille flow.

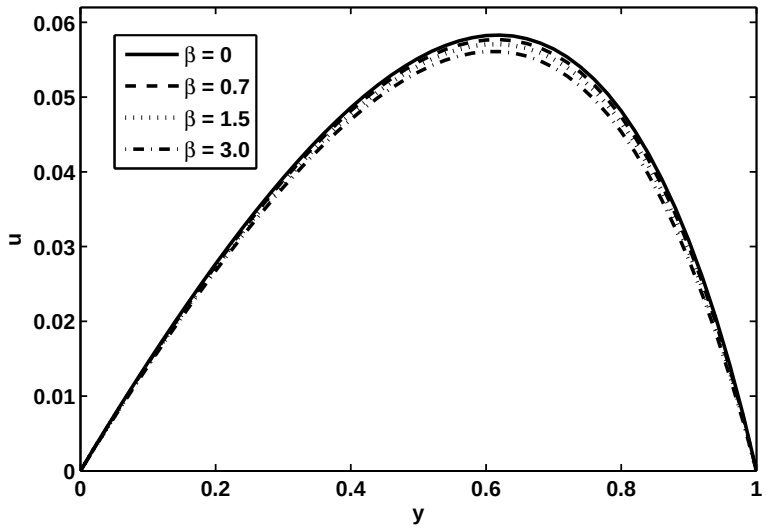

Figure 4.7: Velocity profile for $\mu(p) = A(\frac{p}{p_0})^n$ and $\alpha(p) = Bexp(bp)$ with $\Gamma_1 = 1, \Gamma_2 = 10, \Gamma_3 = 10, \Gamma_4 = 1$ and $n = 2$ in Poiseuille flow.

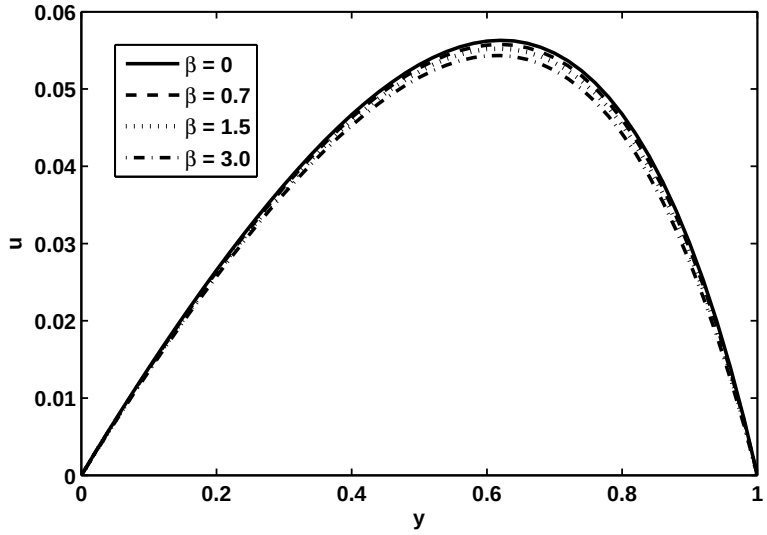

Figure 4.8: Velocity profile for $\mu(p) = A(\frac{p}{p_0})^n$ and $\alpha(p) = B(\frac{p}{p_0})^m$ with $\Gamma_1 = 1, \Gamma_2 = 10, \Gamma_3 = 10, m = 1$ and $n = 2$ in Poiseuille flow.

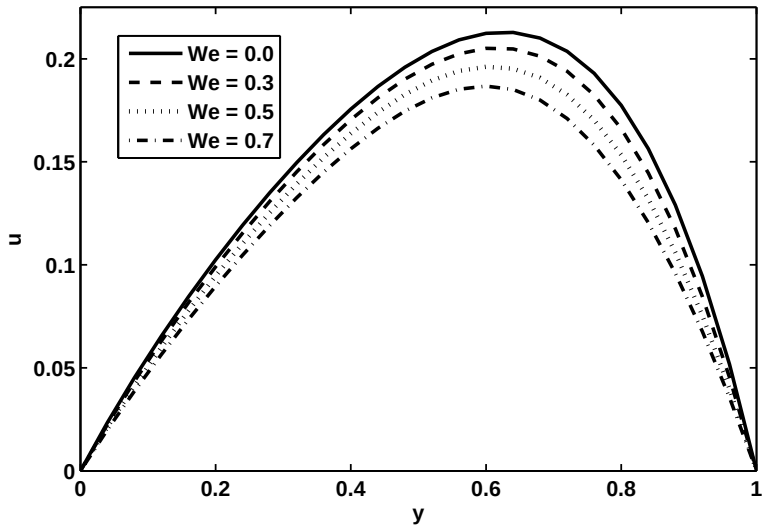

Figure 4.9: Velocity profile for $\mu(p) = Aexp(ap)$ and $\alpha(p) = B(\frac{p}{p_0})^m$ with $\Gamma_1 = 1, \Gamma_2 = 10, \Gamma_3 = 10, \Gamma_4 = 1$ and $\lambda_1 = 0.5$ in Poiseuille flow.

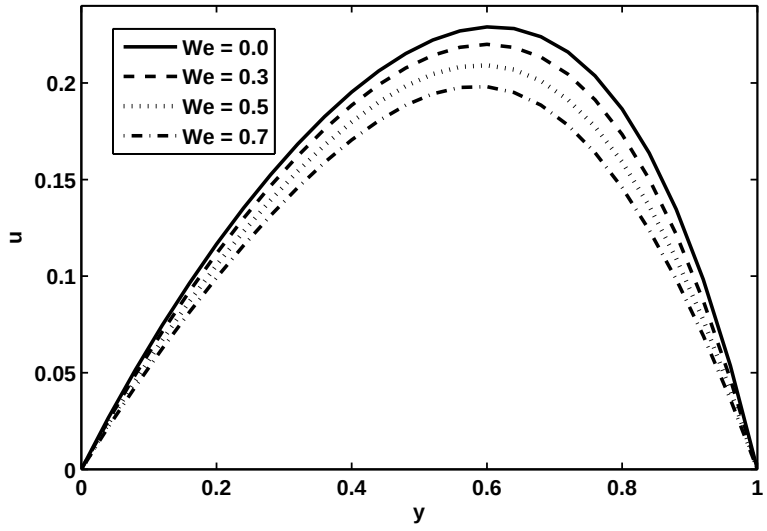

Figure 4.10: Velocity profile for $\mu(p) = A(\frac{p}{p_0})^n$ and $\alpha(p) = Bexp(bp)$ with $\Gamma_1 = 1, \Gamma_2 = 10, \Gamma_3 = 10, \Gamma_4 = 1$ and $\lambda_1 = 0.5$ in Poiseuille flow.

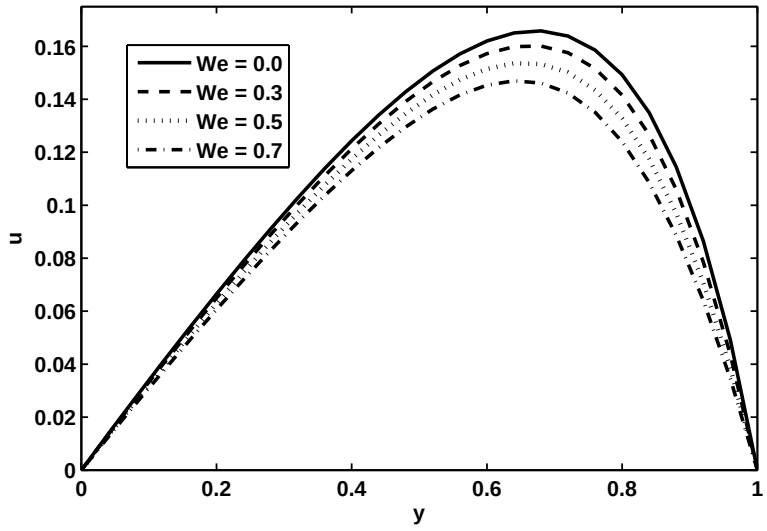

Figure 4.11: Velocity profile for $\mu(p) = A(\frac{p}{p_0})^n$ and $\alpha(p) = B(\frac{p}{p_0})^m$ with $\Gamma_1 = 1, \Gamma_2 = 10, \Gamma_3 = 10, m = 3$ and $\lambda_1 = 0.5$ in Poiseuille flow.

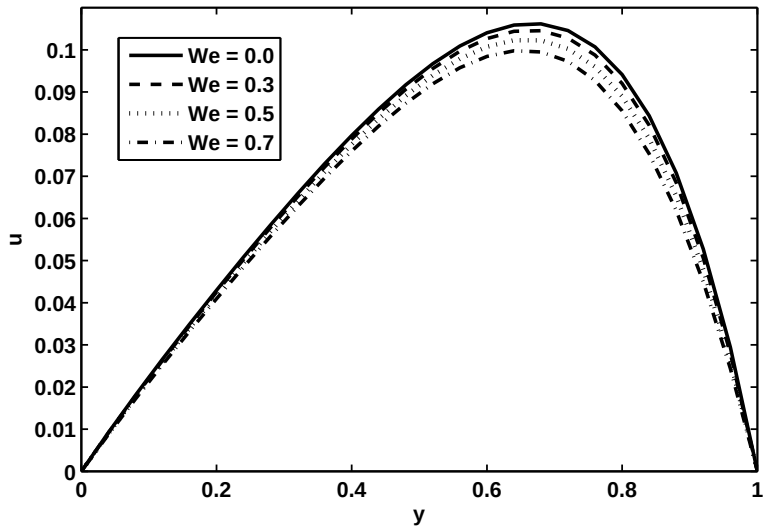

Figure 4.12: Velocity profile for $\mu(p) = A(\frac{p}{p_0})^n$ and $\alpha(p) = B(\frac{p}{p_0})^m$ with $\Gamma_1 = 1, \Gamma_2 = 10, \Gamma_3 = 10, n = 3$ and $\lambda_1 = 0.5$ in Poiseuille flow.

	u(y)			
y	**Case I**	**Case II**	**Case III**	**Case IV**
0	0	0	0	0
0.10	0.075799381	0.067917952	0.085307411	0.061143091
0.20	0.147684133	0.131293524	0.168464456	0.120446899
0.30	0.220579429	0.195616749	0.251125483	0.181760364
0.40	0.298241771	0.265555673	0.334975755	0.248691242
0.50	0.383679550	0.345275435	0.421838510	0.324872584
0.60	0.479381507	0.438555547	0.513816496	0.414185053
0.70	0.587421269	0.548717360	0.613495329	0.520955977
0.80	0.709475104	0.678360359	0.724257030	0.650148720
0.90	0.846773866	0.828910268	0.850793640	0.807554790
1.00	1.00	1.00	1.00	1.00

Table 4.2: Velocity for $\Gamma_1 = 1, \Gamma_2 = 5, \Gamma_3 = 5, \Gamma_4 = 1, \beta = 0.4, m = 3, n = 2, We = 0.1$ and $U_0 = 1$ for Couette flow

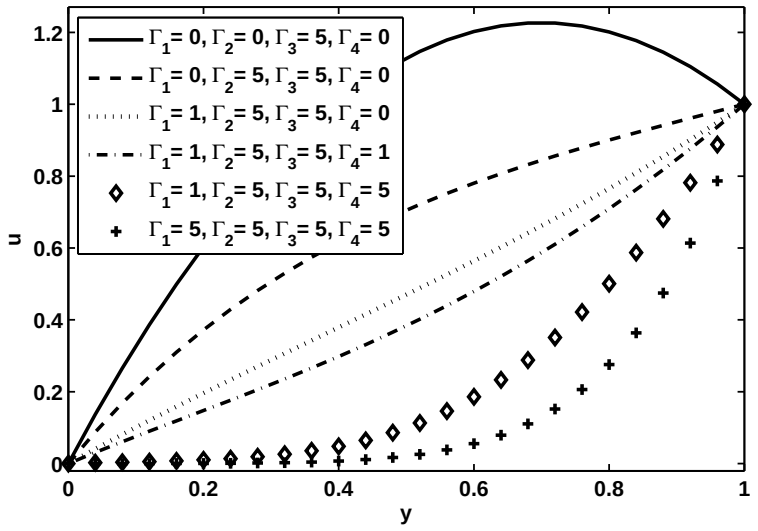

Figure 4.13: Velocity profile for $\mu(p) = Aexp(ap)$ and $\alpha(p) = Bexp(bp)$ with $W_e = 0.05$, and $U_0 = 0.9$ in Couette flow.

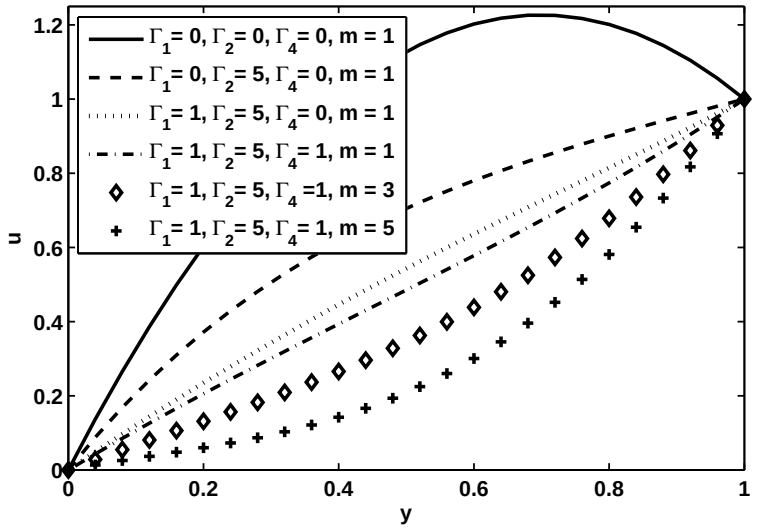

Figure 4.14: Velocity profile for $\mu(p) = Aexp(ap)$ and $\alpha(p) = B(\frac{p}{p_0})^m$ with $\Gamma_3 = 5, W_e = 0.05$ and $U_0 = 0.9$ in Couette flow.

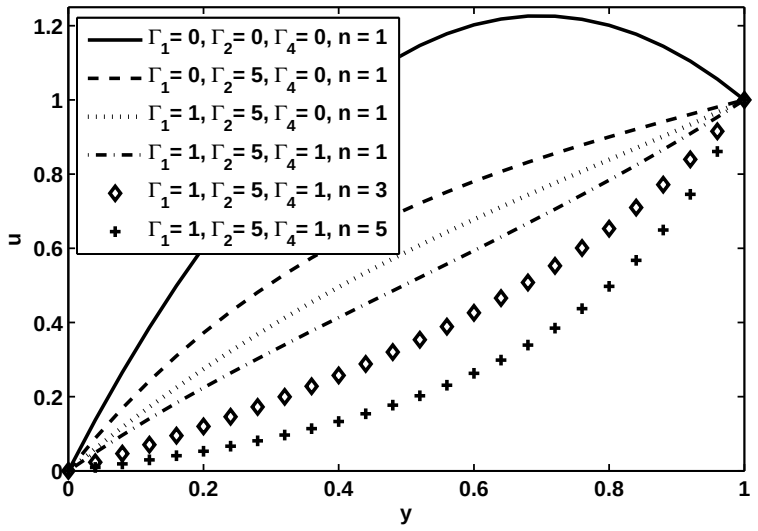

Figure 4.15: Velocity profile for $\mu(p) = A(\frac{p}{p_0})^n$ and $\alpha(p) = Bexp(bp)$ with $\Gamma_3 = 5, W_e = 0.05$ and $U_0 = 0.9$ in Couette flow.

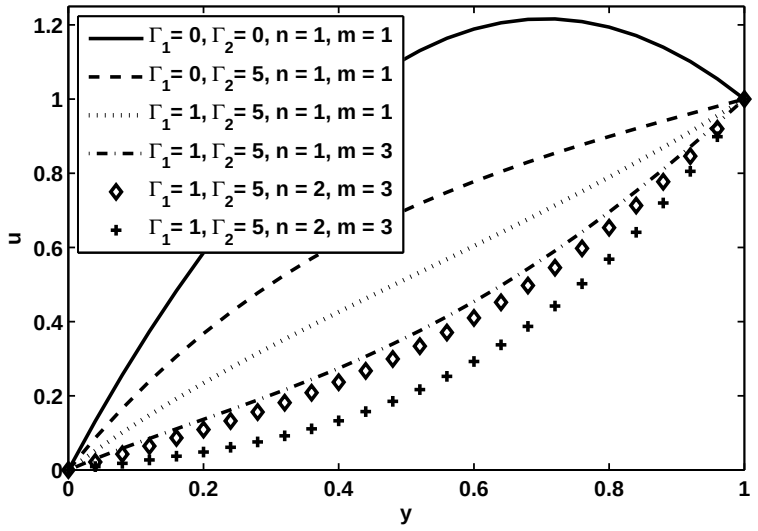

Figure 4.16: Velocity profile for $\mu(p) = A(\frac{p}{p_0})^n$ and $\alpha(p) = B(\frac{p}{p_0})^m$ with $\Gamma_3 = 5, W_e = 0.05$ and $U_0 = 0.9$ in Couette flow.

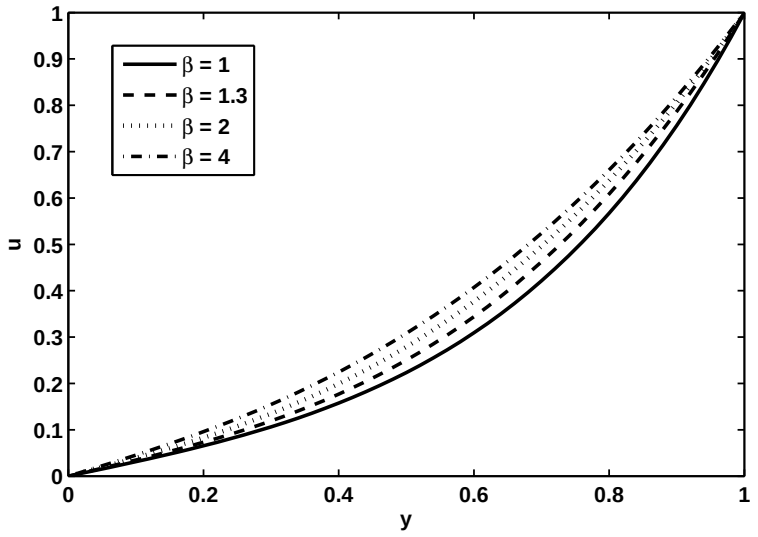

Figure 4.17: Velocity profile for $\mu(p) = Aexp(ap)$ and $\alpha(p) = Bexp(bp)$ with $\Gamma_1 = 1, \Gamma_2 = 5, \Gamma_3 = 1, \Gamma_4 = 1$ and $U_0 = 0.9$ in Couette flow.

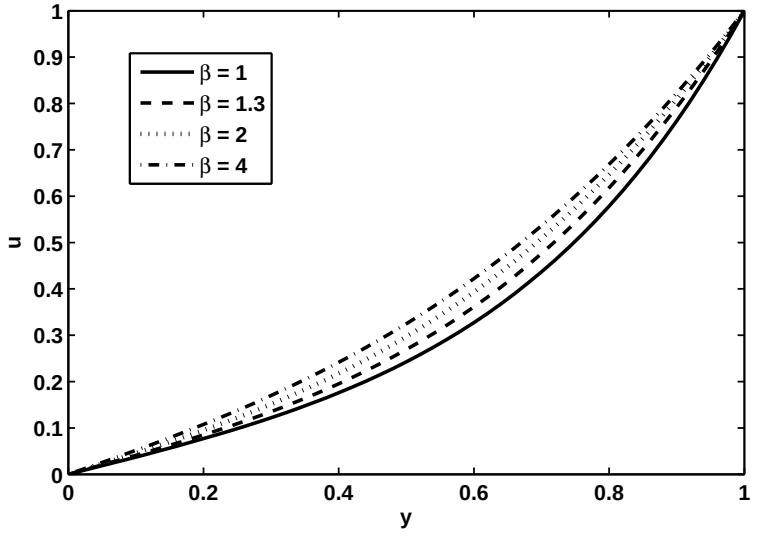

Figure 4.18: Velocity profile for $\mu(p) = Aexp(ap)$ and $\alpha(p) = B(\frac{p}{p_0})^m$ with $\Gamma_1 = 1, \Gamma_2 = 5, \Gamma_3 = 1, \Gamma_4 = 1, U_0 = 0.9$ and $m = 3$ in Couette flow.

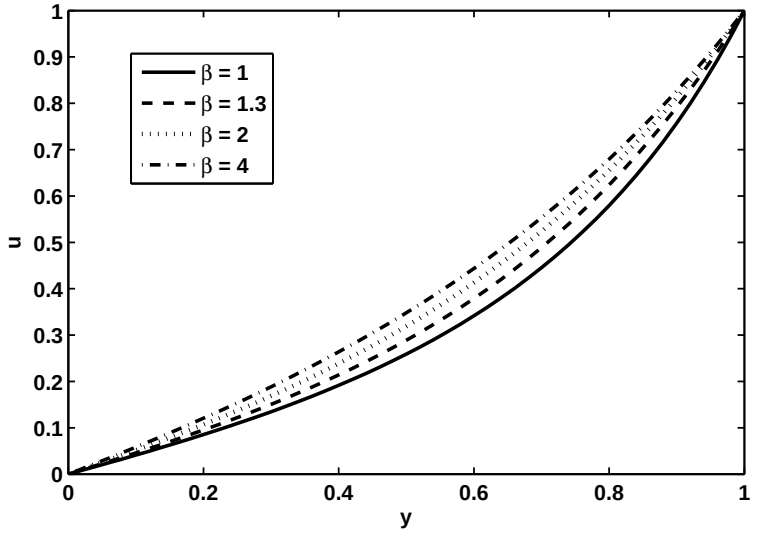

Figure 4.19: Velocity profile for $\mu(p) = A(\frac{p}{p_0})^n$ and $\alpha(p) = Bexp(bp)$ with $\Gamma_1 = 1, \Gamma_2 = 5, \Gamma_3 = 1, \Gamma_4 = 1, U_0 = 0.9$ and $n = 2$ in Couette flow.

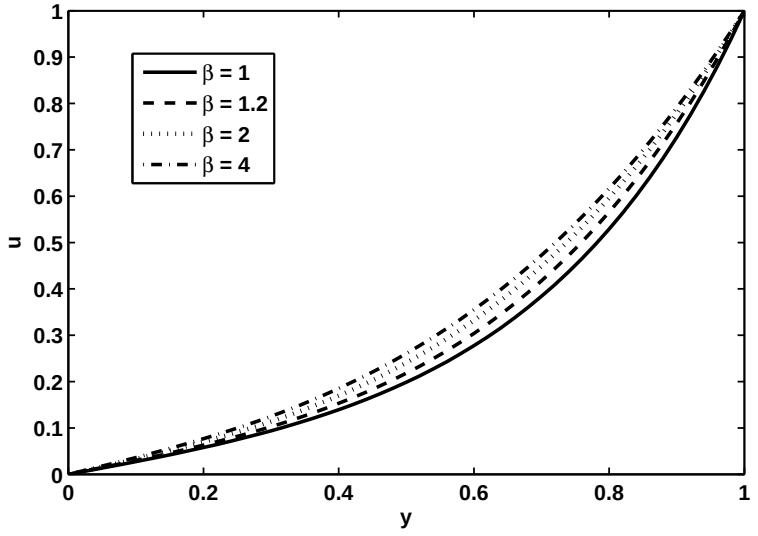

Figure 4.20: Velocity profile for $\mu(p) = A(\frac{p}{p_0})^n$ and $\alpha(p) = B(\frac{p}{p_0})^m$ with $\Gamma_1 = 1, \Gamma_2 = 5, \Gamma_3 = 1, U_0 = 0.9, m = 2$ and $n = 3$ in Couette flow.

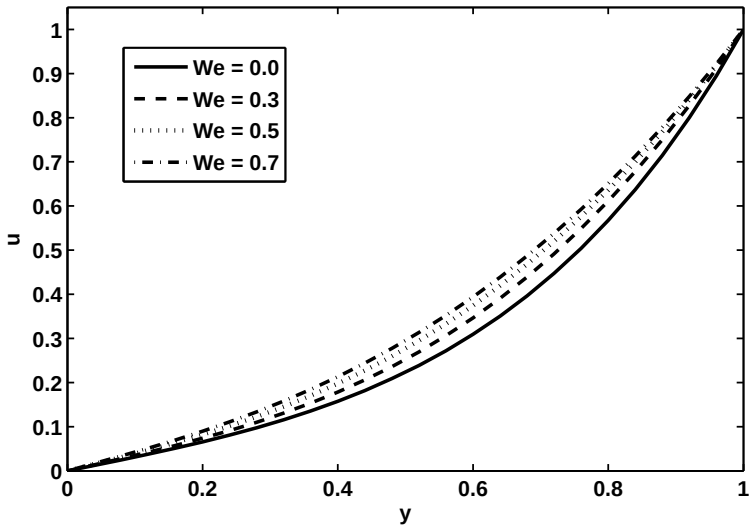

Figure 4.21: Velocity profile for $\mu(p) = Aexp(ap)$ and $\alpha(p) = Bexp(bp)$ with $\Gamma_1 = 1, \Gamma_2 = 5, \Gamma_3 = 1, \Gamma_4 = 1$ and $U_0 = 0.9$ in Couette flow.

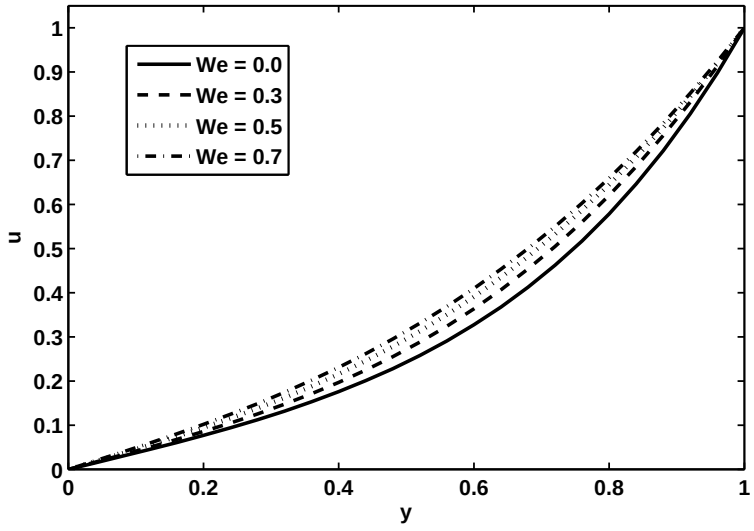

Figure 4.22: Velocity profile for $\mu(p) = Aexp(ap)$ and $\alpha(p) = B(\frac{p}{p_0})^m$ with $\Gamma_1 = 1, \Gamma_2 = 5, \Gamma_3 = 1, \Gamma_4 = 1, U_0 = 0.9$ and $m = 3$ in Couette flow.

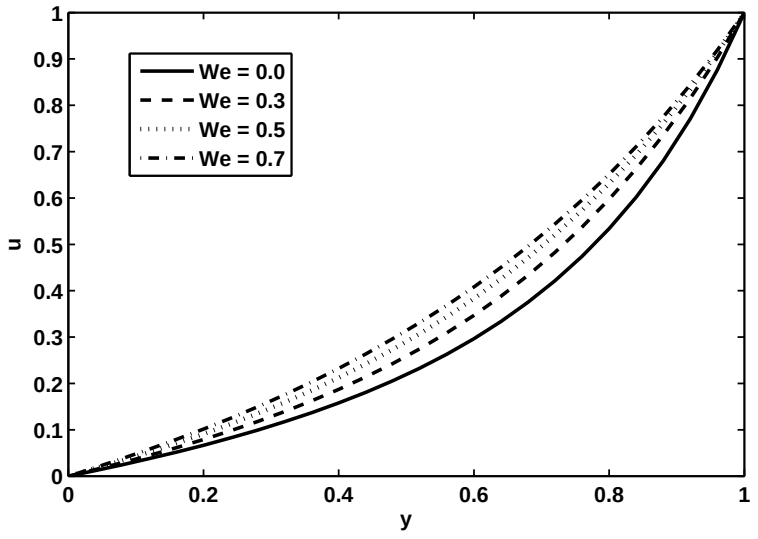

Figure 4.23: Velocity profile for $\mu(p) = A(\frac{p}{p_0})^n$ and $\alpha(p) = Bexp(bp)$ with $\Gamma_1 = 1, \Gamma_2 = 5, \Gamma_3 = 1, \Gamma_4 = 1, U_0 = 0.9$ and $n = 2$ in Couette flow.

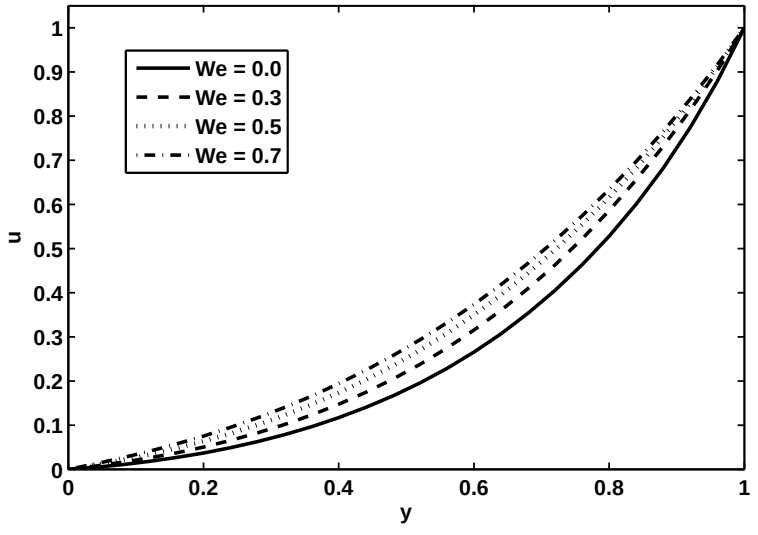

Figure 4.24: Velocity profile for $\mu(p) = A(\frac{p}{p_0})^n$ and $\alpha(p) = B(\frac{p}{p_0})^m$ with $\Gamma_1 = 1, \Gamma_2 = 5, \Gamma_3 = 1, U_0 = 0.9, m = 2$ and $n = 3$ in Couette flow.

Chapter 5

Numerical study of pressure dependent viscosity for Sutterby fluid through porous medium

5.1 Introduction

This chapter is focused on the numerical study of pressure dependent viscosity for Sutterby fluid through porous medium. Four different groupings of pressure dependent viscosity and pressure dependent porous medium parameters are analyzed for two types of fluid flow circumstances namely (i) Poiseuille flow and (ii) Couette flow. The solutions of nonlinear equations have been calculated numerically by shooting method along with Runge-Kutta Fehlberg technique. The physical features of relevant parameters have been discussed through graphs.

5.2 Fluid model

For unidirectional and incompressible flow through inclined channel with pressure dependent viscosity and pressure dependent porosity, the constitutive equation of extra stress tensor for Sutterby fluid is given by [52]

$$\boldsymbol{\tau} = \mu(p)\left[\frac{\sinh C\sqrt{(|\dot{\gamma}|)^2}}{C\sqrt{(|\dot{\gamma}|)^2}}\right]^{\beta}\dot{\gamma}, \tag{5.1}$$

where C is the material constant.

The extra stress tensor can be considered as

$$\begin{aligned}\boldsymbol{\tau} &= \mu(p)\left[\frac{1}{C\sqrt{(|\dot{\gamma}|)^2}}\left(C\sqrt{(|\dot{\gamma}|)^2} - \frac{1}{6}C^3(\sqrt{(|\dot{\gamma}|)^2})^3\right)^{\beta}\dot{\gamma}\right],\\ &= \mu(p)\left[1 - \frac{1}{6}C^2(\sqrt{(|\dot{\gamma}|)^2})^2\right]^{\beta}\dot{\gamma},\\ &= \mu(p)\left[1 - \frac{1}{6}\beta C^2(|\dot{\gamma}|)^2\right]\dot{\gamma}.\end{aligned} \tag{5.2}$$

5.3 Mathematical formulation

With the aid of extra stress tensor of Sutterby fluid and Eq. (1.6), the component form of Eq. (2.1) in the presence of gravity and porous medium take the forms

$$\begin{aligned}-\frac{\partial p}{\partial x} + \mu(p)[1 - \frac{1}{2}\beta C^2(\frac{du}{dy})^2]\frac{d^2u}{dy^2} + [1 - \frac{1}{6}\beta C^2(\frac{du}{dy})^2]\frac{du}{dy}\frac{d}{dy}\mu(p)\\ - \alpha(p)[1 - \frac{1}{6}\beta C^2(\frac{du}{dy})^2]u(y) + \rho g\sin\theta = 0,\end{aligned} \tag{5.3}$$

and

$$-\frac{\partial p}{\partial y} - \rho g\cos\theta = 0. \tag{5.4}$$

Using the following dimensionless quantity

$$\sigma = \frac{C^2 {U_c}^2}{h^2} \tag{5.5}$$

With the help of Eq.(1.9) and Eq.(2.8), Eqs.(5.3) and (5.4) after dropping the bars can be written as

$$[1-\frac{1}{2}\beta\sigma(\frac{du}{dy})^2]\frac{d^2u}{dy^2}+\frac{1}{\mu(p)}[1-\frac{1}{6}\beta\sigma(\frac{du}{dy})^2]\frac{du}{dy}\frac{d}{dy}\mu(p) - h^2\frac{\alpha(p)}{\mu(p)}[1-\frac{1}{6}\beta\sigma(\frac{du}{dy})^2]u(y)+\frac{\rho gh^2\sin\theta}{U_c\mu(p)}=0, \quad (5.6)$$

and

$$\frac{dp}{dy}+\rho gh\cos\theta=0. \quad (5.7)$$

The solution of Eq.(5.7) is

$$p=p_0+\rho gh\cos\theta(1-y). \quad (5.8)$$

By taking into account Eq. (5.7), the solution of Eq. (5.6) has been computed in the next section for two types of boundary conditions termed as

(i) Poiseuille flow

(ii) Couette flow

5.4 Poiseuille flow

In this case the boundaries are at rigid surfaces Eq.(1.26). Therefore, By using Eq.(1.14) to Eq. (1.17), Eq. (5.6) take the following forms

$$[1-\frac{1}{2}\beta\sigma(\frac{du}{dy})^2]\frac{d^2u}{dy^2}-\Gamma_1[1-\frac{1}{6}\beta\sigma(\frac{du}{dy})^2]\frac{du}{dy}-\Gamma_2[1-\frac{1}{6}\beta\sigma(\frac{du}{dy})^2]exp[\Gamma_4(1-y)]u(y) + \Gamma_3 exp[-\Gamma_1(1-y)]=0, \quad (5.9)$$

$$[1-\frac{1}{2}\beta\sigma(\frac{du}{dy})^2]\frac{d^2u}{dy^2}-\Gamma_1[1-\frac{1}{6}\beta\sigma(\frac{du}{dy})^2]\frac{du}{dy}-\Gamma_2[1-\frac{1}{6}\beta\sigma(\frac{du}{dy})^2][1+\Gamma_4(1-y)]^m exp[-\Gamma_1(1-y)]u(y)+\Gamma_3 exp[-\Gamma_1(1-y)]=0, \quad (5.10)$$

$$[1-\frac{1}{2}\beta\sigma(\frac{du}{dy})^2]\frac{d^2u}{dy^2}-\frac{n\Gamma_1}{1+\Gamma_1(1-y)}[1-\frac{1}{6}\beta\sigma(\frac{du}{dy})^2]\frac{du}{dy}-\Gamma_2[1-\frac{1}{6}\beta\sigma(\frac{du}{dy})^2]$$
$$[1+\Gamma_1(1-y)]^{-n}exp[\Gamma_4(1-y)]u(y)+\Gamma_3[1+\Gamma_1(1-y)]^{-n}=0, \quad (5.11)$$

$$[1-\frac{1}{2}\beta\sigma(\frac{du}{dy})^2]\frac{d^2u}{dy^2}-\frac{n\Gamma_1}{1+\Gamma_1(1-y)}[1-\frac{1}{6}\beta\sigma(\frac{du}{dy})^2]\frac{du}{dy}-\Gamma_2[1-\frac{1}{6}\beta\sigma(\frac{du}{dy})^2]$$
$$[1+\Gamma_1(1-y)]^{m-n}u(y)+\frac{\Gamma_3}{[1+\Gamma_1(1-y)]^n}=0, \quad (5.12)$$

5.5 Couette flow

In this case, the lower plate is at rest and the upper plate is moving with the velocity U_h. The boundary conditions for the problem in non dimensional form are Eq. (1.27) The governing equations are same as defined in previous section(Eqs.(5.9) to (5.12)).

5.6 Numerical solution and discussion

The solution for both the cases has been calculated by Shooting method using Runge-Kutta Fehlberg following the same scheme illustrated in chapter two. The nonlinear momentum equation of Sutterby fluid with pressure dependent viscosities has been solved numerically for Poiseuille flow and Couette flow. The results have been displayed through tables and graphs. Table 5.1 describes the outcomes for Poiseuille flow. Numerical results are noted for all the four cases. The analysis of the numerical results shows that when porosity is fixed to be exponentially depending upon pressure, the rational form of pressure dependent viscosity accelerates the fluid flow as compare to the exponential form of viscosity. Similarly when we fix viscosity to be an exponential function of pressure greater fluid velocity is attain for exponentially dependent porosity as compare to the rational function of pressure for porosity. Thus, it is concluded that for Poiseuille flow the case

III generates better results.

Figures 5.1 to 5.4 display the velocity field for different values of $\Gamma's$ for various values of pressure dependent viscosity. It predicts that with the rise in $\Gamma's$, the velocity field decreases for each case of viscosity and porosity. Also, the velocity is maximum at the centre of the channel and gives the maximum values in the absence of $\Gamma's$. The Sutterby fluid model covers the three major classes of fluids i.e., for power law index $\beta = 0$ it represents Newtonian fluids, for $\beta < 1$, it demonstrates the behaviour of shear thinning fluids and for $\beta \geq 1$ it gives results for shear thickening fluids. The velocity profile for different values of power law index β is shown through figures 5.5 to 5.8. It is observed that with an increase in the power law index β, the velocity profile improves for four different cases of viscosity and porosity parameter. The non-dimensional quantity σ is the fluid property parameter. Figures 5.9 to 5.12 present the influence of σ on the fluid flow for different cases of pressure dependent viscosity and porosity. The rise in σ contributes in surging the fluid flow for all the four cases.

Table 5.2 illustrates the numerical results of Couette flow for four different cases of pressure dependent viscosity and porosity. The comparison of the numerical results for case I and case III, viscosity considered as rational function of pressure increases fluid velocity. Also when porosity expression variations are considered, exponential form of porosity plays role in enhancing fluid flow. The general investigation of all the four cases reveals that case III is the better choice of pressure dependent viscosity and porosity to attain more fluid velocity. Figures 5.13 to 5.24 are the graphical illustration for Couette flow. The velocity profile of $\Gamma's$ for Couette flow are shown through the figures 5.13 to 5.16. It is explored that velocity field reduces with an increase in the values of $\Gamma's$ for all the four cases of viscosity and porous medium parameter. Thus, we can determine that the pressure dependent viscosity causes deterioration in velocity. It has been realized that

the velocity field for Couette flow gives larger values in the absence of $\Gamma's$ as Poiseuille flow does. In figures 5.17 to 5.20 the velocity profile for different values of power law index β are displayed. It is seen that the velocity field diminishes with an upturn in power law index β for all the four cases. Variation of fluid property parameter σ for velocity profile in Couette flow is shown through figures 5.21 to 5.24. Velocity profile drops off with a boost in the values of σ for each case of viscosity and porosity. This leads to the fact that for shearing thickening fluids velocity field lessen as compare to the shearing thinning and Newtonian fluids.

	u(y)			
y	**Case I**	**Case II**	**Case III**	**Case IV**
0	0	0	0	0
0.10	0.055982840	0.051346937	0.055620714	0.042314787
0.20	0.103198600	0.093791074	0.104562775	0.078726081
0.30	0.143469991	0.129673748	0.146522910	0.110404749
0.40	0.176783683	0.159600538	0.180599112	0.137479448
0.50	0.201469258	0.182470674	0.205103264	0.158924478
0.60	0.214171348	0.195321400	0.217246224	0.172268350
0.70	0.209656112	0.193033052	0.212601864	0.173064329
0.80	0.180409898	0.167896051	0.184142827	0.153979133
0.90	0.115806704	0.108892644	0.120296995	0.103100376
1.00	0	0	0	0

Table 5.1: Velocity for $\Gamma_1 = 1, \Gamma_2 = 5, \Gamma_3 = 5, \Gamma_4 = 1, \beta = 0.5, m = 3, n = 2$ and $\sigma = 0.3$ for Poiseuille flow

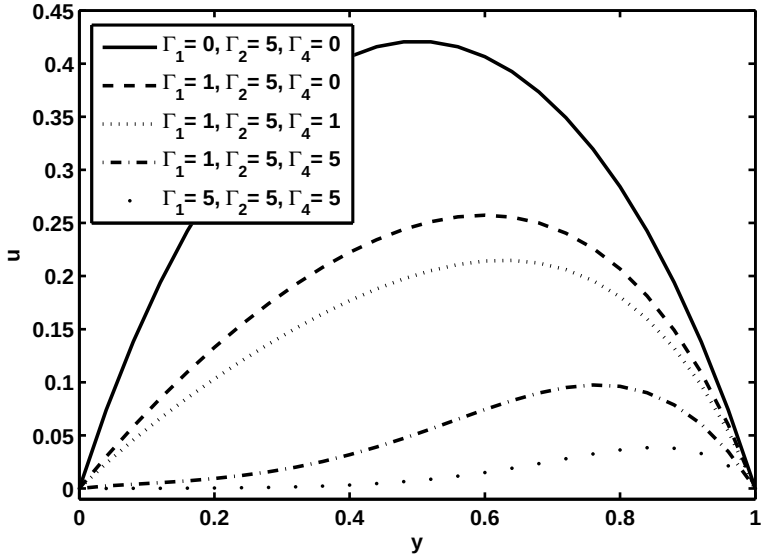

Figure 5.1: Velocity profile for $\mu(p) = Aexp(ap)$ and $\alpha(p) = Bexp(bp)$ with $\beta = 0.4$ and $We = 0.05$ in Poiseuille flow.

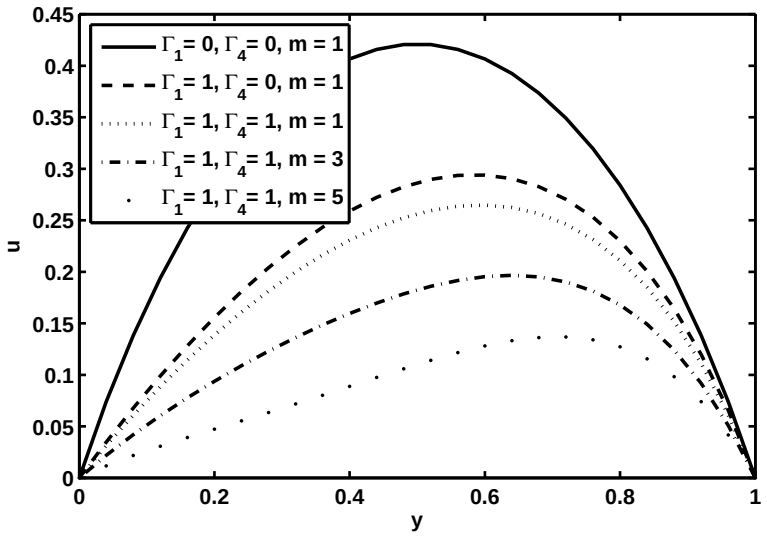

Figure 5.2: Velocity profile for $\mu(p) = Aexp(ap)$ and $\alpha(p) = B(\frac{p}{p_0})^m$ with $\Gamma_3 = 5, \beta = 0.4$ and $We = 0.05$ in Poiseuille flow.

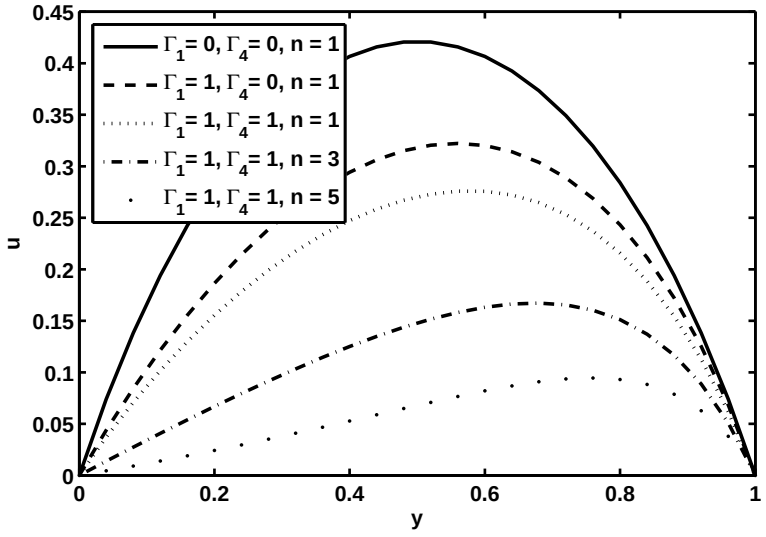

Figure 5.3: Velocity profile for $\mu(p) = A(\frac{p}{p_0})^n$ and $\alpha(p) = Bexp(bp)$ with $\Gamma_3 = 5, \beta = 0.4$ and $We = 0.05$ in Poiseuille flow.

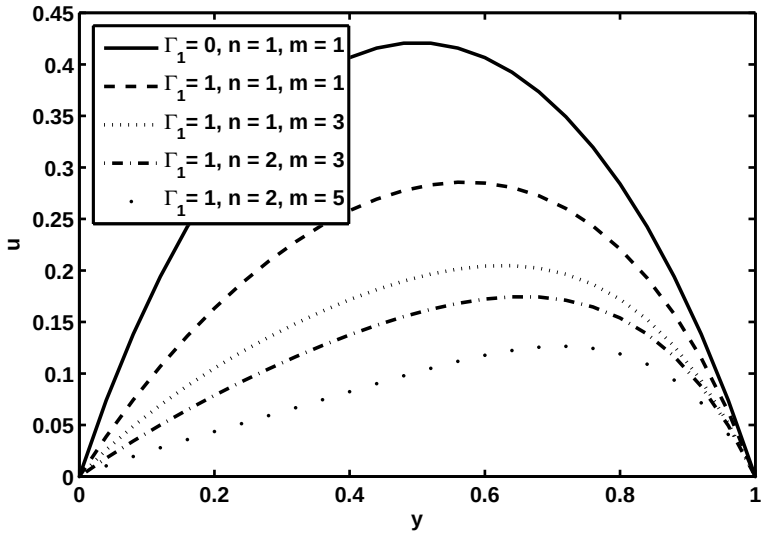

Figure 5.4: Velocity profile for $\mu(p) = A(\frac{p}{p_0})^n$ and $\alpha(p) = B(\frac{p}{p_0})^m$ with $\Gamma_3 = 5, \beta = 0.4$ and $We = 0.05$ in Poiseuille flow.

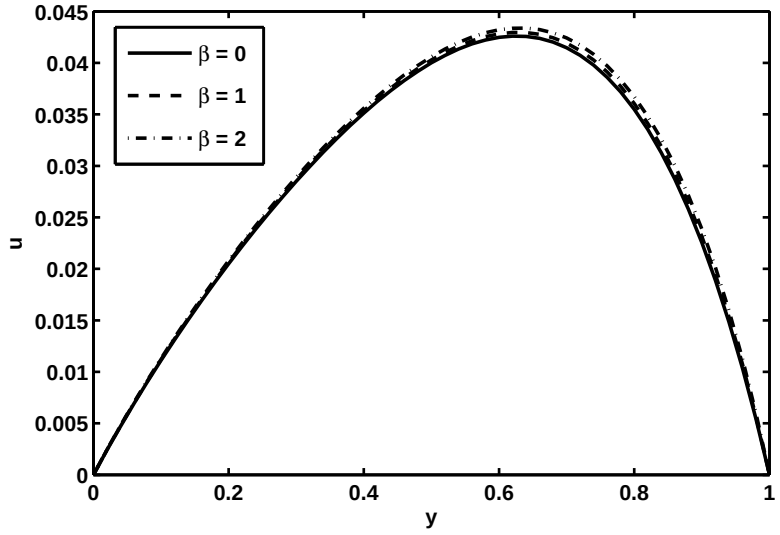

Figure 5.5: Velocity profile for $\mu(p) = Aexp(ap)$ and $\alpha(p) = Bexp(bp)$ with $\Gamma_1 = 1, \Gamma_2 = 10, \Gamma_3 = 10$ and $\Gamma_4 = 1$ in Poiseuille flow.

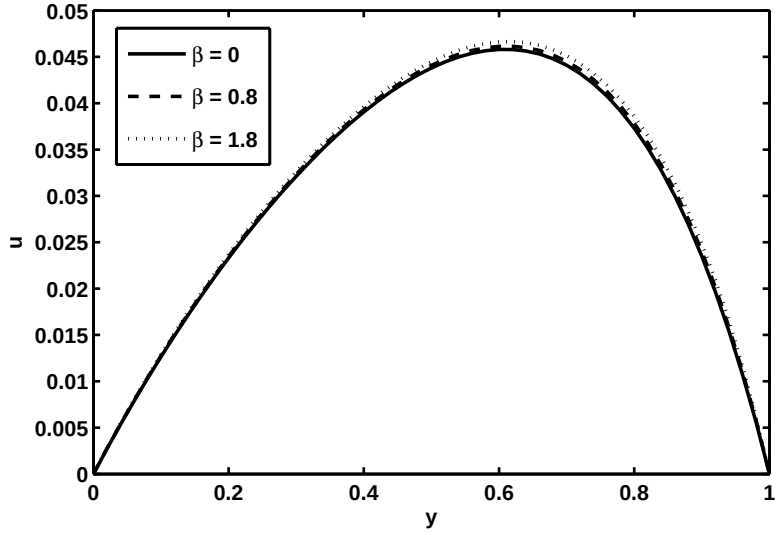

Figure 5.6: Velocity profile for $\mu(p) = Aexp(ap)$ and $\alpha(p) = B(\frac{p}{p_0})^m$ with $\Gamma_1 = 1, \Gamma_2 = 10, \Gamma_3 = 10, \Gamma_4 = 1$ and $m = 2$ in Poiseuille flow.

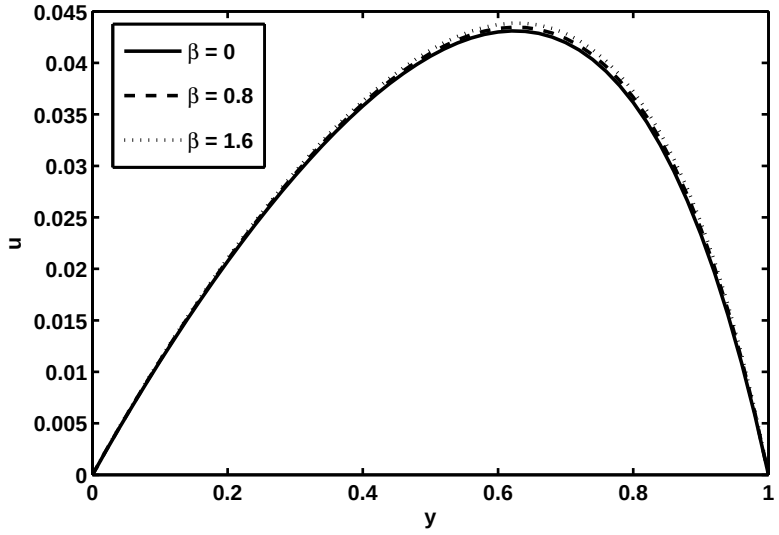

Figure 5.7: Velocity profile for $\mu(p) = A(\frac{p}{p_0})^n$ and $\alpha(p) = Bexp(bp)$ with $\Gamma_1 = 1, \Gamma_2 = 10, \Gamma_3 = 10, \Gamma_4 = 1$ and $n = 2$ in Poiseuille flow.

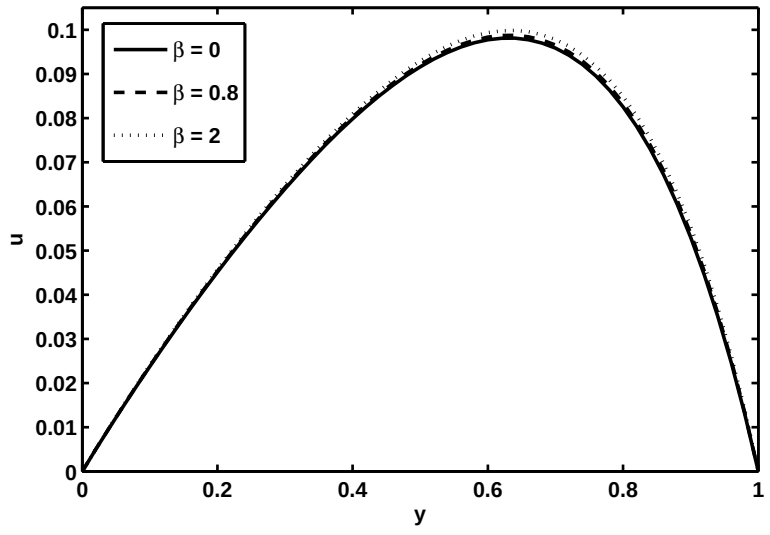

Figure 5.8: Velocity profile for $\mu(p) = A(\frac{p}{p_0})^n$ and $\alpha(p) = B(\frac{p}{p_0})^m$ with $\Gamma_1 = 1, \Gamma_2 = 10, \Gamma_3 = 10, m = 1$ and $n = 2$ in Poiseuille flow.

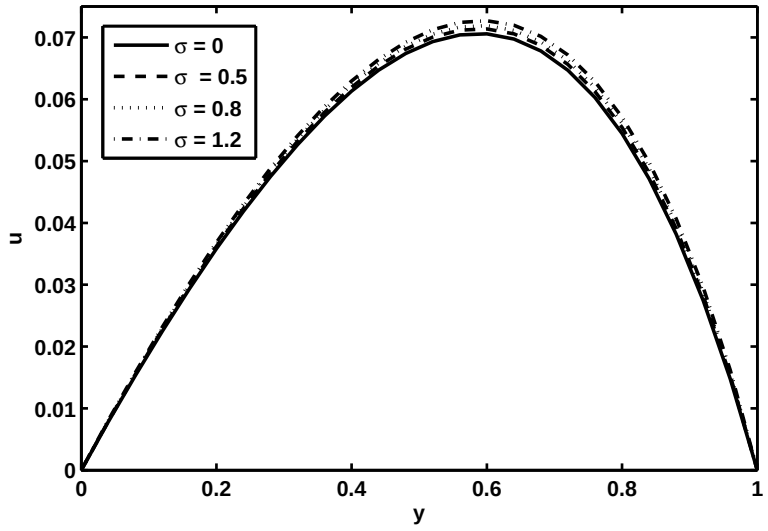

Figure 5.9: Velocity profile for $\mu(p) = Aexp(ap)$ and $\alpha(p) = B(\frac{p}{p_0})^m$ with $\Gamma_1 = 1, \Gamma_2 = 10, \Gamma_3 = 10, \Gamma_4 = 1$ and $\lambda_1 = 0.5$ in Poiseuille flow.

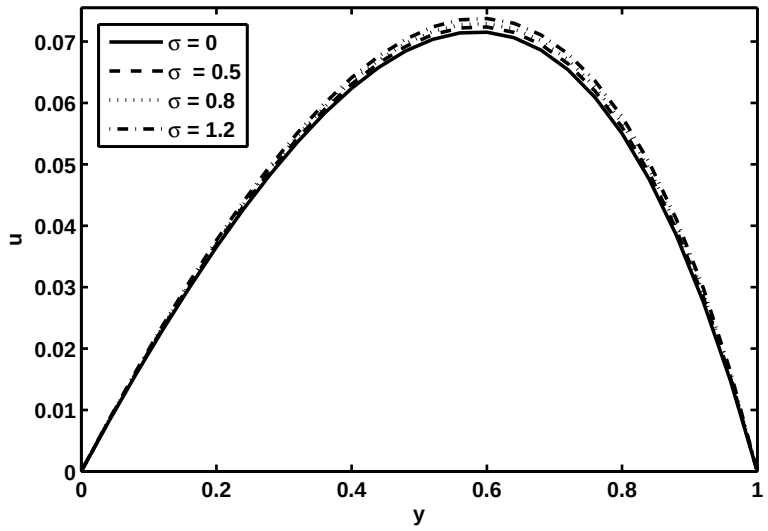

Figure 5.10: Velocity profile for $\mu(p) = A(\frac{p}{p_0})^n$ and $\alpha(p) = Bexp(bp)$ with $\Gamma_1 = 1, \Gamma_2 = 10, \Gamma_3 = 10, \Gamma_4 = 1$ and $\lambda_1 = 0.5$ in Poiseuille flow.

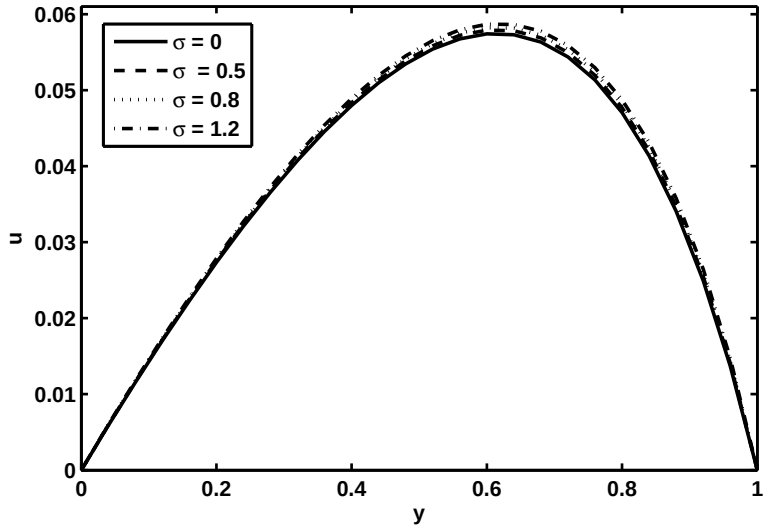

Figure 5.11: Velocity profile for $\mu(p) = A(\frac{p}{p_0})^n$ and $\alpha(p) = B(\frac{p}{p_0})^m$ with $\Gamma_1 = 1, \Gamma_2 = 10, \Gamma_3 = 10, m = 3$ and $\lambda_1 = 0.5$ in Poiseuille flow.

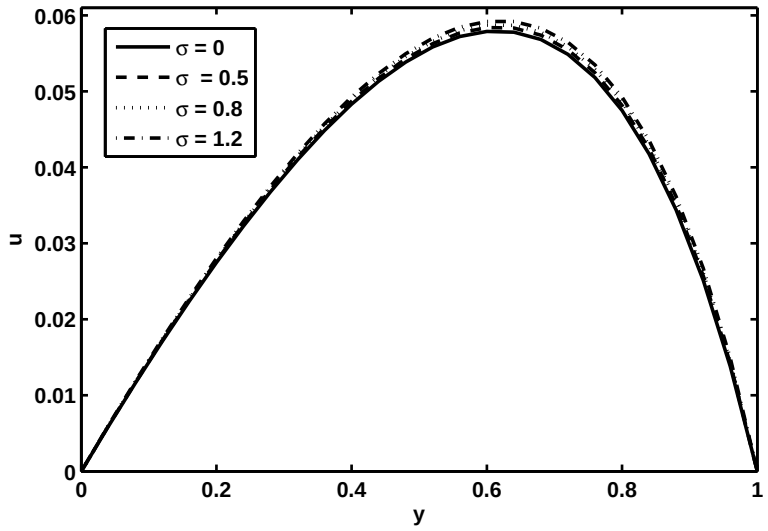

Figure 5.12: Velocity profile for $\mu(p) = A(\frac{p}{p_0})^n$ and $\alpha(p) = B(\frac{p}{p_0})^m$ with $\Gamma_1 = 1, \Gamma_2 = 10, \Gamma_3 = 10, n = 3$ and $\lambda_1 = 0.5$ in Poiseuille flow.

	u(y)			
y	**Case I**	**Case II**	**Case III**	**Case IV**
0	0	0	0	0
0.10	0.076396795	0.068278333	0.086046150	0.061136918
0.20	0.148642742	0.131797769	0.169731130	0.120280743
0.30	0.221792674	0.196150793	0.252750022	0.181300343
0.40	0.299659425	0.266047876	0.336808699	0.247798778
0.50	0.385271706	0.345677379	0.423734833	0.323398845
0.60	0.481112618	0.438846957	0.515621860	0.411991259
0.70	0.589218109	0.548925563	0.615036368	0.517983746
0.80	0.711171134	0.548925563	0.725344935	0.646603362
0.90	0.848003352	0.829173173	0.851276592	0.646603362
1.00	1.00	1.00	1.00	1.00

Table 5.2: Velocity for $\Gamma_1 = 1, \Gamma_2 = 5, \Gamma_3 = 5, \Gamma_4 = 1, \beta = 0.5, m = 3, n = 2, \sigma = 0.3$ and $U_0 = 1$ for Couette flow

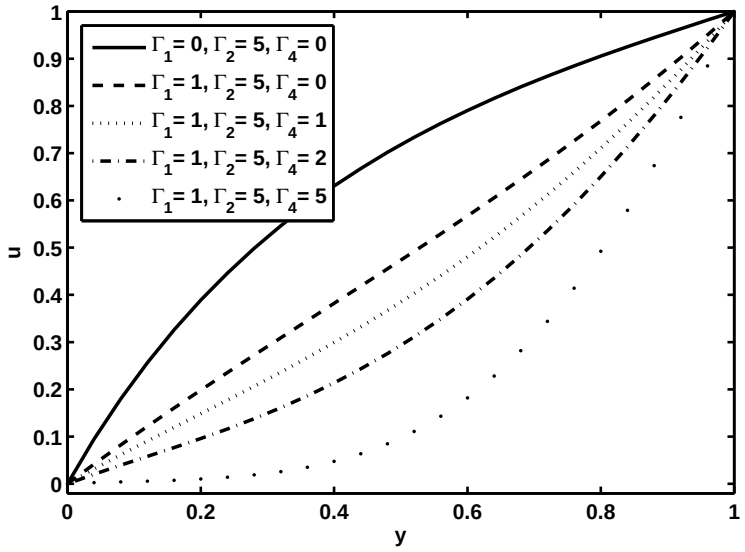

Figure 5.13: Velocity profile for $\mu(p) = Aexp(ap)$ and $\alpha(p) = B(\frac{p}{p_0})^m$ with $\Gamma_3 = 5, W_e = 0.05$ and $U_0 = 0.9$ in Couette flow.

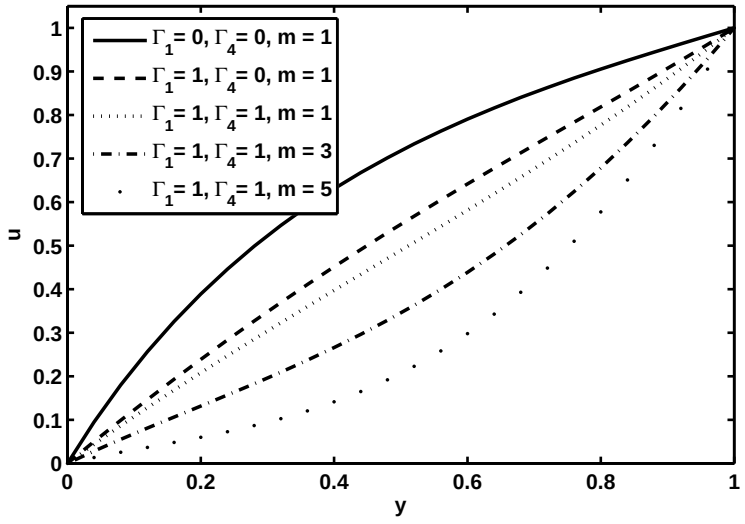

Figure 5.14: Velocity profile for $\mu(p) = Aexp(ap)$ and $\alpha(p) = B(\frac{p}{p_0})^m$ with $\Gamma_3 = 5, W_e = 0.05$ and $U_0 = 0.9$ in Couette flow.

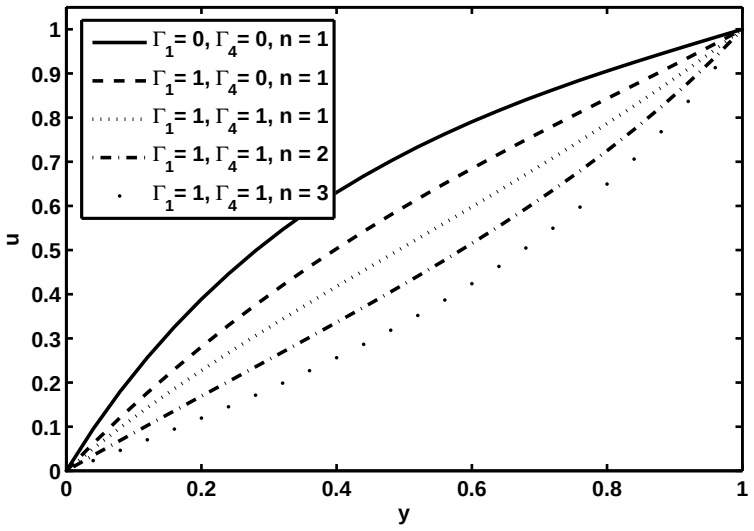

Figure 5.15: Velocity profile for $\mu(p) = A(\frac{p}{p_0})^n$ and $\alpha(p) = Bexp(bp)$ with $\Gamma_3 = 5, W_e = 0.05$ and $U_0 = 0.9$ in Couette flow.

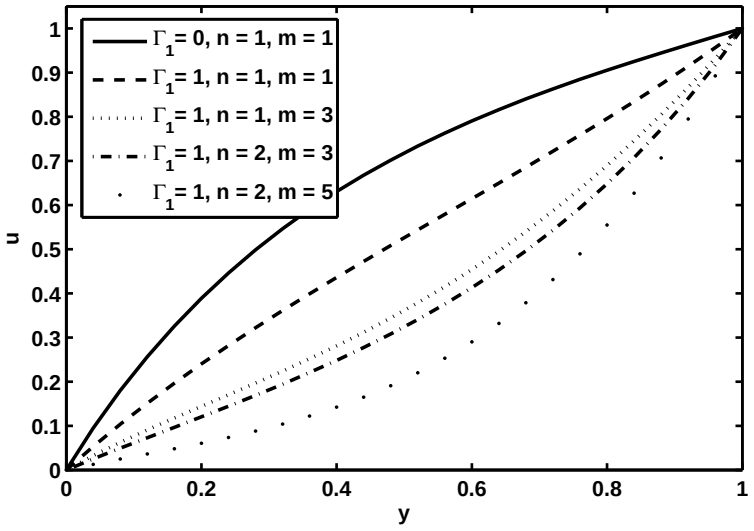

Figure 5.16: Velocity profile for $\mu(p) = A(\frac{p}{p_0})^n$ and $\alpha(p) = B(\frac{p}{p_0})^m$ with $\Gamma_3 = 5, W_e = 0.05$ and $U_0 = 0.9$ in Couette flow.

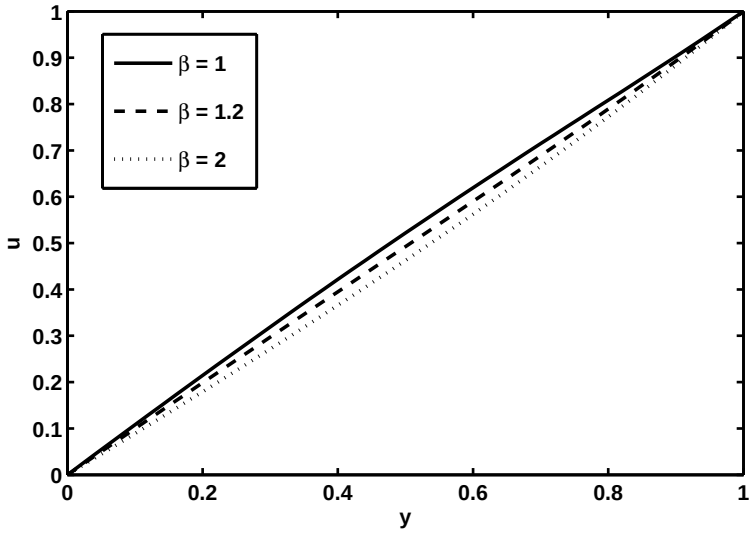

Figure 5.17: Velocity profile for $\mu(p) = Aexp(ap)$ and $\alpha(p) = Bexp(bp)$ with $\Gamma_1 = 1, \Gamma_2 = 5, \Gamma_3 = 1, \Gamma_4 = 1$ and $U_0 = 0.9$ in Couette flow.

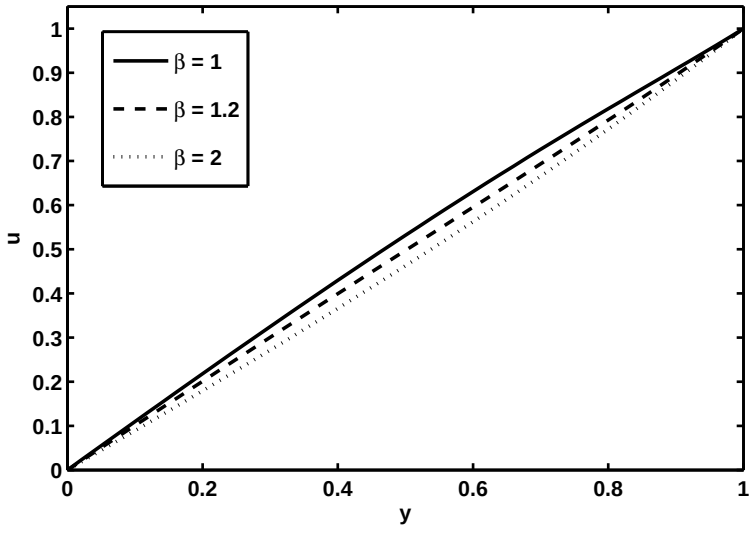

Figure 5.18: Velocity profile for $\mu(p) = Aexp(ap)$ and $\alpha(p) = B(\frac{p}{p_0})^m$ with $\Gamma_1 = 1, \Gamma_2 = 5, \Gamma_3 = 1, \Gamma_4 = 1, U_0 = 0.9$ and $m = 3$ in Couette flow.

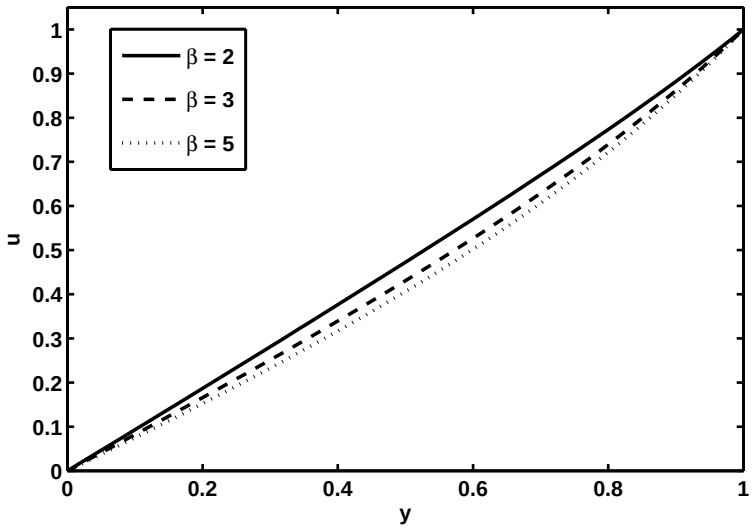

Figure 5.19: Velocity profile for $\mu(p) = A(\frac{p}{p_0})^n$ and $\alpha(p) = Bexp(bp)$ with $\Gamma_1 = 1, \Gamma_2 = 5, \Gamma_3 = 1, \Gamma_4 = 1, U_0 = 0.9$ and $n = 2$ in Couette flow.

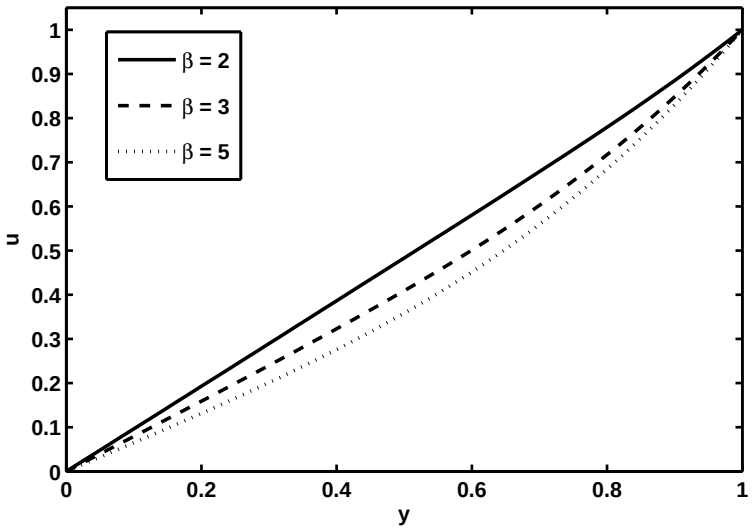

Figure 5.20: Velocity profile for $\mu(p) = A(\frac{p}{p_0})^n$ and $\alpha(p) = B(\frac{p}{p_0})^m$ with $\Gamma_1 = 1, \Gamma_2 = 5, \Gamma_3 = 1, U_0 = 0.9, m = 2$ and $n = 3$ in Couette flow.

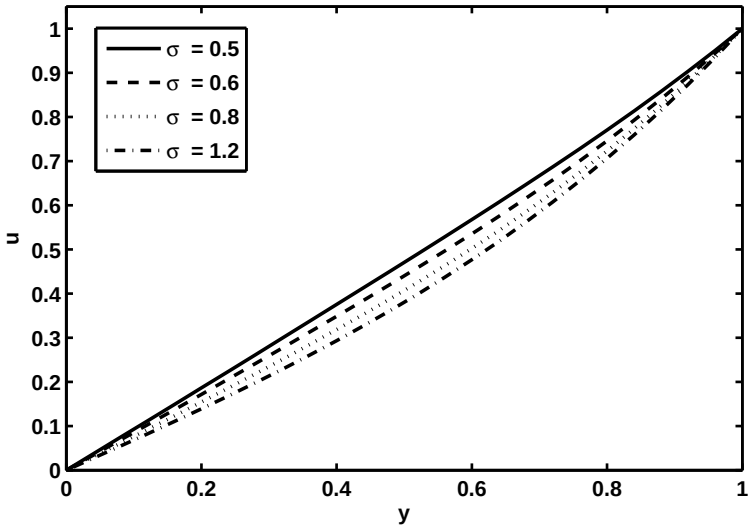

Figure 5.21: Velocity profile for $\mu(p) = Aexp(ap)$ and $\alpha(p) = Bexp(bp)$ with $\Gamma_1 = 1, \Gamma_2 = 5, \Gamma_3 = 1, \Gamma_4 = 1$ and $U_0 = 0.9$ in Couette flow.

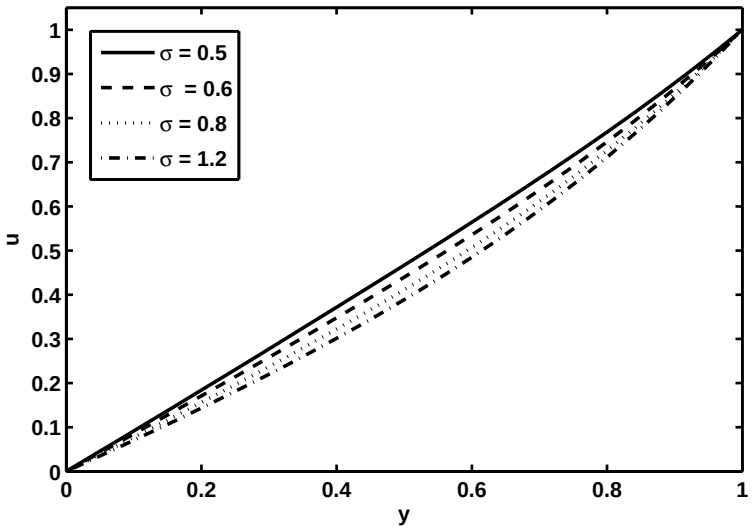

Figure 5.22: Velocity profile for $\mu(p) = Aexp(ap)$ and $\alpha(p) = B(\frac{p}{p_0})^m$ with $\Gamma_1 = 1, \Gamma_2 = 5, \Gamma_3 = 1, \Gamma_4 = 1, U_0 = 0.9$ and $m = 3$ in Couette flow.

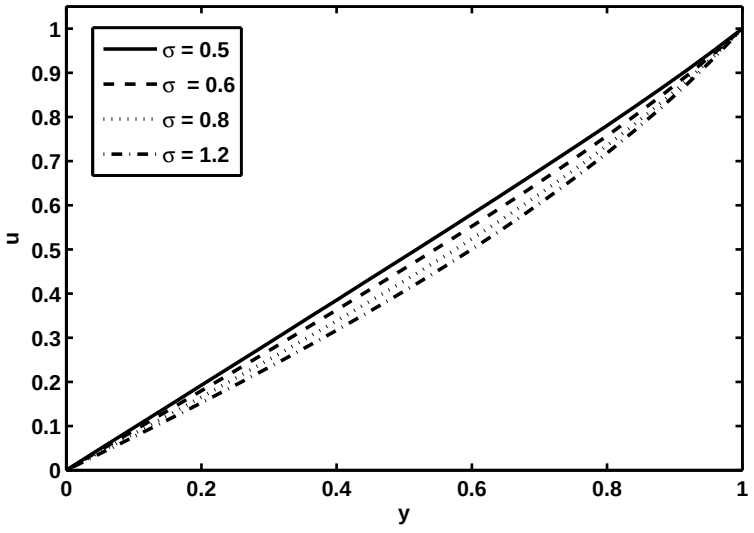

Figure 5.23: Velocity profile for $\mu(p) = A(\frac{p}{p_0})^n$ and $\alpha(p) = Bexp(bp)$ with $\Gamma_1 = 1, \Gamma_2 = 5, \Gamma_3 = 1, \Gamma_4 = 1, U_0 = 0.9$ and $n = 2$ in Couette flow.

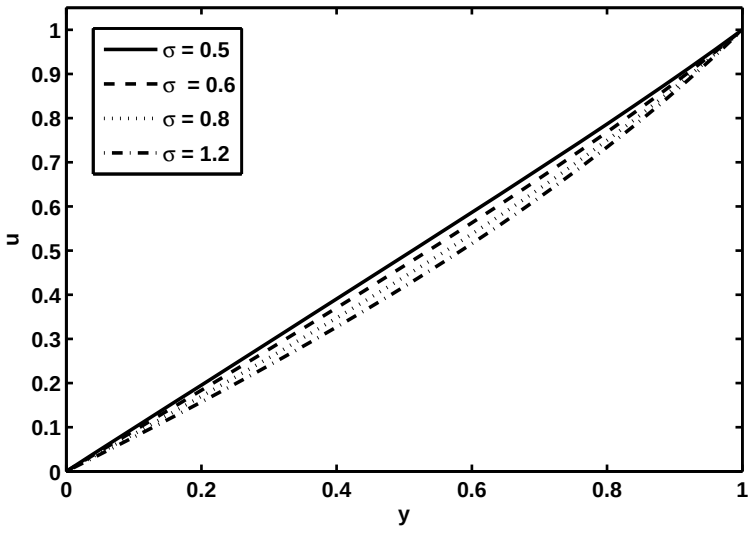

Figure 5.24: Velocity profile for $\mu(p) = A(\frac{p}{p_0})^n$ and $\alpha(p) = B(\frac{p}{p_0})^m$ with $\Gamma_1 = 1, \Gamma_2 = 5, \Gamma_3 = 1, U_0 = 0.9, m = 2$ and $n = 3$ in Couette flow.

Chapter 6

Numerical investigation of couple stress fluid over an elasting stretching sheet with pressure dependent viscosity

6.1 Introduction

In this chapter, we have examined the steady flow of couple stress fluid with pressure dependent viscosity between two parallel plates in which the lower plate is stretched while the upper plate is moving with constant velocity. The governing two dimensional nonlinear partial differential equations are simplified by using suitable supposed form of velocities. The simplified nonlinear ordinary differential equations are solved numerically. The physical features of pertinent parameters have been investigated through graphs and numerical data. The shear stresses at upper and lower plate are also evaluated.

6.2 Fluid model

The basic equations governing the flow of an incompressible couple stress fluid are [53]

$$\rho\frac{D\mathbf{V}}{Dt} = div\mathbf{T} - \eta\nabla^4\mathbf{V} + \rho\mathbf{b}_e, \tag{6.1}$$

where η is the couple stress parameter and the operator D/Dt denotes the material derivative. The Cauchy stress tensor $\mathbf{T}$ can be defined as

$$\mathbf{T} = -p\mathbf{I} + \mu(p)\mathbf{A}_1 \tag{6.2}$$

where p is the dynamic pressure, $\mathbf{I}$ is the unit tensor, $\mathbf{A}_1$ is the first Rivlin-Ericksen tensor and μ is the viscosity which is a function of pressure. Assuming the following two forms

$$\mu(p) = \chi^{\varepsilon p}, \qquad \chi > 0, \qquad \varepsilon > 0, \tag{6.3}$$

and

$$\mu(p) = \chi(1 + \varepsilon p), \qquad \chi > 0, \qquad \varepsilon > 0. \tag{6.4}$$

In both the cases, the viscosity tends to infinity as p tends to infinity. The viscosity form (6.3) is used in problems of elastohydrodynamics, using Barus formula for the viscosity, in which ε is the pressure coefficient for the viscosity, ε^{-1} has units of pressure and it is approximately equals to 50MPa for certain mineral oils, similarly it has different values for other non-Newtonian fluids.

6.3 Mathematical formulation

Consider the steady flow of an incompressible couple stress fluid between an elastic stretching sheet and a rigid plate which are placed a distance H apart. Consider a velocity and pressure fields of the form

$$u = xf'(y) + l'(y), \quad v = -f(y), \quad w = 0, \quad p = p(y), \tag{6.5}$$

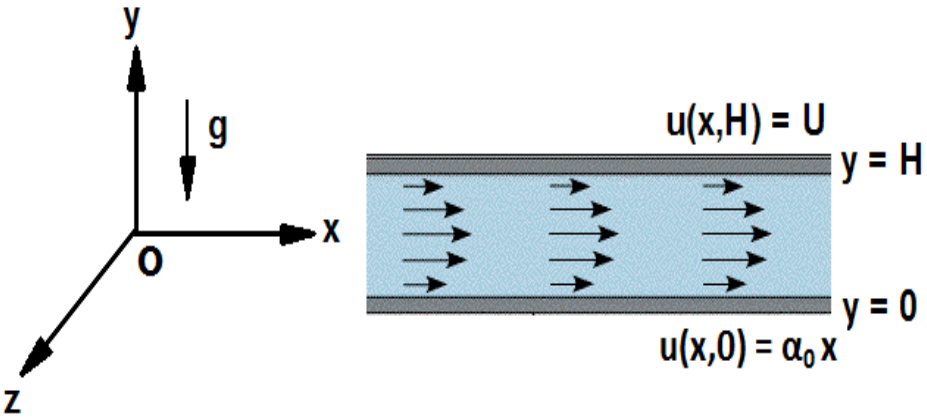

Figure 6.1: Flow between a porous plate and a stretching sheet.

where u, v and w are the x, y and z component of the velocity respectively.

Since the fluid is incompressible, it can only undergo isochoric motions. Under these assumptions, the continuity Eq. (1.1) is identically satisfied and the momentum Eq. (6.1) reduces to

$$\rho(xf'^2 + f'l' - xff'' - fl'') = -\frac{\partial p}{\partial x} + \frac{\partial}{\partial y}(2\mu(p)f') + \frac{\partial}{\partial y}[\mu(p)(xf'' + l'')] - \eta[x\frac{\partial^{(5)}}{\partial y^{(5)}}f(y) + \frac{\partial^{(5)}}{\partial y^{(5)}}l(y)], \quad (6.6)$$

$$\rho ff' = -\frac{\partial p}{\partial y} + \frac{\partial}{\partial x}[\mu(p)(xf''' + l'')] - \frac{\partial}{\partial y}(2\mu(p)f') - \eta\frac{\partial^{(4)}}{\partial y^{(4)}}f(y) - \rho g, \quad (6.7)$$

$$-\frac{\partial p}{\partial z} = 0. \quad (6.8)$$

It follow, from Eqs. (6.3) and (6.4) that

$$\mu(p) = \mu(p(y)). \quad (6.9)$$

Simplification of Eqs. (6.6)–(6.8) by using Eq. (6.9) leads to

$$\rho(xf'^2 + f'l' - xff'' - fl'') = (xf''(y) + l''(y))\frac{d}{dy}\mu(p) + \mu(p)(xf'''(y) + l'''(y)) - \eta[xf^{(5)}(y) + l^{(5)}(y)], \quad (6.10)$$

$$\rho f f' = -\frac{dp}{dy} - \mu(p) f''(y) - 2f'(y)\frac{d}{dy}\mu(p) - \eta f^{(4)}(y) - \rho g, \tag{6.11}$$

It follows from Eq. (6.10) that

$$\rho(f'^2 - f f'') = f''(y)\frac{d}{dy}\mu(p) + \mu(p) f'''(y) - \eta f^{(5)}(y), \tag{6.12}$$

$$\rho(f' l' - f l'') = l''(y)\frac{d}{dy}\mu(p) + \mu(p) l'''(y) - \eta l^{(5)}(y). \tag{6.13}$$

For the three unknowns p, f and l, Eqs. (6.11)-(6.13) form the system of coupled ordinary differential equations. The associated boundary conditions for the problem of the top plate moving with the speed U along the x-direction and the bottom boundary being stretched so that $u(x,0) = \alpha_0 x$, are

$$\begin{aligned} f(0) = 0, \qquad f'(0) = \alpha_0, \qquad f'(H) = 0, \\ l(0) = 0, \qquad l'(0) = 0, \qquad l'(H) = U. \end{aligned} \tag{6.14}$$

As the couple stresses are zero at the plates, $u''(x,0) = 0 = u''(x,H)$ implies that

$$\begin{aligned} f'''(0) = 0, f'''(H) = 0, \\ l'''(0) = 0, l'''(H) = 0. \end{aligned} \tag{6.15}$$

Assume that the pressure for the top plate is p_0,i.e.,

$$p(H) = p_0. \tag{6.16}$$

Introduce the following non-dimensional parameters:

$$\begin{aligned} \bar{x} = \frac{x}{H}, \bar{y} = \frac{y}{H}, \bar{u} = \frac{u}{U}, \bar{\mu} = \frac{\mu}{\mu_0}, \bar{p} = \frac{p}{p_0}, \bar{f} = \frac{f}{U}, \bar{l} = \frac{l}{U}, \\ Re = \frac{\rho U H}{\mu_0}, M = \frac{\mu_0 U}{p_0 H}, N = \frac{\eta}{\mu_0 H^2}, C = \frac{\rho g H}{p_0}, E = \varepsilon p_0. \end{aligned} \tag{6.17}$$

Using these dimensionless parameters, Eqs. (6.11) to (6.13) take the form (dropping bars)

$$MRe f f' = -\frac{dp}{dy} - M\mu(p) f''(y) - 2M f'(y)\frac{d}{dy}\mu(p) - MN f^{(4)}(y) - C, \tag{6.18}$$

$$Re(f'^2 - f f'') = f''\frac{d}{dy}\mu(p) + \mu(p) f'''(y) - N f^{(5)}(y), \tag{6.19}$$

$$Re(f' l' - f l'') = l''(y)\frac{d}{dy}\mu(p) + \mu(p) l'''(y) - N l^{(5)}(y), \tag{6.20}$$

and the corresponding boundary conditions become

$$\begin{gathered} f(0) = 0, f'(0) = \alpha_0, f'(1) = 0, f'''(0) = 0, f'''(1) = 0, \\ l(0) = 0, l'(0) = 0, l'(1) = U, l'''(0) = 0, l'''(1) = 0, p(1) = 1. \end{gathered} \tag{6.21}$$

The dimensionless form of the viscosity are given by

$$\mu(p) = e^{E(p-1)}, \tag{6.22}$$

$$\mu(p) = \frac{1 + Ep}{1 + E}. \tag{6.23}$$

The shear stresses on the lower plate and upper plate are given by

$$\boldsymbol{\tau} = \mu(p)\frac{du}{dy}\bigg|_{y=0,H}, \tag{6.24}$$

and the skin friction coefficient can be written as

$$C_f = x\frac{d}{dy} f'(y)\bigg|_{y=0,1} + \frac{d}{dy} l'(y)\bigg|_{y=0,1} \tag{6.25}$$

6.4 Solution of the problem

We need to solve the system of ordinary differential equations (6.18) to (6.20), subject to the boundary conditions (6.21), and $\mu(p)$ given by (6.22) and (6.23). These equations are solved numerically by using a solver for boundary value problems bvp[traprich] available in Maple.

6.4.1 Numerical results and discussion

The governing equations of couple stress fluid with pressure-dependent viscosities between an elastic stretching sheet and a rigid plate have been solved numerically by trapezoid method that use Richardson extrapolation enhancement. The effect of various non dimensional parameters on velocity components $f(y)$, $l(y)$, pressure field $p(y)$ and shear stress are investigated through graphs and tables respectively. Table 6.1-6.2 gives the numerical values of pressure field for both the form of pressure dependent viscosities with the variation of Reynolds number. It is observed that the pressure on the lower boundary $y = 0$ rises with the increase of Reynolds number while this trend reverses near the upper rigid plate. This behavior is also observed when both exponential as well as linear forms of pressure dependent viscosity are considered. The skin friction at the lower and upper walls of the channel are computed by evaluation of shear stresses on the lower and upper plates from Eq. (6.24) and tabulated in the tables 6.3-6.6. The magnitude of these stresses at the upper plate is signicantly high compared to the respective magnitudes at the lower plate. The components of velocity field for the both form of viscosities are shown in figures 6.2-6.11, for different values of non-dimensional parameters M, N, C, E and Re respectively. Figures 6.2(a)-(b) and figures 6.3(a)-(b) represents the variation of $f(y)$ and $l(y)$ with the non-dimensional parameter M. It is found that $f(y)$ decreases by increasing the values of M and $l(y)$ experiences an enhancement with the increase in M for both

the cases of pressure dependent viscosity. The variation of the couple stress parameter N is displayed in figures 6.4-6.5 for pressure dependent viscosity. The velocity component $f(y)$ gives least values in the absence of couple stress parameter but by increasing the value of couple stress parameter, it increases in both cases of viscosity. The velocity component $l(y)$ decreases by the increase of couple stress parameter for both cases. The non-dimensional number C is a measure of the ratio of pressure in the fluid due to gravity to the atmospheric pressure. The behavior of the velocity field with the variation of C is found in the figures 6.6-6.7. The $f(y)$ gives larger values with the increase of C and the $l(y)$ decreases. The effect of varying the non-dimensional coefficient E of the pressure form of viscosity is shown through figures 6.8-6.9. It is found that the component of velocity $f(y)$ increases by the increase of exponent E and $l(y)$ decreases. Figures 6.10 and 6.11 demonstrate the fluid velocity profile in three dimensional space for both cases of pressure dependent viscosity.

	p(y)			
y	**Re = 0.5**	**Re = 2**	**Re = 5**	**Re = 10**
0	2.478710688	2.507374424	2.557597404	2.625137033
0.2	2.245270630	2.265811234	2.300692347	2.344615296
0.4	1.980360092	1.990295009	2.005865516	2.021983278
0.6	1.683995056	1.683837420	1.682139411	1.676241350
0.8	1.356708707	1.351594279	1.342345163	1.329175066
1.0	1.000000000	1.00000000	1.00000000	1.00000000

Table 6.1: Pressure for $\mu(p) = e^{E(p-1)}$ with $M = 0.2, N = 0.5, E = 0.5, \alpha_0 = 1, x = 1$ and $C = 2$.

y	p(y)			
	Re = 0.5	**Re = 2**	**Re = 5**	**Re = 10**
0	1.717249108	1.828471172	2.023289151	2.284264846
0.2	1.610180425	1.679352619	1.794967860	1.934548060
0.4	1.486549591	1.511707412	1.546758096	1.569390809
0.6	1.345459177	1.334212055	1.307247811	1.252040998
0.8	1.184828152	1.158595039	1.110834431	1.042023824
1.0	1.000000000	1.00000000	1.00000000	1.00000000

Table 6.2: Pressure for $\mu(p) = \frac{1+Ep}{1+E}$ with $M = 1, N = 0.5, E = 0.5, \alpha_0 = 1, x = 1$ and $C = 2$.

C	**I**	**II**	**III**	**IV**	**V**
0	-0.1370	-0.4940	-0.0714	-0.2971	-0.0961
2	-0.1223	-0.3789	-0.0682	-0.2678	-0.0912
4	-0.1049	-0.2877	-0.0643	-0.2369	-0.0854
6	-0.0881	-0.2287	-0.0601	-0.2101	-0.0797
10	-0.062	-0.1601	-0.0519	-0.1697	-0.0696

Table 6.3: Shear stress at lower plate for $\mu(p) = e^{E(p-1)}$ with $\alpha_0 = 1$ and $x = 1$.

C	**I**	**II**	**III**	**IV**	**V**
0	0.1097	0.3446	0.0601	0.2357	0.0815
2	0.1025	0.3053	0.0581	0.2186	0.0779
4	0.0938	0.2633	0.0557	0.1992	0.0737
6	0.0849	0.2303	0.0532	0.1812	0.0693
10	0.0699	0.1837	0.0480	0.1521	0.0612

Table 6.4: Shear stress at upper plate for $\mu(p) = e^{E(p-1)}$ with $\alpha_0 = 1$ and $x = 1$.

C	I	II	III	IV	V
0	-0.1365	-0.4879	-0.0711	-0.2919	-0.0948
2	-0.1278	-0.4489	-0.0690	-0.2792	-0.0923
4	-0.1199	-0.4137	-0.0669	-0.2674	-0.0899
6	-0.1129	-0.3830	-0.0649	-0.2565	-0.0877
10	-0.1009	-0.3331	-0.0613	-0.2371	-0.0835

Table 6.5: Shear stress at lower plate for $\mu(p) = \frac{1+Ep}{1+E}$ with $\alpha_0 = 1$ and $x = 1$.

C	I	II	III	IV	V
0	0.1095	0.3413	0.0599	0.2313	0.0803
2	0.1051	0.3304	0.0586	0.2246	0.0787
4	0.1010	0.3182	0.0573	0.2182	0.0771
6	0.0973	0.3065	0.0561	0.2122	0.0756
10	0.0906	0.2856	0.0538	0.2012	0.0727

	I	II	III	IV	V
M	0.3	0.3	0.7	0.7	1
N	0.2	0.2	0.5	5	1
E	0.5	2	0.5	2	2
Re	2	10	2	10	5

Table 6.6: Shear stress at upper plate for $\mu(p) = \frac{1+Ep}{1+E}$ with $\alpha_0 = 1$ and $x = 1$.

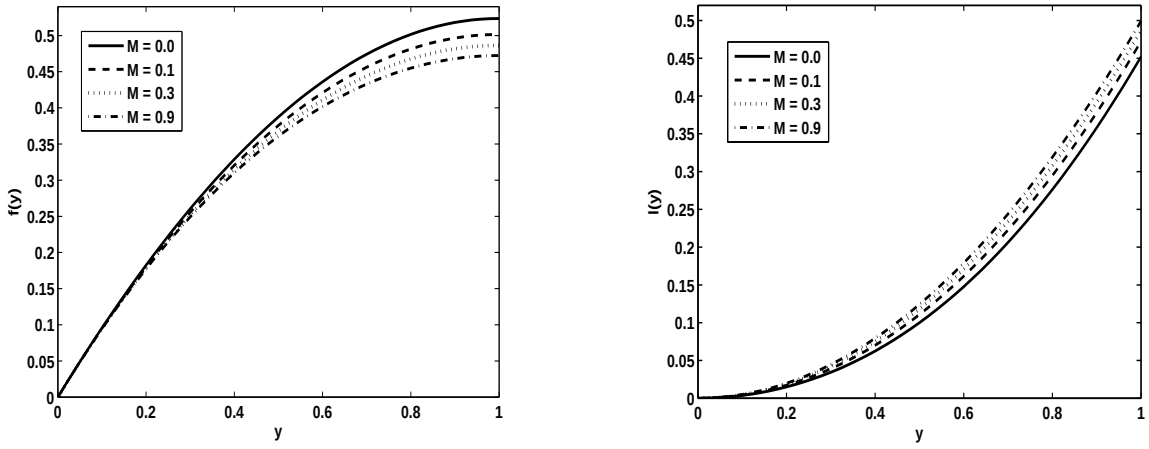

Figure 6.2: Velocity profile for $\mu(p) = e^{E(p-1)}$ with $N = 0.5, C = 2, E = 1, \alpha_0 = 1$ and $Re = 5$.

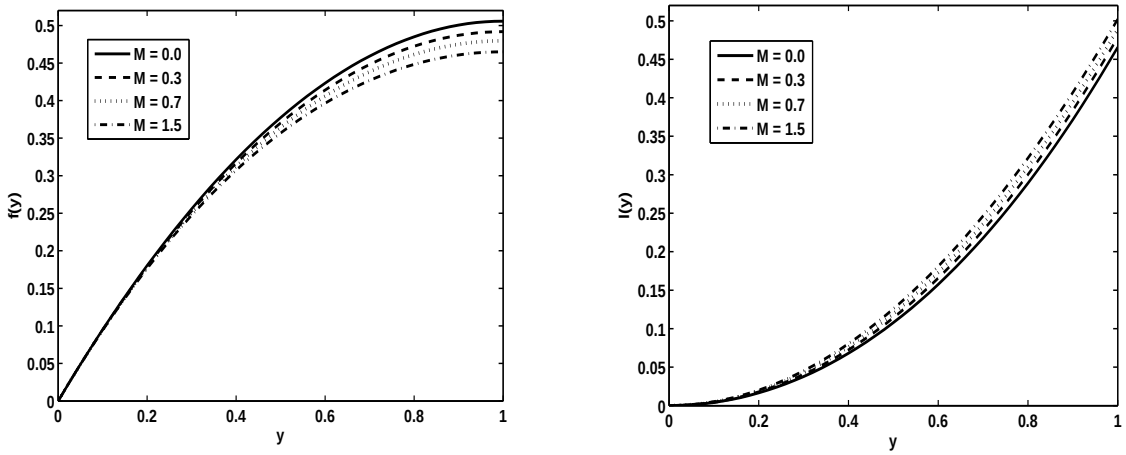

Figure 6.3: Velocity profile for $\mu(p) = \frac{1+Ep}{1+E}$ with $N = 0.1, C = 2, E = 3, \alpha_0 = 1$ and $Re = 2$.

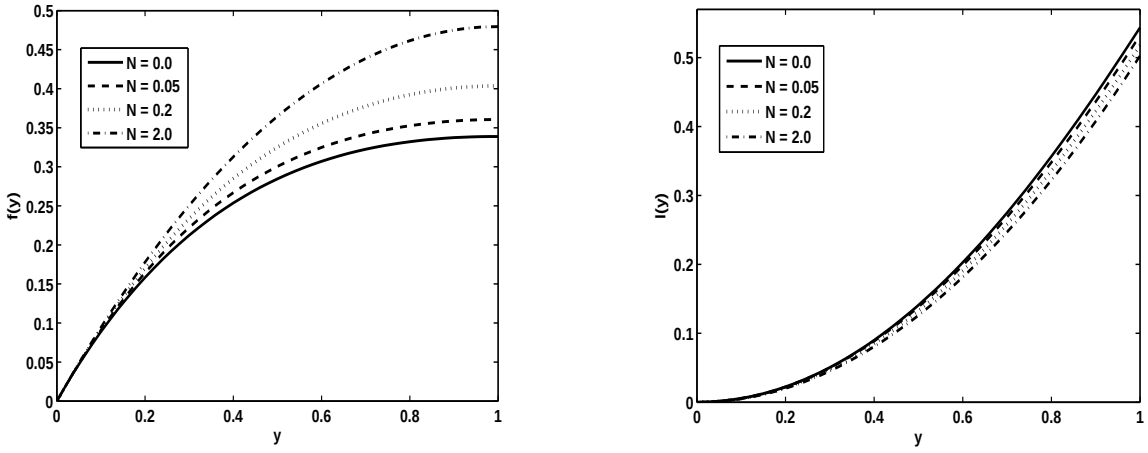

Figure 6.4: Velocity profile for $\mu(p) = e^{E(p-1)}$ with $M = 0.5, C = 2, E = 0.4, \alpha_0 = 1$ and $Re = 10$.

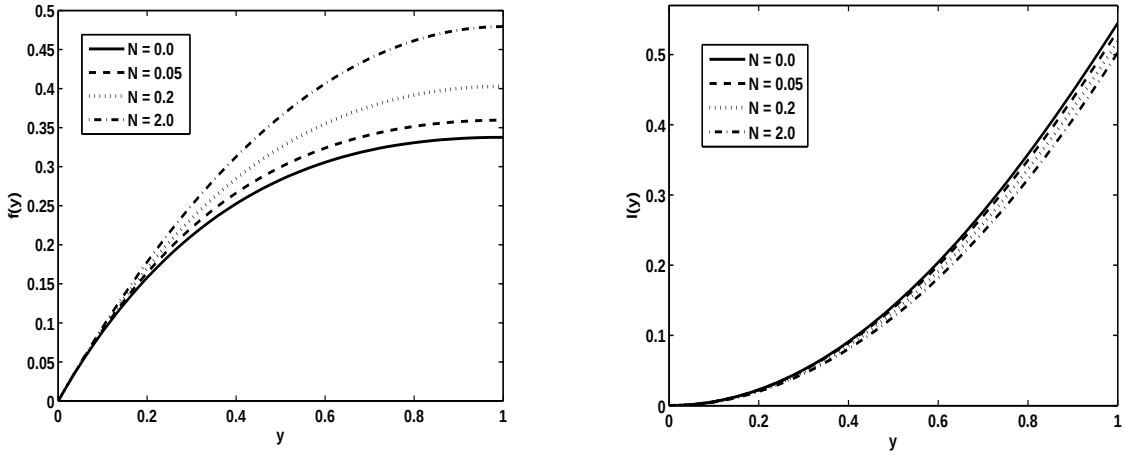

Figure 6.5: Velocity profile for $\mu(p) = \frac{1+Ep}{1+E}$ with $M = 0.5, C = 2, E = 1, \alpha_0 = 1$ and $Re = 10$.

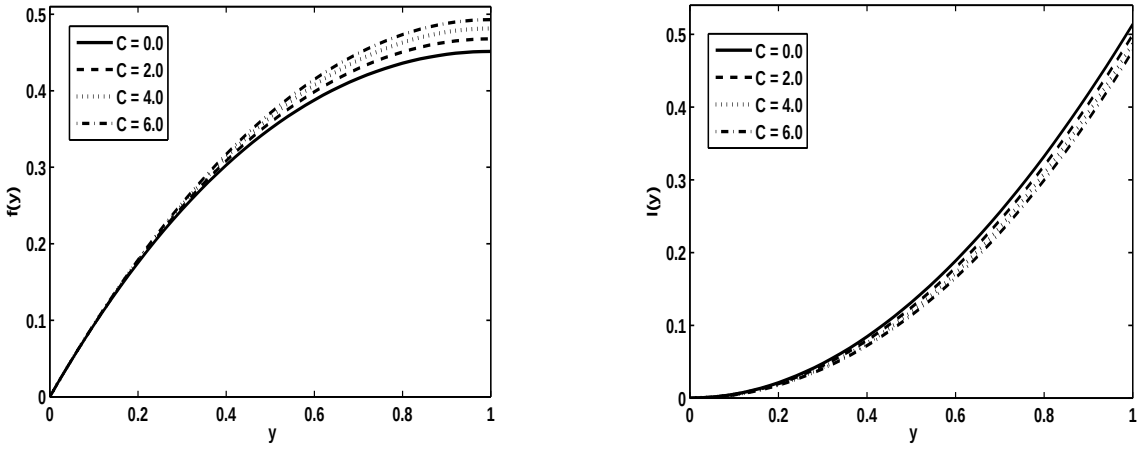

Figure 6.6: Velocity profile for $\mu(p) = e^{E(p-1)}$ with $M = 1, N = 0.5, E = 0.5, \alpha_0 = 1$ and $Re = 5$.

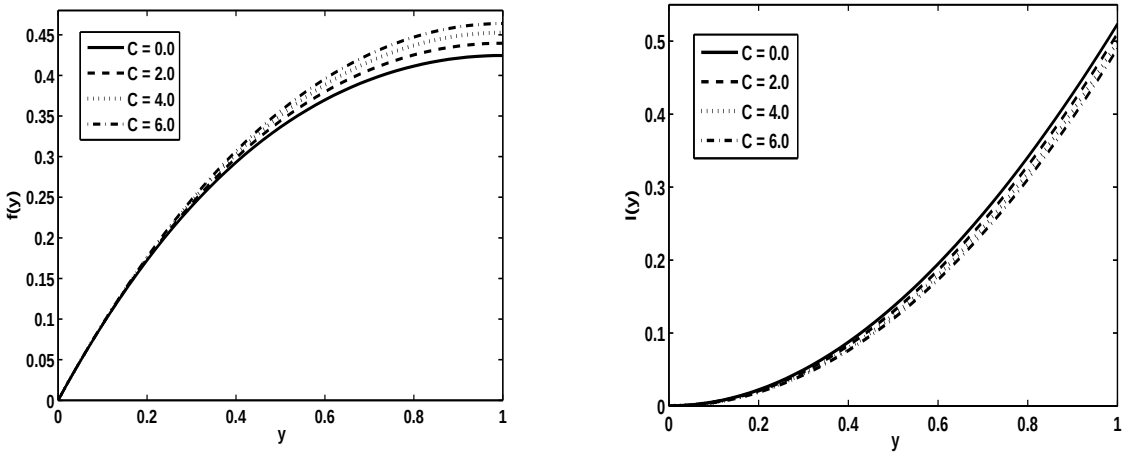

Figure 6.7: Velocity profile for $\mu(p) = \frac{1+Ep}{1+E}$ with $M = 1, N = 0.2, E = 0.5, \alpha_0 = 1$ and $Re = 5$.

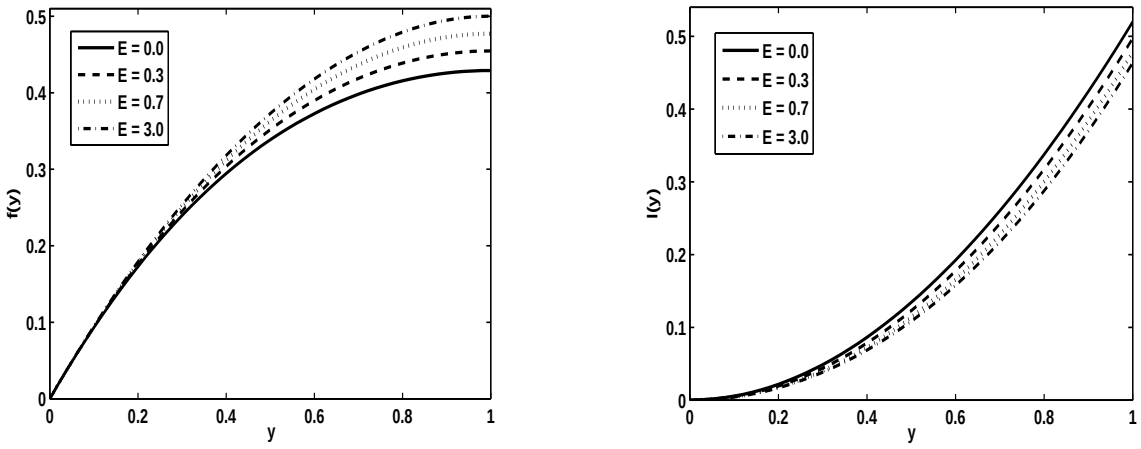

Figure 6.8: Velocity profile for $\mu(p) = e^{E(p-1)}$ with $M = 0.5, N = 0.2, E = 3, \alpha_0 = 1$ and $Re = 5$.

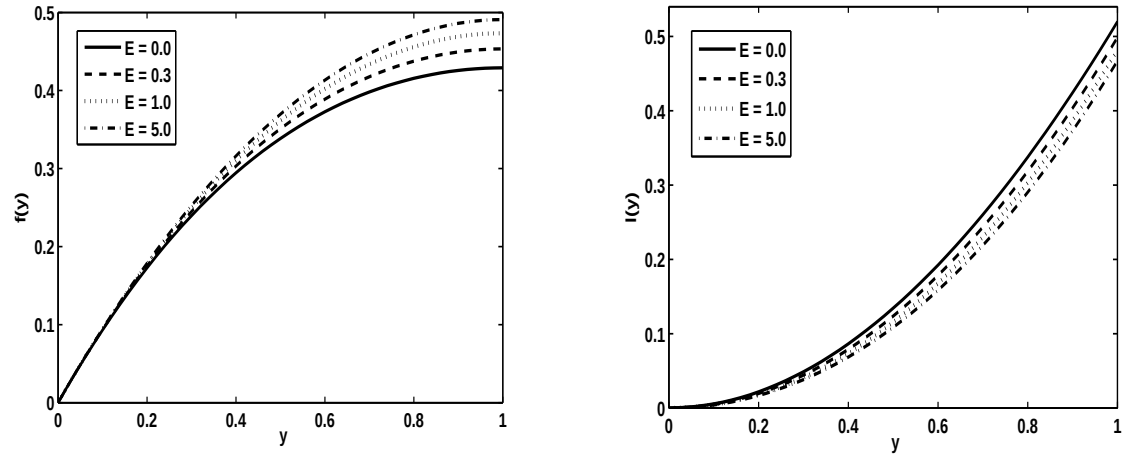

Figure 6.9: Velocity profile for $\mu(p) = \frac{1+Ep}{1+E}$ with $M = 0.2, N = 0.2, C = 4, \alpha_0 = 1$ and $Re = 5$.

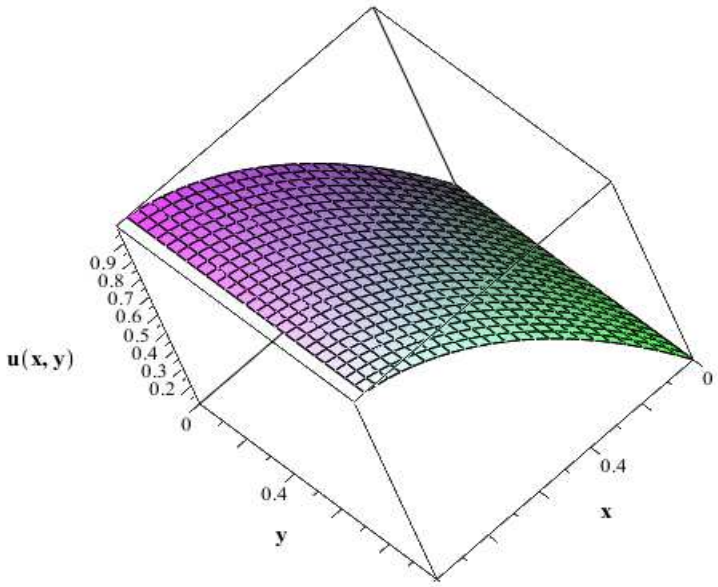

Figure 6.10: Velocity profile for $\mu(p) = e^{E(p-1)}$ with $M = 0.5, N = 0.2, E = 3, \alpha_0 = 1$ and $Re = 5$.

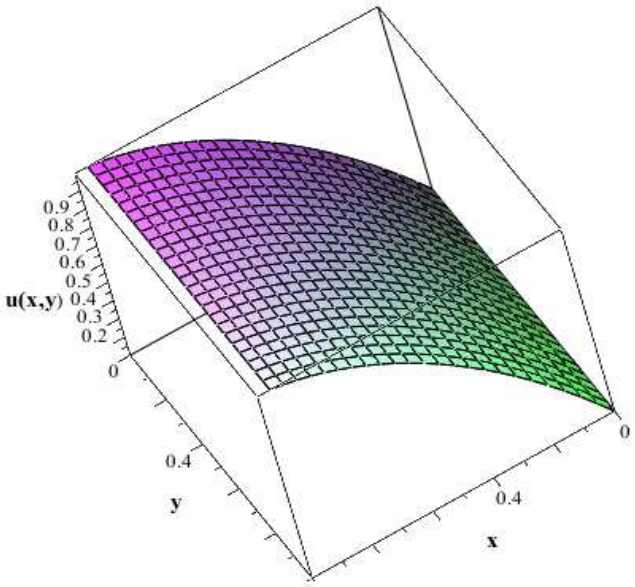

Figure 6.11: Velocity profile for $\mu(p) = \frac{1+Ep}{1+E}$ with $M = 0.2, N = 0.2, C = 4, \alpha_0 = 1$ and $Re = 5$.

Chapter 7

Flow of Jeffrey fluid with pressure dependent viscosity in the annulus of two infinitely long coaxial cylinders

7.1 Introduction

This chapter covers the numerical analysis of flow of Jeffrey fluid with pressure dependent viscosity in the annulus of two infinitely long coaxial cylinders. The governing system of differential equations for exponentially as well as linearly pressure dependent viscosities is simplied by using appropriate non dimensional quantities. The simplified nonlinear coupled differential equations are solved numerically by shooting method with Runge-Kutta Felhberg technique. The results and effects of important parameters are discussed through graphs. In the last sections important concluding remarks are also extracted out.

7.2 Mathematical formulation

Let us consider an incompressible Jeffrey fluid with pressure dependent viscosity in the annulus of two inclined coaxial cylinders. The radius of the inner and outer cylinders are denoted by R_{in} and R_{out}, respectively. The cylinders are assumed to be infinitely long so that end effects are neglected. The outer cylinder is assumed stationary while the inner cylinder rotates with a constant angular velocity Ω . The equations which govern the flow are [54]

$$\rho\frac{d\mathbf{V}}{dt} = div\mathbf{T} + \rho\mathbf{b}_e, \tag{7.1}$$

where $\mathbf{b}_e$ is the body forces. We shall exploit the cylindrical symmetry in the problem by taking recourse to cylindrical coordinates (r, θ, z), with z directed along the axis of the cylinder. We shall assume that the velocity and the pressure are independent of θ in the flow domain. Since the cylinders are infinitely long so we expect the solutions to be independent of z as well. We seek the velocity and the pressure field are of the form

$$\mathbf{V} = (0, v(r), 0) \qquad\qquad p = p(r). \tag{7.2}$$

The velocity field satisfies Eq.(1.1). With the help of Eqs.(1.3)-(1.5) and (7.2) , the component form of Eq.(7.1) in the presence of gravity take the following form

$$-\frac{\rho v^2}{r} = -\frac{dp}{dr} + \rho g\sin\theta, \tag{7.3}$$

and

$$\frac{d}{dr}\left[\frac{\mu(p)}{1+\lambda_1}\left(\frac{dv}{dr} - \frac{v}{r}\right)\right] + \frac{2}{r}\frac{\mu(p)}{1+\lambda_1}\left(\frac{dv}{dr} - \frac{v}{r}\right) - \rho g\cos\theta = 0. \tag{7.4}$$

If the pressure at the inner cylinder surface $r = R_{in}$ is p_i, so that $p(R_{in}) = p_i$. The pressure at the outer cylinder surface $p(R_{out})$ is determined from this boundary condition.

Introducing the following non-dimensional variables

$$\bar{r} = \frac{r}{r_0}, \qquad \bar{v} = \frac{v}{v_0}, \qquad \bar{\mu} = \frac{\mu}{\mu_0}, \tag{7.5}$$

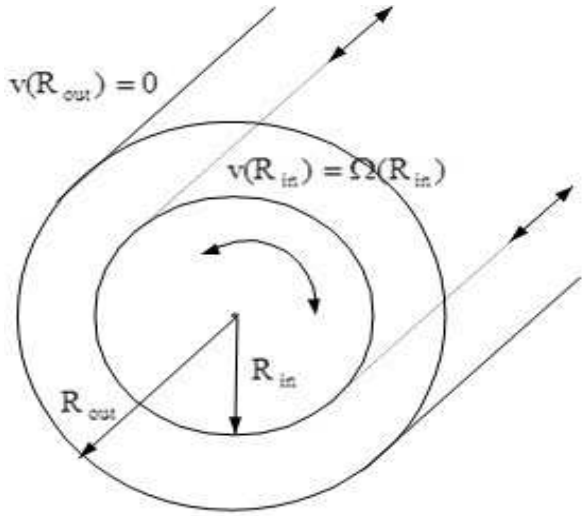

Figure 7.1: Flow in the annulus of two infinitely long coaxial cylinders.

where r_0, v_0 and μ_0 are the representative quantities. Choose $r_0 = R_{in}, v_0 = \Omega R_{in}, \mu_0 = \mu(p_0)$ and $p_0 = \rho v_0^2$. The above non-dimensionalization leads to the following non-dimensional parameters

$$\zeta = \frac{R_{out}}{R_{in}}, \qquad k = \frac{p_i}{p_0}, \qquad \Gamma_5 = \frac{\rho g r_0}{p_0}\sin\theta, \qquad \Gamma_6 = \frac{\rho g r_0^2}{\mu_0 v_0}\cos\theta. \tag{7.6}$$

The appropriate boundary conditions are

$$v(R_{in}) = v_0, \qquad and \qquad v(R_{out}) = 0. \tag{7.7}$$

Using Eq. (6.16) and (7.6), the non-dimensional form of the governing equations with boundary conditions, after dropping the bars are as follows

$$\frac{dp}{dr} - \frac{v^2}{r} - \Gamma_5 = 0, \tag{7.8}$$

$$\frac{d^2v}{dr^2} + \frac{1}{r}\frac{dv}{dr} - \frac{1}{r^2}v + \frac{1}{\mu(p)}\left(\frac{dv}{dr} - \frac{v}{r}\right)\frac{d\mu(p)}{dr} - \frac{1+\lambda_1}{\mu(p)}\Gamma_6 = 0, \tag{7.9}$$

$$v(1) = 1, \qquad and \qquad v(\zeta) = 0. \tag{7.10}$$

The non dimensional form of the viscosity given by Eqs.(6.22) and (6.23) after dropping the bars are

$$\frac{d^2v}{dr^2}+\frac{1}{r}\frac{dv}{dr}-\frac{1}{r^2}v+E\left(\frac{dv}{dr}-\frac{v}{r}\right)\frac{dp}{dr}-\Gamma_6(1+\lambda_1)e^{E(1-p)}=0, \tag{7.11}$$

$$\frac{d^2v}{dr^2}+\frac{1}{r}\frac{dv}{dr}-\frac{1}{r^2}v+\frac{E}{1+Ep}\left(\frac{dv}{dr}-\frac{v}{r}\right)\frac{dp}{dr}-\Gamma_6(1+\lambda_1)\frac{1+E}{1+Ep}=0. \tag{7.12}$$

7.3 Numerical solution and discussion

We solve Eqs.(7.8), (7.11) and (7.12) subject to the boundary conditions Eq.(7.10) numerically by shooting method with Runge Kutta Fehlberg technique. The numeric scheme explained in chapter two is followed. The results have been discussed through graphs.
The governing equations of Jeffrey fluid with pressure-dependent viscosities in the annulus of two inclined coaxial cylinders have been solved numerically. We select $\zeta=\frac{R_{out}}{R_{in}}=2$ for our problem. Table 7.1 illustrates the numerical results for pressure as well as velocity profiles for both linear and exponential forms of pressure dependent viscosities. The comparison of linear and exponential forms of viscosity for pressure profile reveals that pressure increases when linearly pressure dependent viscosity is chosen. Similarly, viscosity taken as a linear function of pressure generates more fluid velocity as compare to the exponential pressure dependent viscosity. Thus, it can be established that exponential pressure dependent viscosity resist to the fluid flow remarkably. The velocity corresponding to the Navier Stokes fluid is always larger than the corresponding solution for the pressure-dependent fluid. It depicts that as the pressure increases radially, the viscosity increases leading to a decrease in the velocity. Also, it is analyzed from the figures 7.2 and 7.3 that the velocity field decreases by the increase in the values of $\Gamma's$ for both the cases of viscosity. The effects of non-dimensional quantity E are shown in figures 7.4 and 7.5. E is a coefficient of pressure in both expressions of pressure dependent viscosity. Figure

7.4 displays the impact of E when viscosity is an exponential function of pressure. It is noted that the bigger the coefficient E lesser will be the fluid velocity. Similarly the effect of coefficient E when viscosity depends on pressure linearly is displayed in figure 7.5. Here it is seen that the higher value of coefficient E leads to the rise in fluid velocity. The contribution of pressure ratio comes from the parameter k. It is observed that the velocity profile ascents by the growing value of k for exponential as well as linear form of viscosity as shown in figures 7.6 and 7.7. Figures 7.8 and 7.9 demonstrate the effect of Jeffrey fluid parameter λ_1 on fluid flow. The velocity field is diminishing for both the exponential and linear form of viscosity by increasing the Jeffrey fluid parameter λ_1. Figures 7.10 to 7.13 are the graphical illustration of pressure profile for different values of important parameters. Figures 7.10 and 7.11 display the effect of $\Gamma's$ on pressure profile. Notably for both cases of pressure dependent viscosity i.e., exponential and linear, pressure upsurges with the rise in $\Gamma's$. Coefficient of pressure E contribution is shown in figures 7.12 to 7.13. It is concluded that the rising values of E reduces the pressure. However, this trend is more visible when viscosity is taken to be an exponential function of pressure.

	p(r)		v(r)	
y	**Linear**	**Exponential**	**Linear**	**Exponential**
1.00	2.000000000	2.000000000	1.000000000	1.000000000
1.10	2.174970764	2.164974781	0.775328413	0.664188156
1.20	2.316073271	2.291980200	0.599773744	0.455259171
1.30	2.438517379	2.403778808	0.459339415	0.315262243
1.40	2.550525973	2.509016029	0.345578800	0.217909340
1.50	2.656710796	2.611323652	0.252930410	0.148712255
1.60	2.759705775	2.712308456	0.177498565	0.098775675
1.70	2.861019977	2.812701082	0.116427951	0.062295438
1.80	2.961507646	2.912837789	0.067553479	0.035346906
1.90	3.061637450	3.012873119	0.029190281	0.015216589
2.00	3.161651155	3.112876861	0.000000000	0.000000000

Table 7.1: Pressure and Velocity profile for $\Gamma_5 = 1, \Gamma_6 = 1, k = 2, E = 2$ and $\lambda_1 = 0.5$.

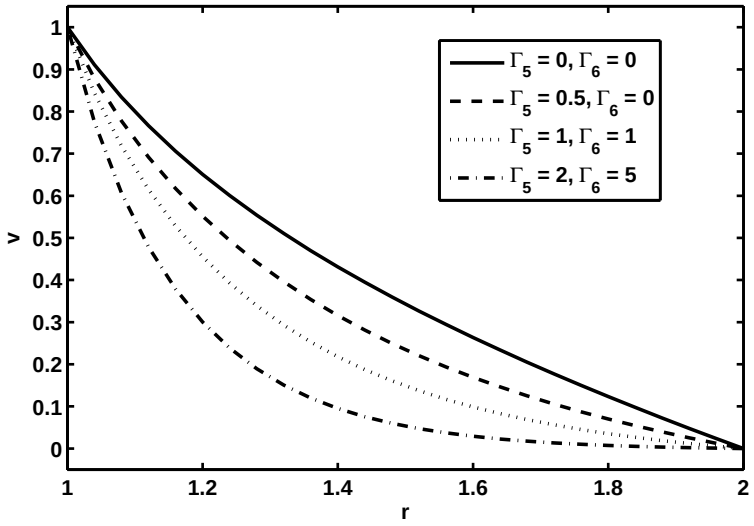

Figure 7.2: Velocity profile for $\mu(p) = e^{E(p-1)}$ with $k = 2, E = 2$ and $\lambda_1 = 0.5$.

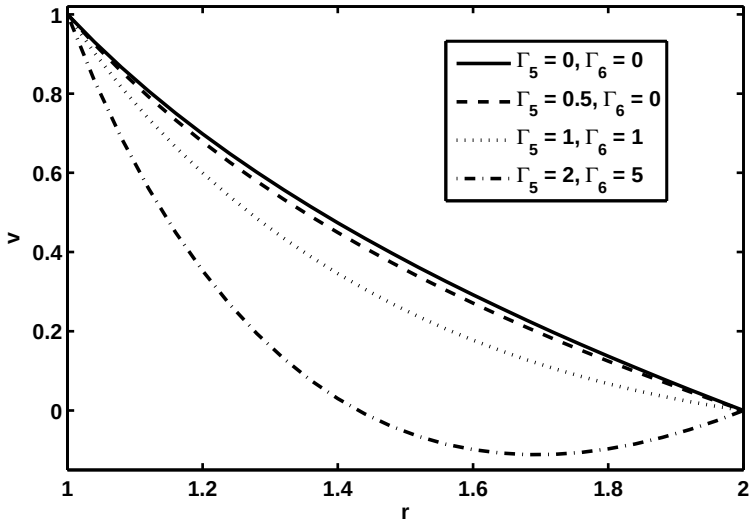

Figure 7.3: Velocity profile for $\mu(p) = \frac{1+Ep}{1+E}$ with $k = 2, E = 2$ and $\lambda_1 = 0.5$.

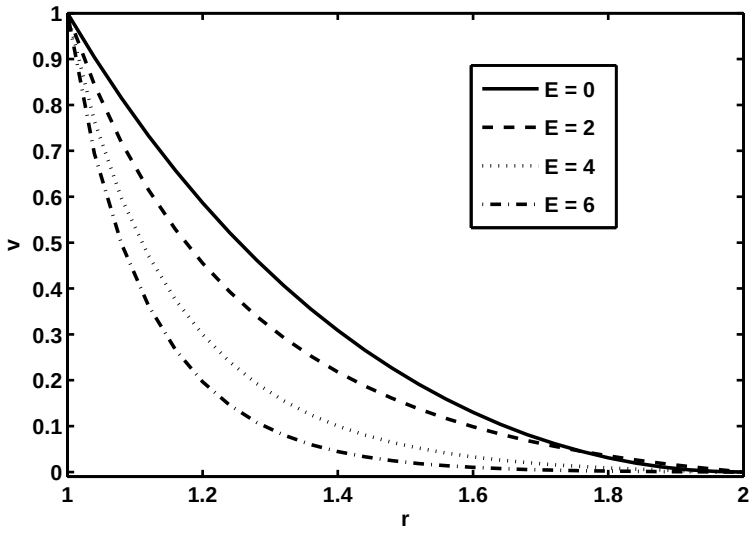

Figure 7.4: Velocity profile for $\mu(p) = e^{E(p-1)}$ with $\Gamma_5 = 1, \Gamma_6 = 1, k = 2$ and $\lambda_1 = 0.5$.

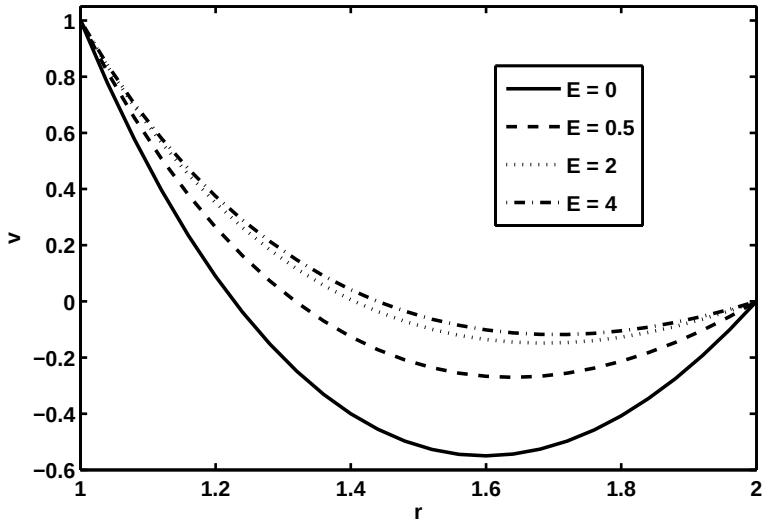

Figure 7.5: Velocity profile for $\mu(p) = \frac{1+Ep}{1+E}$ with $\Gamma_5 = 1, \Gamma_6 = 5, k = 2$ and $\lambda_1 = 0.5$.

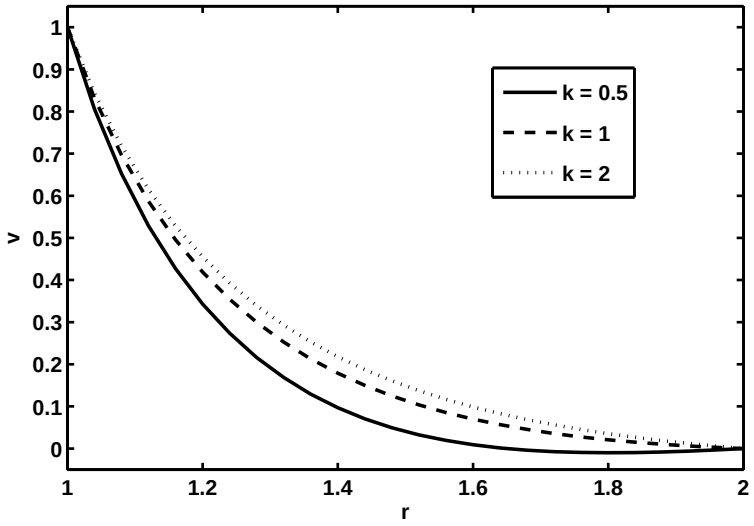

Figure 7.6: Velocity profile for $\mu(p) = e^{E(p-1)}$ with $\Gamma_5 = 1, \Gamma_6 = 1, E = 2$ and $\lambda_1 = 0.5$.

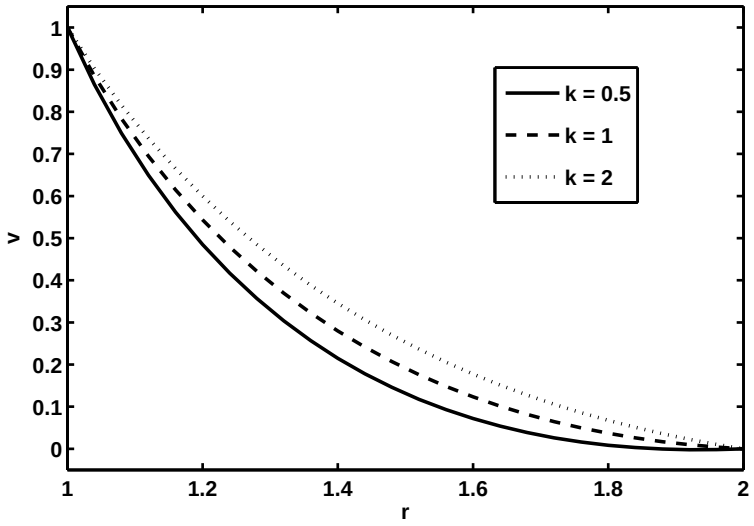

Figure 7.7: Velocity profile for $\mu(p) = \frac{1+Ep}{1+E}$ with $\Gamma_5 = 1, \Gamma_6 = 1, E = 2$ and $\lambda_1 = 0.5$.

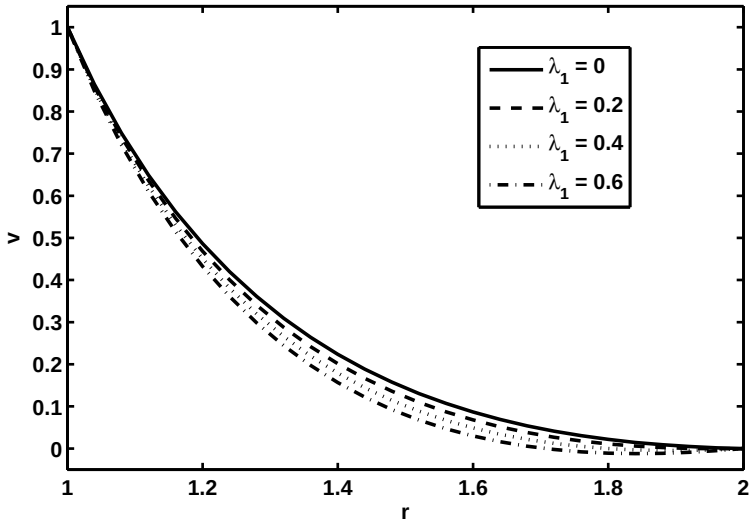

Figure 7.8: Velocity profile for $\mu(p) = e^{E(p-1)}$ with $\Gamma_5 = 1, \Gamma_6 = 5, k = 2$ and $E = 1$.

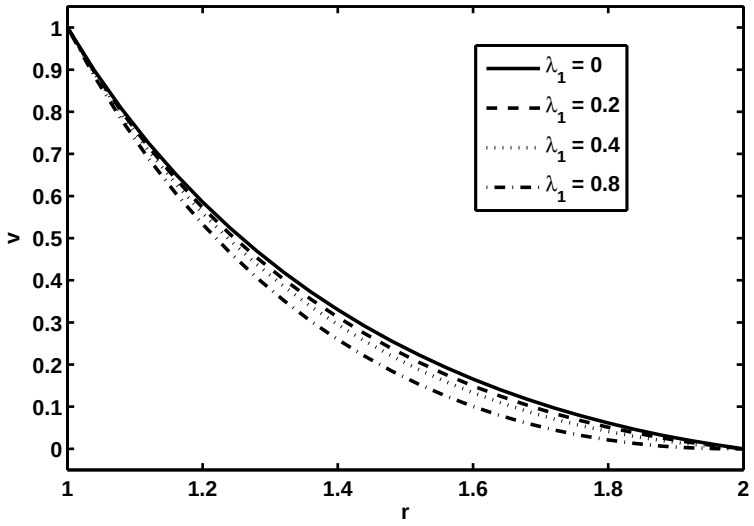

Figure 7.9: Velocity profile for $\mu(p) = \frac{1+Ep}{1+E}$ with $\Gamma_5 = 1, \Gamma_6 = 1, k = 1$ and $E = 1$.

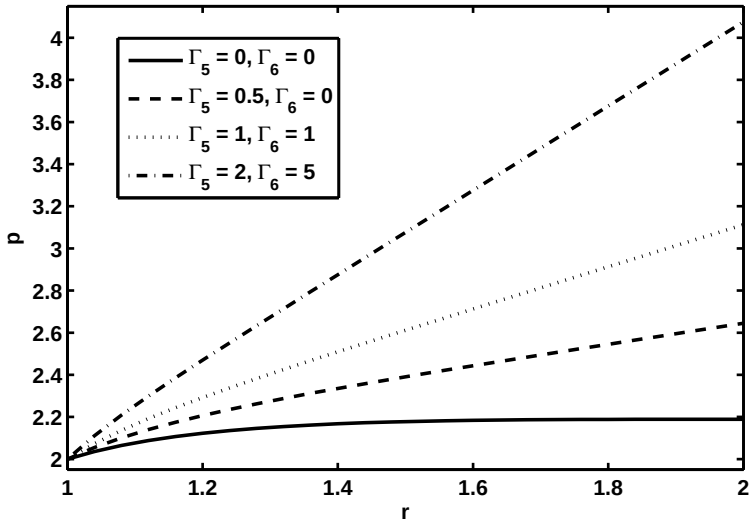

Figure 7.10: Pressure profile for $\mu(p) = e^{E(p-1)}$ with $k = 2, E = 2$ and $\lambda_1 = 0.5$.

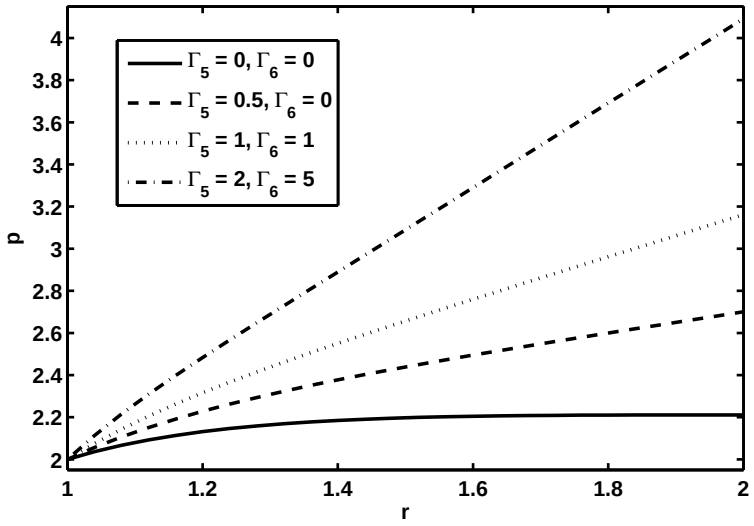

Figure 7.11: Pressure profile for $\mu(p) = \frac{1+Ep}{1+E}$ with $k = 2, E = 2$ and $\lambda_1 = 0.5$.

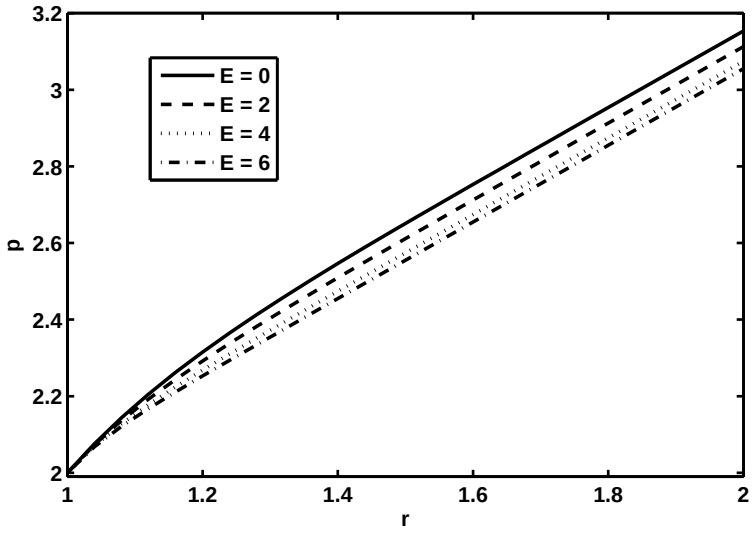

Figure 7.12: Pressure profile for $\mu(p) = e^{E(p-1)}$ with $\Gamma_5 = 1, \Gamma_6 = 1, k = 2$ and $\lambda_1 = 0.5$.

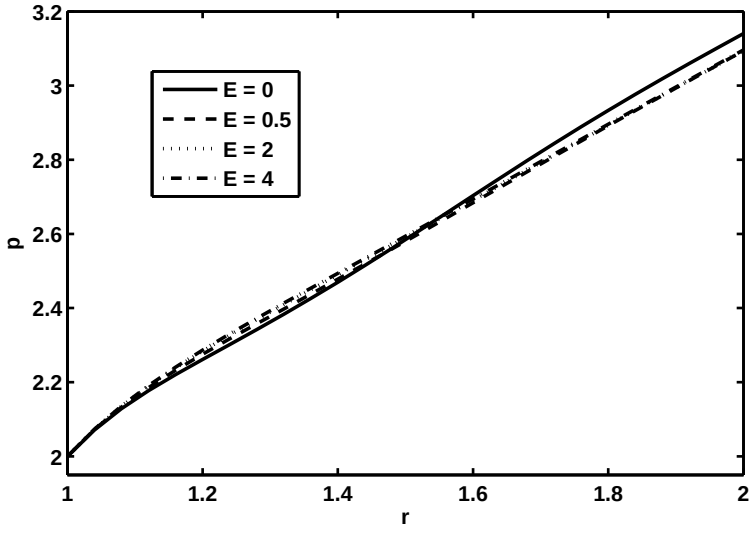

Figure 7.13: Pressure profile for $\mu(p) = \frac{1+Ep}{1+E}$ with $\Gamma_5 = 1, \Gamma_6 = 5, k = 2$ and $\lambda_1 = 0.5$.

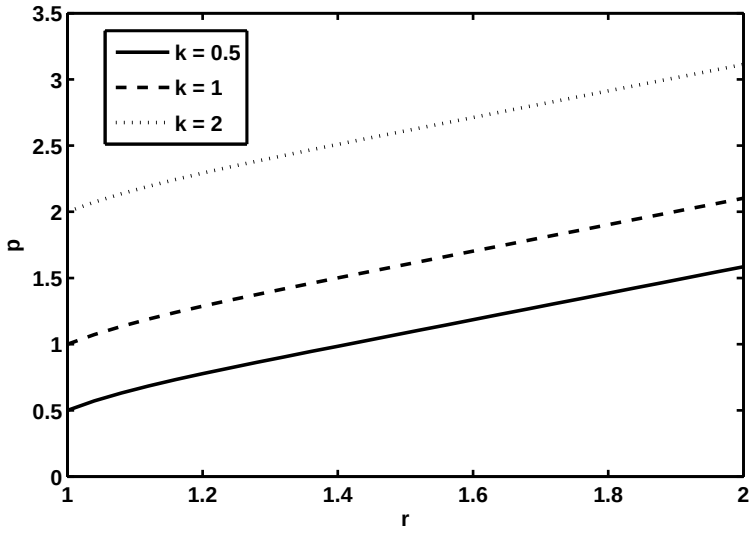

Figure 7.14: Pressure profile for $\mu(p) = e^{E(p-1)}$ with $\Gamma_5 = 1, \Gamma_6 = 1, E = 2$ and $\lambda_1 = 0.5$.

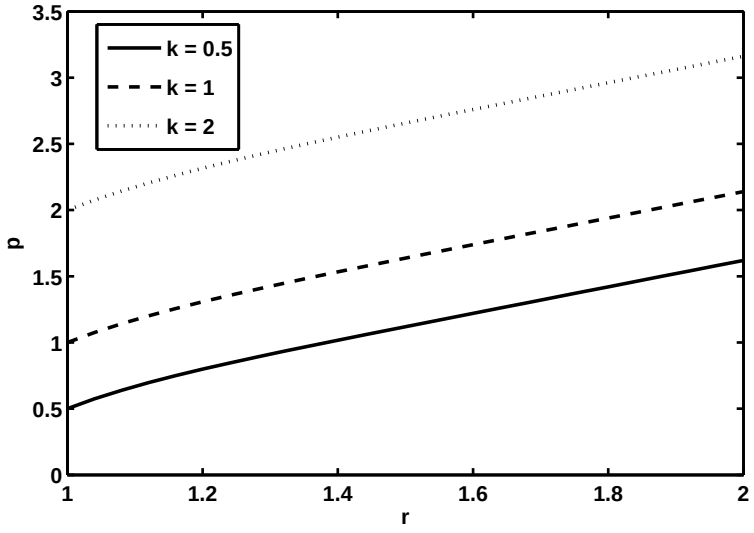

Figure 7.15: Pressure profile for $\mu(p) = \frac{1+Ep}{1+E}$ with $\Gamma_5 = 1, \Gamma_6 = 1, E = 2$ and $\lambda_1 = 0.5$.

Chapter 8

Conclusion

This chapter is devoted to the conclusions extracted from the previous chapters. In this thesis different types of non-Newtonian fluid models having pressure dependent viscosity are taken into account. It is also important to note that three types of geometries (i.e. inclined channel, parallel porous plates with stretching and annulus of two infinite coaxial cylinders) are assumed. Main aim of the present research is to examine the effect of pressure dependent viscosity on shear thinning and shear thickening fluid models with different geometries. Different functional forms of viscosity and porosity in the form of case I, II, III and IV (see chapter 1) are chosen. Numerical techniques (e.g. shooting method in conjunction with Runge-Kutta-Fehlberg method and finite difference scheme) are used to obtain their solutions. The results are compared using tables and graphs after varying physical parameters. The conclusive remarks are as follows:

- Increase in $\Gamma's$ decreases the fluid velocity both for Poiseuille and Couette flow with Jeffrey, Williamson, hyperbolic tangent, Carreau and Sutterby fluid models.
- The fluid property parameters i.e., λ_1, We and σ enhances fluid flow in case of Poiseuille flow whereas this trend reverses in the case of Couette flow.

- In case II where viscosity depends on pressure exponentially and porosity is a rational function of pressure, increase in the power of rational expression reduces fluid velocity while in case IV where both viscosity and porosity are taken to be rational functions of pressure, rising the power of rational expression term upsurges fluid velocity.

- For cases III and IV where viscosity is taken to be a rational function of pressure the rise in power drops down the fluid velocity.

- For both Poiseuille and Couette flows in case of Jeffrey, Williamson and hyperbolic tangent fluid models, case II is the most suitable selection for pressure dependent viscosity and porosity.

- The power law index β contribution is witness in enhancing the fluid flow for both types of flows (i.e. Poiseuille and Couette flow) of hyperbolic tangent fluid while the trend reverses for the case of Carreau and Sutterby fluid models.

- For both Poiseuille and Couette flows in case of Carreau and Sutterby fluid models, case III is the most suitable selection for pressure dependent viscosity and porosity.

- Pressure profile enhances with the rising values of Reynolds number near the lower stretching sheet while decays near the upper rigid plate.

- The magnitude of shear stresses at the upper rigid plate is signicantly high when compared to the respective magnitudes at the lower stretching sheet.

- Couple stress fluid property parameter N contributes in raising the velocity component $f(y)$ while sinking the velocity component $l(y)$.

- The mounting values of pressure ratio C upsurges the velocity component $f(y)$ and drops the velocity component $l(y)$.

- The non-dimensional coefficient of pressure E influences in fluid flow by rising the velocity component $f(y)$ and dropping the velocity component $l(y)$.

- Pressure profile enhances with the rising values of $\Gamma's$. This rise is more rapid near the wall of the outer cylinder for both types of pressure dependent viscosities.

- The non-dimensional quantity E which appears as a coefficient of variable viscosity contributes in reducing the pressure. Its contribution is more significant in the case of viscosity depending upon pressure exponentially.

- The non-dimensional pressure ratio k play a significant role in increasing the pressure for both cases of pressure dependent viscosities.

- The increasing values of $\Gamma's$ pays in reducing the fluid velocity for both forms of pressure dependent viscosities.

- The non-dimensional quantity E contributes in reducing the fluid velocity for exponentially pressure dependent viscosity while rising values of E upsurges fluid flow when viscosity is taken as a linear function of pressure.

- The pressure ratio k tends to reduce fluid velocity for both cases of pressure dependent viscosities.

Bibliography

[1] C. Andrade, *Viscosity of liquids*, Nature, 125 (1930) 309–310.

[2] G.G. Stokes,*On the theories of the internal friction of fluids in motion, and of the equilibrium and motion of elastic solids*, Trans. Camb. Phil. Soc., 8 (1845) 287–305 .

[3] J. Aho and S. Syrjala, *On the measurement and modeling of viscosity of polymers at low temperatures*, Polym. Tes., 27 (2008) 35–40.

[4] J. Aho and S. Syrjala, *Shear viscosity measurements of polymer melts using injection molding machine with adjustable slit die*, Polym. Tes., 30 (2011) 595–601.

[5] J. Hron, J. Malek and K.R. Rajagopal, *Simple flows of fluids with pressure-dependent viscosities*, Proc. R. Soc. Lond. A, 457 (2001) 1603-1622.

[6] J. Hron, J. Malek, V. Prusa and K.R. Rajagopal, *Further remarks on simple flows of fluids with pressure-dependent viscosities*, NonLin. Anal. Real World Appl., 12 (2011) 394-402.

[7] C. Barus *Isothermals, Isopiestics and isometrics relative to viscosity*, Am. J. Sci., 45 (1893) 87–96.

[8] W.G. Cutler, R.H. McMickle, W. Webb and R.W. Schiessler, *A Study of the compressions of several high molecular weight hydrocarbons*, J. Chem. Phys., 29 (1958) 727–740.

[9] E.M. Griest, W. Webb and R.W. Schiessler, *Effect of pressure on viscosity of high hydrocarbons and their mixtures*, J. Chem. Phys., 29 (1958) 711–720.

[10] N. Mills, *Incompressible mixtures of Newtonian fluids*, Int. J. Eng. Sci., 4 (1966) 97–112.

[11] K.L. Johnson and R. Cameron, *Shear behavior of elastohydrodynamic oil films at high rolling contact pressures*, Proc. Inst. Mech. Eng. 182 (1967) 307–327.

[12] K.L. Johnson and J.L. Tevaarwerk,*Shear behavior of elastohydrodynamic oil film*, Proc. Roy. Soc. Lond., A356 (1977) 215–236.

[13] A.Z. Szeri, *Fluid Film Lubrication,Theory and Design*, Camb. Uni. Press, 1998.

[14] S. Bair and P. Kottke, *Pressure–viscosity relationships for elastohydrodynamics*, Tri. Trans. 46 (2003) 289–295.

[15] P.W. Bridgman, *The Physics of High Pressure*, MacMillan, New York, 1931.

[16] P.W. Bridgman, *The effect of pressure on the viscosity of forty–three pure fluids*. Proc. Am. Acad. Arts Sci., 61 (1926) 57–99.

[17] S. Bair and W.O. Winer, *The high pressure high shear stress rheology of liquid lubricants*, J. Trib., 114 (1992) 1-9.

[18] M. Renardy, *Some remarks on the Navier-Stokes equations with a pressure dependent viscosity*, Comm. Part. Diff. Eq., 11 (1986) 779-793.

[19] F. Gazzola, *A note on the evolution of Navier-Stokes equations with a pressure dependent viscosity*, Zeit. Angew. Math. Phys., 48 (1997) 760-773.

[20] J. Malek, J. Necas and K.R. Rajagopal, *Global analysis of the flows of fluids with pressure-dependent viscosity*, Arch. Rat. Mech. Anal. 165 (2002) 243-269.

[21] M. Franta, J. Malek and K.R. Rajagopal, *On steady flows of fluids with pressure and shear-dependent viscosities*, Proc. R. Soc. Lond. A 461 (2005) 651-670.

[22] M. Bulicek, J. Malek, and K.R. Rajagopal, *Navier's slip and evolutionary Navier–Stokes-like system with pressure and shear–rate dependent viscosity*, Ind. Univ. Math. J., 56 (2007) 51–85.

[23] K. Kannan and K.R. Rajagopal, *Flow through porous media due to high pressure gradients*, Appl. Math. and Comput. 199 (2008) 748–759.

[24] H. Darcy *Les Fontaines Publiques de la Ville de Dijon*, Dalmont, Paris, (1856).

[25] S.Whitaker, *Flow in porous media I: A theoretical derivation of Darcy's law*, Tran. Por. Med., 1 (1986) 3-25.

[26] H.C. Brinkman, *A calculation of the viscous force exerted by a flowing fluid on a dense swarm of particles*, Appl. Sci. Res., A 1 (1947) 27-34.

[27] H.C. Brinkman, *On the permeability of media consisting of closely packed porous particles*, Appl. Sci. Res., A 1 (1949) 81–86.

[28] W.G. Gray and C.T. Miller, *Examination of Darcy's Law for Flow in Porous Media with Variable Porosity*, Environ. Sci. Technol., 38 (2004) 5895-5901.

[29] J.G. Savins, *Non-Newtonian flow through porous media*, Ind. Eng. Chem., 61 (1969) 18-47.

[30] E.H. Wissler, *Viscoelatic effects in the flow of non–Newtonian fluids through porous media*, Ind. Eng. Chem. Fund., 10 (1971) 411–417.

[31] H. Pascal, *Rheological behaviour effect of non–Newtonian fluids on steady and unsteady flow through porous medium* Int. J. Numer. Anal. Meth. Geomech., 7 (1983) 289–303.

[32] Y.S. Wu and K. Pruess, *A numerical method for simulating non–Newtonian fluid flow and displacement in porous media*, Adv. Wat. Res., 21 (1998) 351–362.

[33] J.R.A. Pearson and P.M.J. Tardy, *Models for flow of non–Newtonian and complex fluids through porous media*, J. Non-Newt. Fluid Mech., 102 (2002) 447–473.

[34] K.R. Rajagopal, G. Saccomandi and L. Vergori ,*Couette flow with frictional heating in a fluid with temperature and pressure dependent viscosity*, Int. J. Heat Mass Transfer, 54 (2011) 783–789.

[35] P. Schafer and H. Herwig *Stability of plane Poiseuille flow with temperature dependent viscosity* Int. J. Heat Mass Transfer. 36 (1993) 2441–2448.

[36] K.B. Nakshatrala and K.R. Rajagopal,*A numerical study of fluids with pressure dependent viscosity flowing through a porous medium*, Int. J. Numer. Meth. Fluids., 67 (2011) 342–368.

[37] T. Hayat, A.H. Kara,*Couette flow of a third grade fluid with variable magnetic field*, Math. Comp. Model., 43 (2006) 132–137.

[38] T. Hayat, M. Khan, M. Ayub, *Couette and Poiseuille flows of an Oldroyd 6–constant fluid with magnetic field*, J. Math. Anal. App., 299 (2004) 225–244.

[39] T. Hayat, R. Ellahi, F.M. Mahomed,*Exact solutions for Couette and Poiseuille flows for forth grade fluids*, Act. Mech., 188 (2007) 69–78.

[40] S. Abbasbandy, T. Hayat,, R. Ellahi, S. Asghar, *Numerical results of a flow in a third grade fluid between two porous walls*, Zeit. Nat. A., 64 (2009) 59–64.

[41] Z. Abbas, T. Hayat, M. Sajid, S. Asghar *Unsteady flow of a second grade fluid film over an unsteady stretching sheet* Math. Comp. Model., 118 (2008) 518–526.

[42] M. Sajid, T. Hayat *Non-Similar series solution for boundary layer flow of a third order fluid over a stretching sheet* App. Math. Comp., 181 (2007) 1576–1585.

[43] K.W. Morton and D.F. Mayers, *Numerical Solution of Partial Differential Equations, An Introduction*, Camb. Uni. Press, (2005).

[44] M.K. Jain, S.R.K. Iyengar and R.K. Jain, *Numericals Methods for scientific and engineering computation*, New Age Int. Ltd. Pub., (2009).

[45] R.L. Burden and J.D. Faires *Numerical Analysis* , Thomson Brooks/Cole, (2005).

[46] E. Fehlberg,*Low-order classical Runge-Kutta formulas with step size control and their application to some heat transfer problems*, NASA Tech. Report, 315, (1969).

[47] C.H.B. Narayana, S. Sreenadh and P. Devaki, *Oscillatory flow of a Jeffrey fluid in an elastic tube of variable cross-section*, Adv. App. Sci. Res., 3 (2012) 671–677.

[48] R.V. Williamson, *The flow of pseudoplastic materials*, Ind. Eng. Chem. 21 (1929) 1108–1111.

[49] I.Dapra and Garpi, *Perturbation solution for pulsatile flow of a non-Newtonian Williamson fluid in a rock fracture*, Int. J. Rock Mech. Min. Sci., 44 (2007) 271–278.

[50] A. Michalke, *On the inviscid instability of the hyperbolic-tangent velocity profile*, J. Fluid Mech., 19 (1964) 543–56.

[51] P.J. Carreau, D.D. Kee and M. Daroux, *An analysis of the viscous behaviour of polymeric solutions*, Canad. J. Chem. Eng., 57 (1979) 135–140.

[52] R.L. Batra and M. Eissa, *Laminar forced convection heat transfer of a Sutterby model fluid in an eccentric annulus*, Mech. Res. Comm., 21 (1994) 147–152.

[53] S.C.Prasad and K.R.Rajagopal *Flow of a fluid with pressure dependent viscosity due to a boundary that is being stretched*, App. Math. Comp., 173 (2006) 50–68.

[54] S. Srinivasan and K.R. Rajagopal, *A note on the flow of a fluid with pressure-dependent viscosity in the annulus of two infinitely long coaxial cylinders*, App. Math. Model., 34 (2010) 3255–3263.